UNIVERSITÀ
DI PAVIA

Ph.D. IN BIOMEDICAL SCIENCES

DEPARTMENT OF BRAIN AND BEHAVIORAL SCIENCES
UNIT OF NEUROPHYSIOLOGY

In vivo characterization of cerebellar modulation over prefrontal cortex activity.

Supervisors:
Prof. Lisa Mapelli, Supervisor
Prof. Egidio D'Angelo, Co-Supervisor

Doctoral Dissertation of
Danila Di Domenico

Academic Years 2021/2022

Declaration

I hereby declare that the contents and organization of this dissertation constitute of my original work and do not compromise in any way the rights of third parties, including those relating to the security of personal data.

Danila Di Domenico, 2023

Table of Contents

Chapter 1

INTRODUCTION

1.1 The Cerebellum

The cerebellum, also known as “little brain”, is located in the posterior cranial fossa above the brain stem and separated from the occipital lobe of the cerebral cortex by the tentorium cerebelli. It comprises two hemispheres and a median zone called the vermis. The cerebellar surface is composed of grey matter with numerous convolutions, known as cerebellar laminae, each one named lobule, and divided mediolaterally by two deep transverse fissures into three lobes: anterior, posterior, and flocculo-nodular. The white matter of the cerebellum is arranged in a tree-like pattern and is referred to as the *arbor vitae*. The cerebellar outputs originate from four symmetrical pairs of nuclei located in the white matter, known as deep cerebellar nuclei (DCN). These include the fastigial nucleus (FN), the globose and emboliform nuclei (which combine to form the interposed nucleus -IN- in non-primate mammals), and the dentate nucleus (DN) (Fig. 1.1).

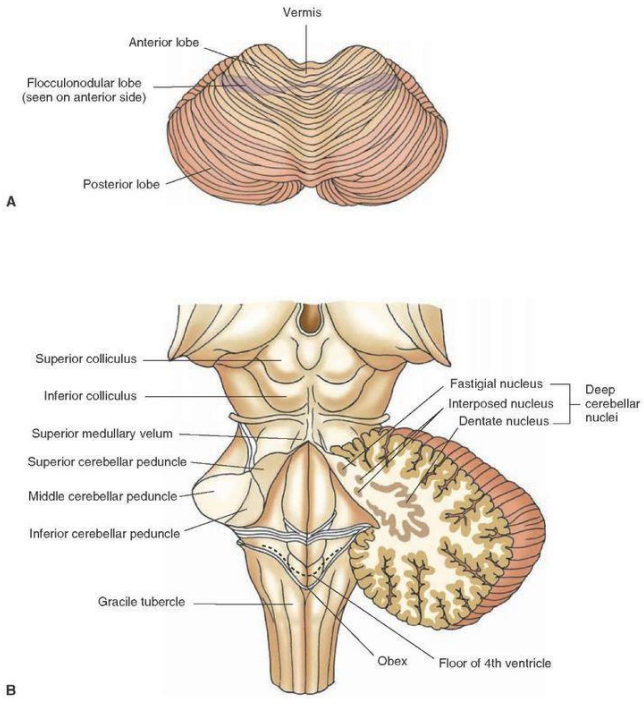

Figure 1.1|(A) Dorsal view of the cerebellum. **(B)** Midsagittal cut through the cerebellum and brain stem showing white matter within the vermal lobules.

All cerebellar connections travel through the brainstem, which is connected to the cerebellum by three pairs of cerebellar peduncles. The superior peduncle, also known as the brachium conjunctivum, is formed mainly by efferent fibres from DCN directed towards the red nucleus, thalamus, and reticular formation, giving rise respectively to the cerebellorubral, cerebellothalamic, and fastigioreticular tracts. Afferent fibres include the anterior spinocerebellar and tectocerebellar tracts. The middle peduncle, also known as the brachium pontis, connects the cerebellum to the pons and carries afferent fibres from the contralateral pontine nuclei, whose axons are connected to the cerebral cortex and superior colliculus. Lastly, the inferior peduncle contains both afferent fibres from the medulla, including posterior spinocerebellar, cuneocerebellar, trigeminocerebellar tracts, olivocerebellar, and vestibulocerebellar fibres, as well as efferent fibres to the vestibular nuclei arising from the vestibulocerebellum (SWENSON 2006; Swenson, Kosinski, and Castro 1984).

The anatomy and cytoarchitecture of the cerebellum are relatively conserved across mammals, including humans (Apps and Hawkes 2009)(Fig. 1.2).

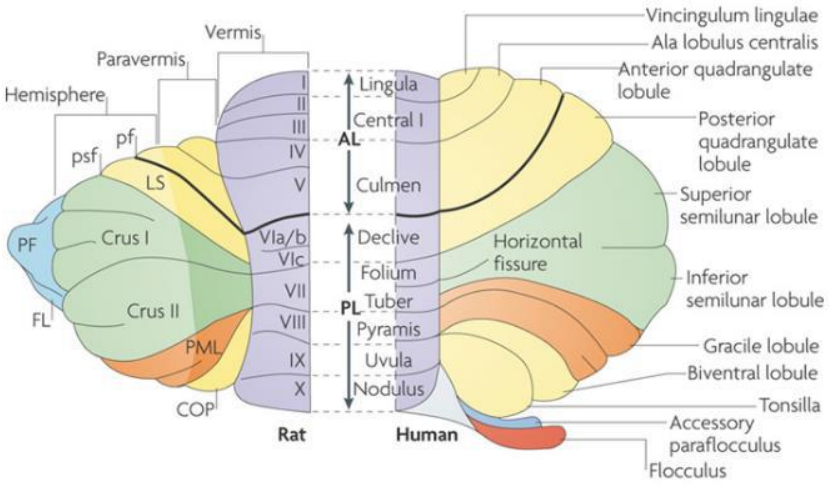

Figure 1.2| Simplified dorsal view of rat (on the left) and human (on the right) cerebellum. Similar areas in the rat and human cerebellum are marked with the same colour. In rats, the fastigial nucleus is found in the vermis, the interposed nucleus (which consists of the globose and emboliform nuclei in humans) is situated in the intermediate zone of the cerebellar hemisphere (paravermis), and the dentate nucleus is located in the lateral zone of the hemisphere. In humans, the cerebellar hemispheres are larger on the medio-lateral axis for the increased number of folia and number of corticopontocerebellar projections from higher brain areas. On the other hand, the parafloccular lobule is larger in rats. Pf, primary fissure; AL, anterior lobe; COP copula pyramidis; Crus I and Crus II, ansiform lobule; FL, flocculus; LS, lobulus simplex; PF, paraflocculus; PL, posterior lobe; PML, paramedian lobule; psf, posterior superior fissure (Apps and Hawkes 2009).

According to phylogenetic and functional criteria, the cerebellum can be divided into three subdivisions, each of which forms connections with a specific part of the brain. The medial zone (nodulus, formerly known as vestibulocerebellum), is located in the flocculo-nodular lobe, and is involved in regulating balance and eye movements, with bidirectional communication with the vestibular nuclei in the medulla oblongata. The vermis and paravermial zone (formerly known as spinocerebellum), comprises the vermis, intermediate zone, IN and FN, and receive sensitive inputs from the spinocerebellar tract. It regulates body and limb movements and is involved in adapting motor coordination by integrating sensory input with motor commands. Finally, the lateral zone of the hemispheres (formerly known as cerebrocerebellum), includes the lateral parts of the hemispheres and DN, receives projections exclusively from the nuclei located in the pons, which relay information from the cerebral cortex. It is involved in planning and timing of movements, as well as cognitive functions of the cerebellum (Apps and Hawkes 2009; SWENSON 2006).

1.1.1 The cerebellar circuit

The cerebellar cortex is characterized by a highly organized structure consisting of three layers that exhibit a repetitive circuit scheme. The cerebellum, due to its organized and relatively simple structure, is an ideal model for studying the mechanisms that regulate neuronal network function. The outermost layer is the molecular layer, containing molecular layer interneurons (MLIs), Purkinje cells (PCs), and parallel fibres (PFs). PCs receive excitatory synapses from PFs and inhibitory synapses from MLIs, while climbing fibres (CFs) originating from the inferior olive (IO) make excitatory synapses with PCs. The PC layer contains the somata of PCs, whose axons make inhibitory synapses with DCN neurons in the white matter. Recent studies have shown that PCs send recurrent collaterals to other PCs and MLIs (Witter et al. 2016). The innermost layer is the granular layer, consisting of granule cells (GrCs) and Golgi cells (GoCs), which are inhibitory interneurons making GABAergic synapses with GrCs. GrCs receive excitatory inputs from mossy fibres (MFs). The sole cerebellar output projecting to other parts of the central nervous system is provided by the DCN. Before entering the cerebellar cortex, MFs and CFs send collaterals to the DCN. Other interneurons, such as unipolar brush cells, Lugaro cells, synarmotic neurons, candelabrum neurons, and perivascular neurons have also been described but their functions are still under debate (Ambrosi et al. 2007).

Additional research has revealed that the DCN has both inhibitory and excitatory effects on its targets. DCN neurons that project GABAergic signals reach the IO, creating a feedback loop with the cerebellar cortex that endows the cerebellum with complex processing abilities (Houck and Person 2014; Uusisaari and de Schutter 2011). Meanwhile, DCN neurons that project glutamatergic signals reach the spinal cord and various brainstem nuclei that are involved in motor control, as well as the thalamus, which relays signals to motor and associative areas in the cerebral cortex. These anatomical connections suggest that the cerebellum may be involved not only in precise motor control but also in cognitive functions. The presence of feedback projections from the cerebral cortex to the cerebellum through the pontine nuclei, which form a closed-loop network, supports this hypothesis (for a deeper insight into the anatomical and functional connections between the cerebellum and associative brain areas see Chapter 1.3).

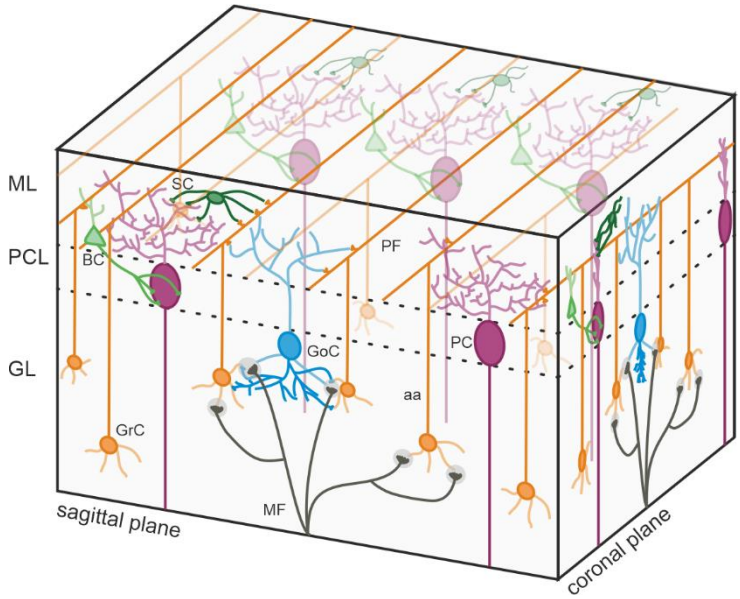

Figure 1.3| Schematic representation of the cerebellar circuit. The cerebellum receives two main afferents: mossy fibres (MFs) and climbing fibres (CFs). MFs coming from precerebellar structures form synaptic contacts with granule cells (GrCs) and deep cerebellar nuclei (DCN) neurons. CFs coming from the inferior olive (IO) contact both DCN neurons and Purkinje cells (PCs). DCN neurons integrate excitatory synaptic inputs coming from MFs and CFs and inhibitory inputs coming from the GrC - PC pathway regulating the cerebellar output. PF: parallel fibre; MLI: molecular layer interneuron; PC: Purkinje cell; GrC: granule cell; GoC: Golgi cell; UBC: unipolar brush cell; NTc: non-traditional cell; MF: mossy fibre; DCN: deep cerebellar nuclei; IO: inferior olive. Figure modified from (Monteverdi et al. 2023).

1.1.2 Deep Cerebellar Nuclei

Together with a small portion of the cortex, the DCN represent the main output of the cerebellum. These neurons project directly to the lateral and medial vestibular nuclei of the brainstem, as well as to other higher structures. The DCN are located in the innermost portion of the *arbor vitae*, immersed in the cerebellar white matter. The preponderance of input received by the DCN comes from PCs (estimated approximately 60-80%) but they also receive collateral projections from MFs and CFs (Shepherd 2004).

There are four pairs of DCN bilaterally arranged on each side of the midline: the FN, IN (consisting of the globular and emboliform nuclei), and DN (Fig. 1.4). They have specific functions and connectivity with different parts of the brain and are essential in relaying information to subcortical regions. In the human cerebellum, afferent fibres outnumber by almost three times the efferent fibres, making it a hub for brain processing (Haroun 2016).

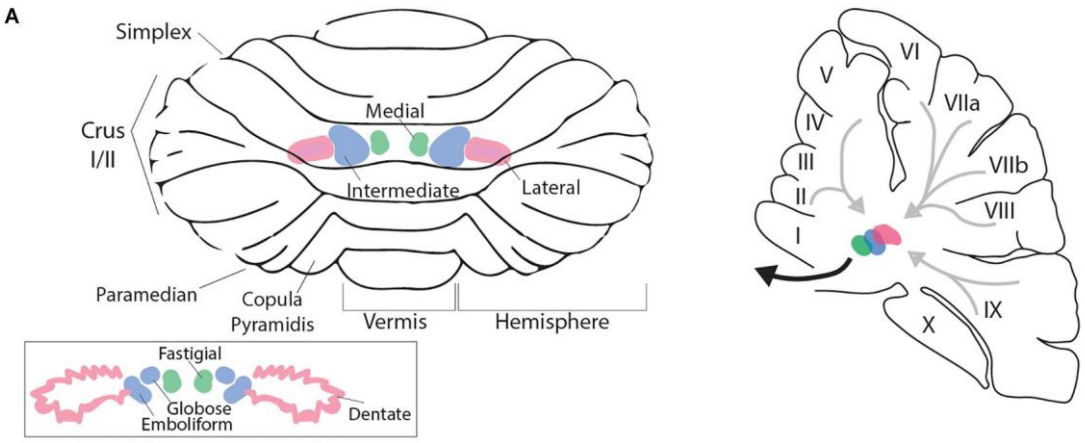

Figure 1.4| Rodent cerebellum with focus on the DCN. The left panel displays the dentate nucleus (*pink*), the fastigial nucleus (*green*), and the interposed nuclei, consisting of the globular and emboliform nuclei (*blue*). The right panel shows the parasagittal view of the DCN, with the same colour code. The Purkinje cell output is indicated by light grey arrows, while the thick black arrow represents DCN efferent towards the cerebral cortex and brainstem (Gill and Sillitoe 2019).

The FN is the oldest cerebellar nucleus and a renowned motor coordination hub. FN has been implicated in regulating multiple non-somatic processes such as feeding, cardiovascular, and respiratory functions, as well as emotional activities (X. Y. Zhang, Wang, and Zhu 2016). It

receives afferent inputs from the vermis and sends efferent outputs to the vestibular nuclei and the reticular formation. One of the most important efferent pathways is the uncinate fasciculus, which decussates within the cerebellar white matter and passes posteriorly through the superior peduncle to reach the vestibular nuclei laterally. The FN also originates a set of uncrossed fibres that reach the vestibular nuclei via the inferior peduncles. Additionally, some fibres do not form synaptic contacts in the vestibular nuclei but proceed to the spinal cord to form the fastigiospinal tract, or reach the medial reticular formation of the pons, forming the tract that controls horizontal eye movements.

The globose and emboliform nuclei in humans, are a paired formation located in the right and left hemisphere of the cerebellum. The globose nucleus is located medially and holds its position in front of the emboliform nucleus (Shyian 2016). The function of the globose nucleus has been up for debate, but it seems to be active during process of conditioned eye blink responses (Haroun 2016). The emboliform nucleus is a wedge-shaped cerebellar structure that is composed of grey matter and, in rodents, is often included in the IN together with the globose nucleus.

In rodents, the IN receives afferents from the paravermal cortex, and projects to the red nucleus, contributing to the rubrospinal tract. Additionally, the globus pallidus, as well as the DN and FN, send efferents to the lateral nucleus of the thalamus, which is connected to the motor and premotor cortex (Trobe 2008).

Lastly, the DN is the largest and most lateral of all cerebellar nuclei. It is built of folded laminae of grey matter and resembles a tooth. It is the largest neuronal structure linking the cerebellum with the rest of the brain and is involved in processes such as voluntary motor function, planning, movement initiation, and other cognitive processes (Akakin et al. 2014). The DN originates the main efferent pathway of the cerebellum, called the conjunctival fasciculus. The DN also receives afferents from the cerebellar hemispheres and projects to the ventromedial and ventrolateral nuclei of the thalamus, contributing to the corticospinal and corticobulbar tracts (Trobe 2008).

In humans, two portions of the DN can be identified: a dorsal (microgyric) and a ventral (macrogyric) one, which projects to the PFC passing through thalamic nuclei (Middleton and

Strick 2001). Furthermore, the DN appears to be divided into separate motor and non-motor domains that converge onto functionally distinct neocortical systems (Fig. 1.5).

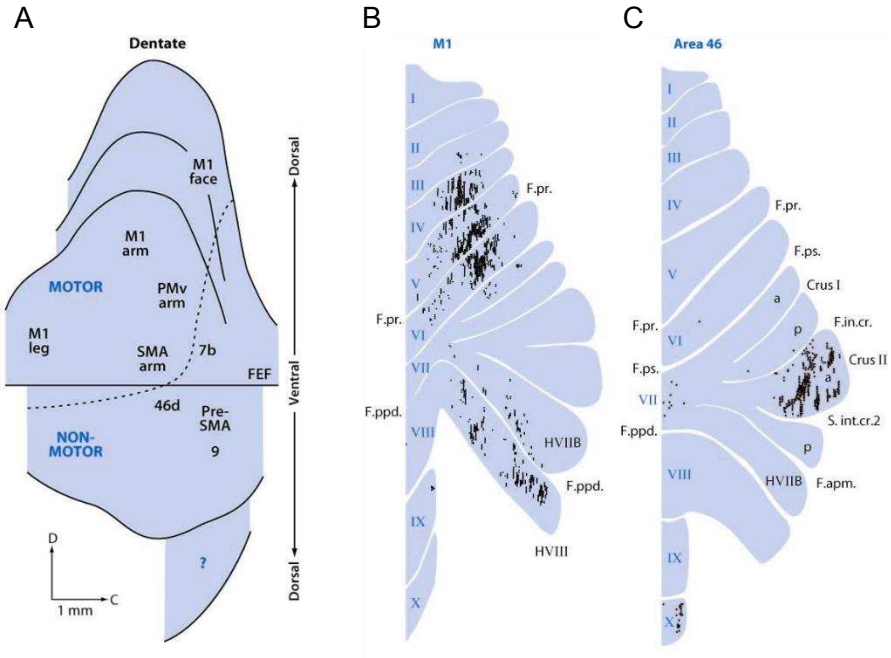

Figure 1.5| (A) Topographic map of the DN. The DN can be divided into motor and non-motor domains based on the projections to different cortical targets in the cebus monkey (FEF, frontal eye field; M1, primary motor cortex; PMv, ventral premotor area; Pre-SMA, presupplementary motor area; SMA, supplementary motor area). **(B-C)** Projections of cerebellar cortical areas to specific cortical regions. The black dots on the cerebellar cortex map indicate the position of PCs that project to M1 (in the centre) or to area 46 of the prefrontal cortex (on the right) in primates (Strick, Dum, and Fiez 2009).

In all DCN, six populations of neurons can be identified, which in turn are divided into three subcategories that differ in morphology, neurotransmitter, and connectivity (De Zeeuw and Berrebi 1995). These subcategories are: large glutamatergic neurons that provide contralateral excitatory input to areas outside the cerebellar circuit; medium-sized GABAergic neurons that provide feedback to the IO; and small GABAergic and glycinergic interneurons that are involved in lateral inhibition (Uusisaari, Obata, and Knöpfel 2007). Furthermore, unlike other cerebellar neurons, DCN neurons have much larger receptive fields with low specificity for the numerous input modalities they receive (Rowland and Jaeger 2008). The individual efferent axons of DCN branch out and project to various extracerebellar structures, including the spinal cord and medulla oblongata. This information suggest that the output of

the DCN impacts generalized aspects of behaviour, movement planning, and execution (Middleton and Strick 1994), and timing (Ivry and Spencer 2004; De Schutter and Steuber 2009).

1.2 The Prefrontal Cortex

The prefrontal cortex is thought to be the main association area in the mammalian cortex. It is positioned in the frontal part of the frontal lobe and its main functions comprehend task flexibility and planning, selective attention, attentional-set shifting, rule learning, strategy switching, and goal-directed behaviour. Because of this large range of functions, it is one of the most studied areas of the brain in different mammalian species, but differences in PFC nomenclature and subdivisions in humans, rodents, and non-human primates complicate the approach to PFC studies. In humans, the granular and orbital parts of the frontal cortex, such as the orbitofrontal cortex and the granular frontal cortex, are typically associated with the PFC. In contrast, most rodent studies focus on the medial frontal areas, such as the prelimbic cortex (PrL) and the anterior cingulate cortex (ACC) (Laubach et al. 2018). Despite these differences, researchers have recognized that the rodent mPFC (in particular the PrL) can be considered a functional homolog of the human dorsolateral prefrontal cortex (dlPFC) and ACC, playing a crucial role in top-down inhibitory control and reward mechanisms (Terraneo et al. 2016). Therefore, it is not uncommon to use information about rodent prefrontal areas to infer primate prefrontal cortex functioning.

Another important aspect to consider is the difference in the development of human and rodent brains. While rodents are widely used in scientific research, their brains lack the unique molecular, cellular, and anatomical features found in the human cerebral cortex. Understanding the intricacies of top-down functions such as inhibitory control, working memory, and salience detection requires a deep understanding of the respective cerebral and neuronal processes in both species. Therefore, it is important to consider the evolutionary differences in anatomy and gene expression between humans and rodents to better understand normal and abnormal cerebral activity.

Gene expression plays a crucial role in cortical expansion in primates, resulting in the development of vital sites in the neocortex that are not present in rodent models. Expression of specific genes in prospective association areas such as the prefrontal cortex is apparent in

human foetal brain development but not seen in rodents (Johnson et al. 2009). These expressions are responsible for the individualized granular cortex construction as well as agranular and dysgranular formation in mammalian animals. Agranular brain areas are more primitive than granular brain areas in the prefrontal cortex, and the level of granularity in specific prefrontal areas is deposited through development and forms more prominent and functional structures in mammals (Carlén 2017) (Fig. 1.6).

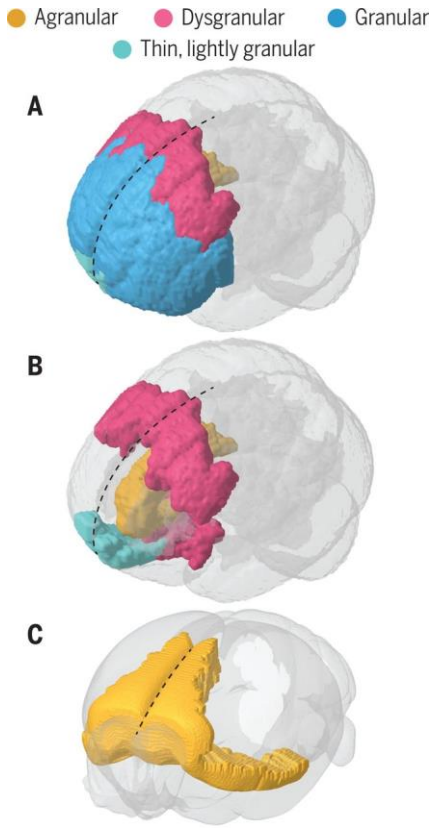

Figure 1.6| Cortical types in the human and mouse prefrontal cortex (A-B) Frontal-side view of the human brain showing four cortical types in the prefrontal cortex. **(C)** Tilted frontal-side view of the mouse brain illustrating the agranular prefrontal cortex (Carlén 2017).

1.2.1 Medial Prefrontal Cortex

The rodent medial prefrontal cortex (mPFC) can be divided into four areas: the medial precentral area (PrCm), the anterior cingulate cortex (ACC), the prelimbic area (PrL), and the infralimbic cortex (ILC), arranged along the dorsal to ventral axis (Heidbreder and

Groenewegen 2003). The majority (80-90%) of neurons in the mPFC are excitatory pyramidal cells, with the remaining 10-20% being inhibitory GABAergic interneurons (Ascoli et al. 2008; Defelipe et al. 2013; Riga et al. 2014). Within the GABAergic interneurons, there are four subpopulations based on the expression of specific proteins: fast-spiking parvalbumin (PV) interneurons that target the perisomatic region, somatostatin (SST) interneurons that target dendrites, and vasoactive intestinal polypeptide (VIP) interneurons that express ionotropic serotonin receptor 5HT3a (Rudy et al. 2011). Another subtype of interneuron in the cortex is neuropeptide Y (NPY)-expressing neurons, which inhibit pyramidal neurons in ipsilateral PrL through activation in the ILC, thus regulating the activation of downstream targets (Saffari et al. 2016). GABAergic interneurons are distributed throughout the cortex, but their arrangement is different in the PFC (Saffari et al. 2016), (Fig. 1.7). These interneurons play an important role in local circuits by synchronizing pyramidal cells firing and generating neuronal oscillations (Kvitsiani et al. 2013).

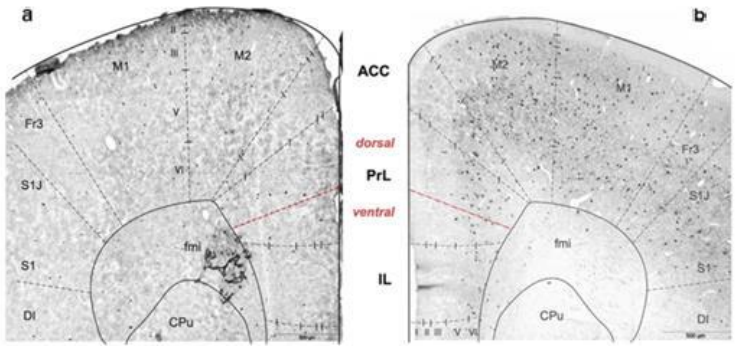

Figure 1.7| The distribution of GABAergic neurons is different in ACC, PrL and ILC. **(A)** NPY+–stained coronal sections of PFC in higher magnification and schematic drawing of different areas. **(B)** Overview of PV-stained coronal sections of PFC and quantification of the overall density of $PV^{+/-}$ GABAergic neurons in M2, ACC, PrL and ILC. (Adapted from Saffari et al. 2016).

According to several optogenetic studies, the activity of GABAergic interneurons plays a crucial role in gamma oscillations and emotional behaviour (Cruikshank et al. 2012; Little and Carter 2013; Vertes 2006; Yizhar 2012). Specifically, photostimulation of PV interneurons has been found to result in fast, powerful, and uniform inhibition on pyramidal cells firing, which affects their outputs. SST neurons have been shown to modulate input signals reaching principal pyramidal neurons, resulting in a weak, more variable, and prolonged inhibitory

effect on pyramidal cells firing (Kvitsiani et al. 2013). Pyramidal neurons in the mPFC can be classified based on their projection patterns and expression of dopamine receptors, which are involved in the reward circuit (Dembrow and Johnston 2014; Floresco et al. 2006). Usually, pyramidal neurons express just one type of dopamine receptor (either D1-like or D2-like) and the co-presence of both receptors types is rare (Gaspar, Bloch, and Le Moine 1995). Photostimulation of long-range projecting pyramidal cells revealed their connections to both PV and SST interneurons, but PV interneurons have a stronger inhibitory effect on subcortically projecting pyramidal neurons (A. T. Lee, Gee, et al. 2014).

1.2.2 Layers and connectivity of the mPFC

The mPFC consists of functional microcolumns that process information in a supramodal manner. The rodent mPFC displays a unique organization, lacking the classical cortical input layer IV, while deep layers V and VI provide efferent projections to subcortical areas (Douglas and Martin 2004; Opris et al. 2013; Swadlow, Gusev, and Bezdudnaya 2002; Uylings, Groenewegen, and Kolb 2003). Inputs from various sources such as the contralateral mPFC, medio-dorsal (MD) thalamus, basolateral amygdala (BLA), and ventral hippocampus (HPC) reach mPFC, among these we found projections to layer II PrL pyramidal neurons at specific dendritic locations (Humeau et al. 2005; Little and Carter 2013). The mPFC anatomical and functional connectivity enables the integration of inputs from different afferent origins. Thalamo-cortical interactions are crucial for sensation, perception, and consciousness. The midline and paralaminar thalamic nuclei send excitatory projections to late-spiking interneurons in layer I, instead of pyramidal cells (Alitto and Usrey 2003; Cruikshank et al. 2012; Roy John 2002). Cortical interneurons regulate pyramidal cell firing through feed-forward inhibition and control activity gain. Repetitive photostimulation of thalamo-cortical projections has been shown to elicit strong, sustained synaptic responses in mPFC interneurons, suggesting that their prolonged activation is necessary for working memory function (Cruikshank et al. 2012; Ferguson and Gao 2018).

Several studies indicate that various subcortical regions, including the Ventral Tegmental Area (VTA) and medio-dorsal (MD) thalamic nuclei project to neurons in the mPFC at layer III (Hoover and Vertes 2007; Kuroda et al. 1996). The activation of pyramidal neurons through these pathways allows relaying information horizontally and downstream to pyramidal

neurons in layer V (Thomson and Bannister 2003). Additionally, layer V pyramidal neurons receive long-range inputs from the same subcortical regions and the MD region of the thalamus (Kuroda et al. 1993, 1996), which they integrate with the inputs from layer III. The important role of cortical GABAergic interneurons in cognitive functions has been demonstrated through *in vivo* experiments using pharmacological tools and electrophysiological recordings. These studies showed that most of the projections from MD nuclei reach PV interneurons in layer III, which contact pyramidal neurons in layer V (Paine, Slipp, and Carlezon 2011; Sawaguchi, Matsumura, and Kubota 1989). Moreover, the activation of PV interneurons is mainly due to excitatory inputs from MD (Floresco and Grace 2003; Povysheva et al. 2006). Thus, it is reasonable to hypothesize that MD glutamatergic projections to mPFC provide strong excitation of PV interneurons, which exert their inhibitory effect onto pyramidal neurons in layer V (Fig. 1.8). This circuit organization fine-tunes the balance between excitation and inhibition (E/I balance), which has significant implications for mPFC-dependent cognitive behaviour.

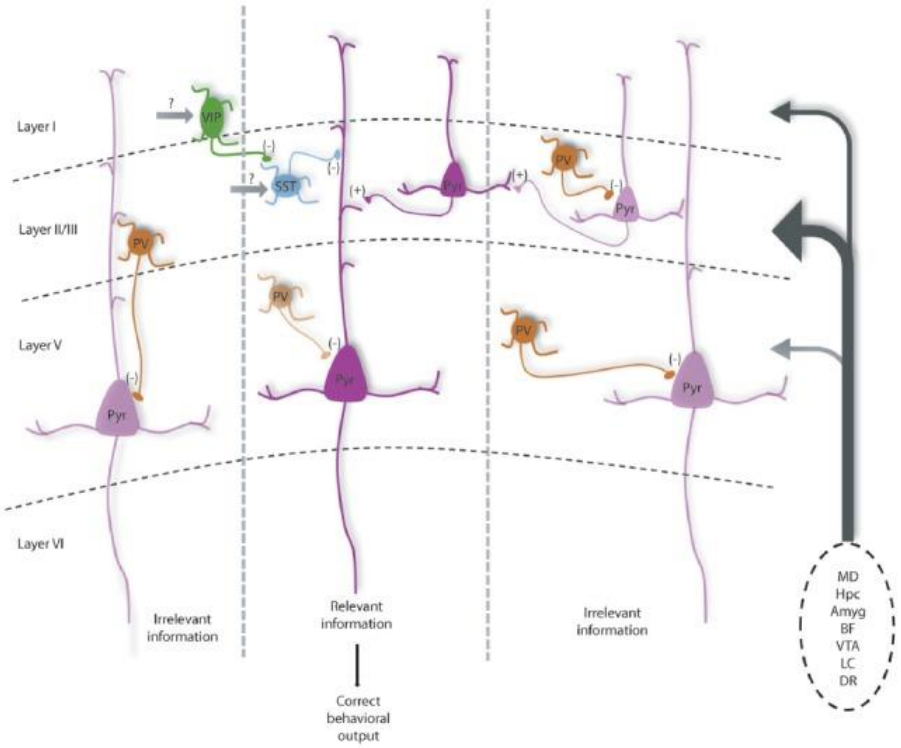

Figure 1.8| Activity of PV interneurons in regulating the excitation/inhibition balance in PFC circuits. Under normal conditions, PV neurons are highly active and contribute to inhibiting pyramidal neurons (mediated by inputs from the MD). This suppresses the activity of neurons in functional units (cortical columns on the left of the diagram) that represent distractor information, increasing the signal-to-noise ratio of incoming information

from PFC afferents (listed on the right). VIP interneurons may further refine activity by inhibiting SST neurons that disinhibit the distal dendrites of groups of pyramidal neurons. Darker and lighter neurons represent high and low levels of activity, respectively. Amig, amygdala; BF, basal forebrain; DR, dorsal raphe; Hpc, hippocampus; LC, locus coeruleus; MD, mediodorsal thalamus; VTA, ventral tegmental area (Ferguson and Gao 2018).

The observation that dysfunction in thalamic connection to mPFC causes cognitive impairment provides further evidence of the importance of the mPFC in various functions related to visceral, autonomic, limbic, and cognitive processes. Long-range projections from the mPFC to other cortical and subcortical brain areas play a crucial role in these functions (Hoover and Vertes 2007; Miller and Cohen 2001). Optogenetic studies have identified glutamatergic and GABAergic projections of the mPFC to the nucleus accumbens, indicating that not all GABAergic neurons in the mPFC are local interneurons (A. T. Lee, Vogt, et al. 2014). Glutamatergic PrL projections to the BLA are involved in higher cognitive processes associated with innate emotional responses (Britt et al. 2012; Suska et al. 2013). Two distinct pyramidal cell populations in PFC layer II project either to the contralateral mPFC or the BLA (Little and Carter 2013). The interconnectivity between the PrL and other brain regions is essential for efficient bi-directional communication and top-down control when responding to emotional stimuli.

1.3 Cerebello-prefrontal cortex interactions

Beyond its traditional association with motor control, it is now acknowledged that the cerebellum plays a role in cognitive functions, through specific connections between the cerebellum and areas of the cerebral cortex involved in cognitive processes such as the PFC (Palesi et al. 2015). Anatomical studies and tractographic reconstruction of cerebellar projections passing through the superior cerebellar peduncle have unveiled cerebello-cerebral connections in humans. The superior cerebellar peduncle carries cerebellar outputs directed to motor nuclei of the thalamus [the ventro-anterior (VA) and ventro-lateral (VL)] projecting to motor cortices, but also to intralaminar nuclei and the MD thalamic nucleus, which ultimately project to the PFC (Schmahmann 1996). Notably, tractography has revealed that around 80% of cerebellar connections are directed to cerebral cortex areas involved in cognitive functions, rather than sensorimotor control (Palesi et al. 2015) (Fig. 1.9). In non-human primates, a study using trans-synaptic viral tracers determined that the primary motor cortex mainly projects to cerebellar lobules with well-established roles in skilled motor control, whereas afferents from the prefrontal area reached regions in cerebellar

hemispheres that are not connected with the primary motor cortex (R. M. Kelly and Strick 2003).

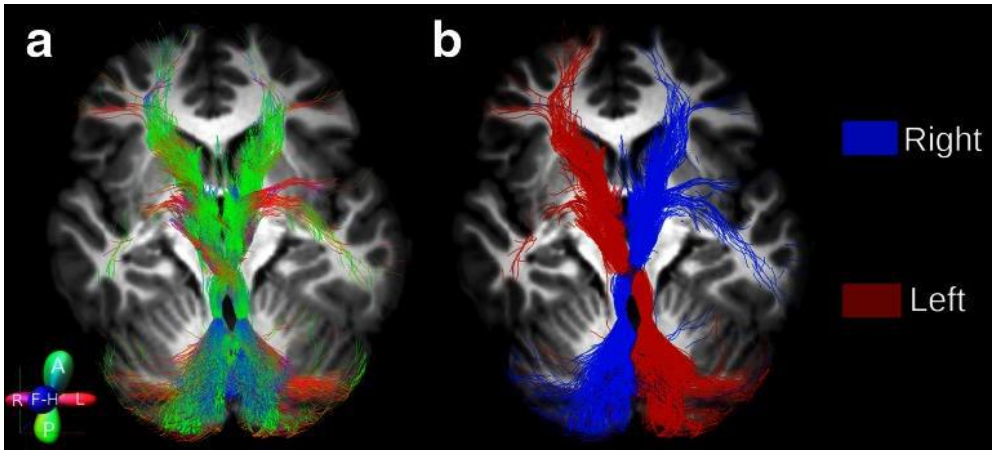

Figure 1.9| 2D rendering of cerebello-thalamo-cortical pathways of a representative subject**. (a)** The tracts are color-coded by direction to represent their anatomy **(b)** A single solid colour has been used for each tract to distinguish the streamlines from the left (*red*) and right (*blue*) pathways (Palesi et al. 2015).

Furthermore, tracing studies and lesion-symptom mapping have shown a functional coherence between the PrL of the mPFC in rodents and the PFC in humans and non-human primates (Seamans, Lapish, and Durstewitz 2008a; Uylings, Groenewegen, and Kolb 2003). *In vivo* electrophysiological experiments in rodents have also supported the existence of cerebello-prefrontal interconnections, showing that stimulation of the PrL of the mPFC elicits local field potentials (LFP) responses in PCs (Thomas C. Watson, Jones, and Apps 2009) (Fig. 1.10). LFPs were more pronounced in the lobule VII of the contralateral vermis, which is known to be involved in eye movement control through projections from the fastigial nucleus (FN). These findings suggest that cerebello-cerebral connections involved in eye movement are more related to goal-directed behaviour than purely cortical information processing (Thomas C. Watson, Jones, and Apps 2009). An additional study conducted *in vivo* found that DCN stimulation elicited a range of response patterns in mPFC neurons in rats, indicating the bidirectional influence between the cerebellum and the prefrontal cortex (Thomas C. Watson et al. 2014) (Fig 1.11).

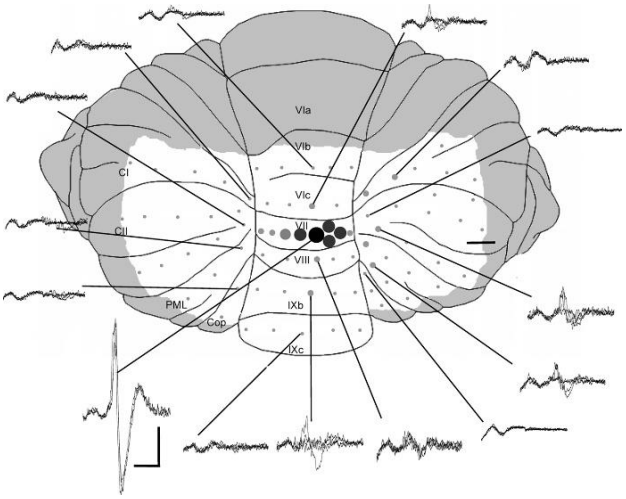

Figure 1.10| PrL contribution to population activity in cerebellar vermis of a rat. Schematic representation of the dorsal view of the cerebellum reporting the distribution of LFP responses evoked by the stimulation of the mPFC. The amplitude of the LFPs responses is represented by example waveforms recorded within each cerebellar region and the size of circles. Taken from Watson, Jones, and Apps 2009.

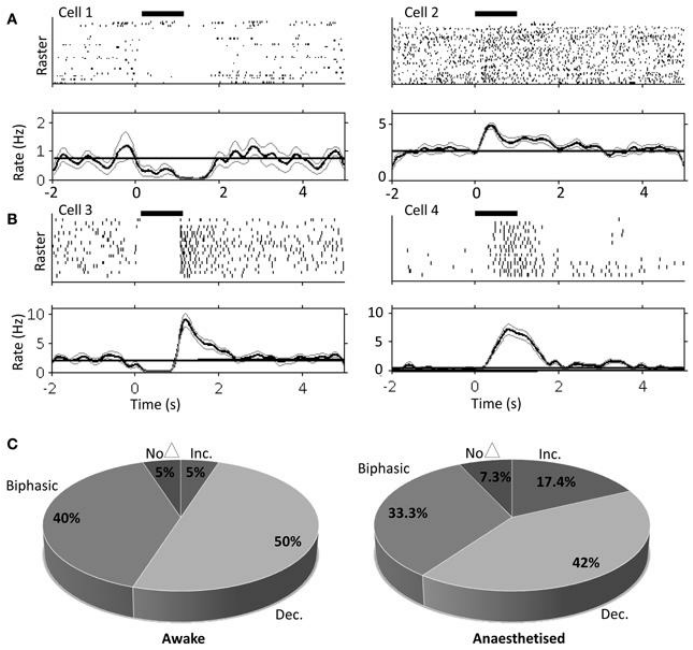

Figure 1.11| PrL single units response pattern following cerebellar stimulation. Raster plots and peri-stimulus time histograms of typical responsive neurons in the PrL of awake (A) and urethane-anesthetized rat (B). High frequency FN stimulation (100 Hz, 100 stimuli, 1s duration, 100 μA) evokes 3 typical response patterns in both awake and anesthetized animals: decrease of firing rate compared to baseline activity (cell 1 in Figure A); increase of spike discharge (cell 2 in Figure A; cell 4 in Figure B); biphasic response consisting in a decrease of firing rate followed by a rebound increase (cell 3 in Figure B). In (C) are reported the response patterns percentages following FN stimulation in awake (n=20) and anesthetized (n=69) rats (Thomas C. Watson et al. 2014).

Various studies have reported a connection between the stimulation of the DN and dopamine (DA) release in the mPFC, which may regulate cortical neuron responses to cerebellar stimulation (Mittleman et al. 2008). The cerebellar output-induced release of DA in the mPFC can occur via several pathways, including the VTA, thalamus (Kehr, Lindqvist, and Carlsson 1976; Snider and Maiti 1976; Snider, Maiti, and Snider 1976; Thomas C. Watson et al. 2014), substantia nigra or basal ganglia (Nieoullon, Cheramy, and Glowinski 1978). The diverse response patterns observed in the mPFC may be due to the expression of various DA receptors in mPFC neurons, including those belonging to the D1-like and D2-like receptor families (Thomas C. Watson et al. 2014). Hence, the release of dopamine in the mPFC leads to a diverse range of effects on both cortical pyramidal cells and local interneurons (for a detailed description see chapter 4). However, the complex reciprocal connections between these cells complicate the interpretation of responses elicited in mPFC by cerebellar activation (Dembrow and Johnston 2014) (Fig. 1.12). Recent optogenetic studies on freely moving mice suggest that the induction of dopaminergic release in mPFC via cerebello-VTA pathway activation is insufficient to cause significant behavioural changes (Carta et al. 2019). Therefore, it is reasonable to assume that the involvement of the cerebellum in cognition cannot be fully explained solely by the contribution of the cerebello-VTA pathway.

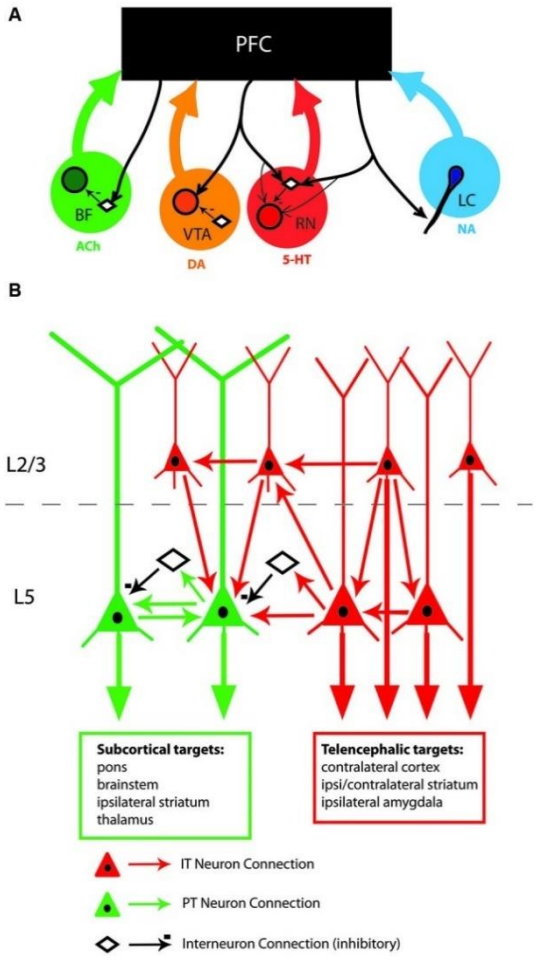

Figure 1.12| Schematic representation of anatomy and network connectivity within and across the rodent mPFC. (A) Schematic representation of projections to and from the PFC. Noradrenaline (NA) is released from the locus coeruleus (LC) terminals; Acetylcholine (ACh) from the basal forebrain (BF); Serotonin (5-HT) from the raphe nuclei (RN); Dopamine (DA) from the ventral tegmental area (VTA) and substantia nigra (SN). PFC neurons project to the neuromodulatory centres, contacting back the neuromodulator-synthesizing neurons (*shaded circles*), inhibitory interneurons (*open diamonds*), or both. **(B)** Schematic representation of the connections within the mPFC. The pyramidal tract (PT, *green*) neurons are located in layers V/VI (L5/6); intratelencephalic (IT, *red*) neurons throughout L2-6. PT neurons receive input from other PT neurons, IT, and inhibitory interneurons. IT neurons receive inputs only from other IT neurons (Dembrow and Johnston 2014).

Furthermore, it is essential to examine the other cerebellar pathways that reach the mPFC and contribute to cortical activity. The thalamic projections that receive cerebellar output are of particular interest, since the thalamus plays a critical role in many processes, including sensation, perception, and consciousness (Alitto and Usrey 2003; Roy John 2002). Therefore, the analysis of the functional interaction between the cerebellum and prefrontal cortex must focus on the glutamatergic projections from the thalamus to the mPFC.

Thalamic nuclei that receive axons from the cerebellum are either involved in sensory-motor control (VA and VL nuclei) or cognitive processes (intralaminar and MD nuclei) (Schmahmann

1996). Interestingly, there is evidence indicating that the mPFC receives significant innervation from the MD thalamic region, which appears to be crucial for various cognitive processes, including working memory, cognitive flexibility, and social interaction (Ferguson and Gao 2018; Parnaudeau, Bolkan, and Kellendonk 2018).

In addition, it has been reported that *in vivo* stimulation of the cerebellar DN has a dopamine-mediated neuromodulatory effect on the mPFC through activation of the glutamatergic ventral or MD thalamic nuclei (Hoover and Vertes 2007). However, more research is needed to completely understand the neural mechanisms that are involved in the modulation of mPFC activity caused by the cerebellar output.

1.4 Cerebellar role in cognition

Over the past few decades, numerous studies have focused on cerebellar role in movement by examining the interactions between the motor cortex and the cerebellum and their contribution to motor learning. However, it has been demonstrated that the cerebellum is involved in functions beyond the motor domain. Indeed, anatomical and functional neuronal pathways have been discovered between the cerebellum and the PFC in both directions (R. M. Kelly and Strick 2003; Palesi et al. 2015; Thomas C. Watson et al. 2014; Thomas C. Watson, Jones, and Apps 2009). The PFC, in particular, is primarily associated with higher cognitive functions rather than motor control. One intriguing theory suggests that the brain is capable of selecting and executing motor commands through anticipatory control loops and internal (forward and inverse) models (Ito 2008) (Fig. 1.13). In this way, the brain is able to create internal models which allow for the prediction of movement and the real-time control of the dynamic properties of body parts without requiring sensory feedback, similar to how movement is replicated (Ito 2008). Expanding this theory to cognition may provide insights into how the brain processes information that is eventually transformed into thoughts. The forward model calculates the inputs to a system solely by comparing the current state and the system output without using feedback inputs, and therefore it is incapable of correcting errors. In contrast, the inverse model involves some of the system output returning to the input, enabling the system to adapt or compensate for errors.

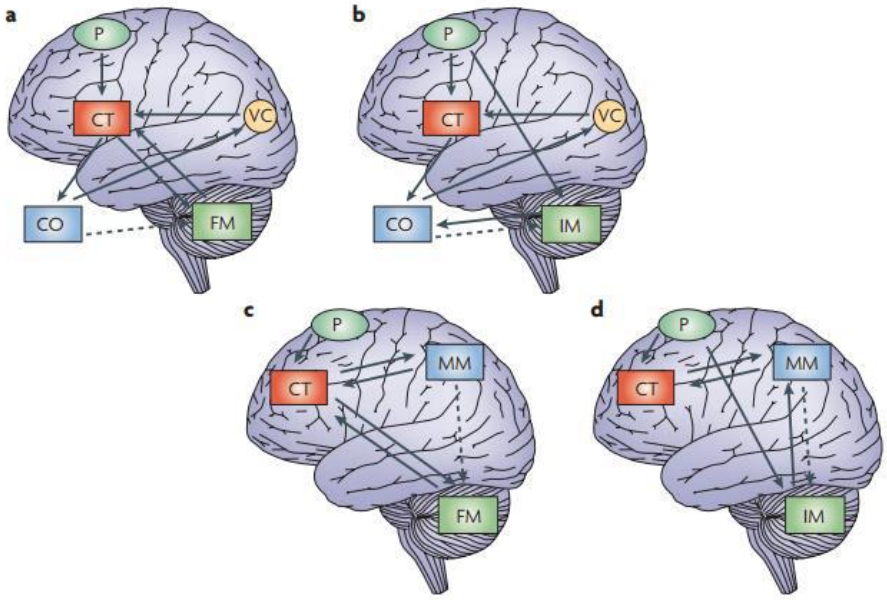

Figure 1.13|Internal-model control systems for voluntary movement and mental activity. 'Forward' **(a)** and 'inverse' **(b)** model control systems for movement. According to the instruction given by the instructor (P) in the premotor cortex, the controller (CT) in the motor cortex sends command signals to the controlled object (CO), a body part or a lower motor centre. The visual cortex (VC) mediates feedback from the body part to the motor cortex. The dashed arrow indicates that the body part is copied into an internal model in the cerebellum (either a forward model (FM) or an inverse model (IM)). In the forward-model control system, control of the CO by the CT can be precisely performed by referring to the internal feedback from the forward model. In the inverse-model control system, feedback control by the CT is replaced by the inverse model itself. (**c,d)** Forward- and inverse model control systems for mental activities. In response to an instructor, the controller in the prefrontal cortex initially controls a mental model (MM) that is expressed in the temporo–parietal cortex. The dashed arrow shows that the mental model is copied to a forward model or an inverse model in the cerebellum. (Adapted from Ito 2008)

The cerebellar involvement in anticipatory control loops is essential for the coordination, dynamics, and fluidity of movements. These qualities reflect the learning mechanisms of adaptation that depend on sensory prediction errors and are responsible for the internal modelling of the body state (D'Angelo and Casali 2012; Shadmehr and Krakauer 2008). Precisely, when a specific mental model is used repeatedly, a corresponding internal model (either forward or inverse) is formed in the cerebellum (Ito 2008). The observations that cerebellar impairments have been demonstrated to have effects in both motor and cognitive domains (Schmahmann 2004) sustain this hypothesis. Indeed, neural substrates for abstract or symbolic cognition are not separated from those used for other forms of cognition. Overall, thought may be considered as an implicit form of action that uses the same anticipatory control loops that are involved in on-line action control and adaptive behaviour. The

formation of abstract internal models and action prediction relies on a combination of inhibition processes, working memory, event representation, and learning (Pezzulo 2012).

Since the similar organization of motor pathways also supports cognitive processing during behaviour, it is possible to control action in real-time whilst facilitating the prediction of abstract consequences of said actions, as well as the generation and assessment of new actions. Specifically, the cerebellar cortex is organized in microcomplexes whose closed-loop circuits generate cerebellar interconnections with the neocortex (Apps and Hawkes 2009; R. M. Kelly and Strick 2003; Middleton and Strick 1994). Cerebellar microcomplexes serve as the functional unit for learning and are ultimately connected to the same group of neurons in the DCN and IO (Apps and Hawkes 2009). In each microcomplex, inputs from MFs to GrCs are transmitted to PCs, which also receive error signals conveyed by CFs originating from the IO. These error signals drive an LTD-based learning process at PF-PC synapses. The cerebellar ability to create and adapt internal models is based on this error-based learning process, allowing each microcomplex to form an internal model for a specific function.

The neocortical region responsible for conscious control of thought and action, including abstract reasoning and problem solving, is the PFC (Miller and Cohen 2001). Within the PFC, neurons encode information about goals and how to achieve them through the working memory system. This is accomplished by the maintenance of specific patterns of pyramidal cells activity over an extended period (Miller and Cohen 2001), depending on lateral inhibition from GABAergic interneurons (Rao, Williams, and Goldman-Rakic 2000). To both regulate attention levels and develop the appropriate mental model during the thinking process, the PFC system collaborates with the novelty system, which involves the hippocampal CA1 area and dopaminergic neurons in the VTA (Lisman and Grace 2005). Moreover, the cerebellar output reaches the VTA, which is one of the subcortical structures that modulate the neuronal activity in the PFC through dopaminergic projections (Dembrow and Johnston 2014; Mittleman et al. 2008; Rogers et al. 2011). Additionally, recent studies in mice have shown that there is an anatomical and functional relationship between the cerebellum and the hippocampus, which suggests that the cerebellum could also have an impact on hippocampal neuronal activity and associative learning (Bohne et al. 2019; Froula, Hastings, and Krook-Magnuson 2023; Thomas Charles Watson et al. 2019).

When faced with a new problem, there is a discrepancy between the existing mental models and the novel situation, prompting the brain to develop new strategies to solve it (new mental models). In such cases, the novelty activates the attentional system, which increases the magnitude and duration of working memory (Nestor, Lam, and Gray 1996). This, in turn, sends command signals that enable the adaptation of mental models to the new situation.

In addition to the attentional and novelty system, the thalamus is another subcortical structure that plays a crucial role in regulating cortical neuron activity and it is also linked to the cerebellum. The thalamus facilitates cerebello-cortical interplay relaying cerebellar outputs to both motor and prefrontal regions of the brain (Hoover and Vertes 2007; Schmahmann 1996). The thalamus is involved in various motor, cognitive, and sensory processes (Alitto and Usrey 2003; Roy John 2002) and supports rapid on-line and feedback processing, which enables the synchronization of sequences of thought and action (Koziol et al. 2014).

In general, alterations in cerebello-cortical pathways, underpinning the regulation of firing activity in PFC neurons, are known to be associated with several cognitive disorders, such as autism and schizophrenia (Andreasen et al. 1996; D'Angelo and Casali 2012; Rogers et al. 2011).

1.4.1 Cerebellum and autism

When referring to the cerebellum in autism spectrum disorders (ASDs), the first correlation that comes to mind is the link of ASDs with motor impairments. Indeed, Lebarton and Iverson (2013) have demonstrated that autistic subjects experience changes in motor coordination, movements of the upper and lower limbs, and difficulties in maintaining posture. In addition, research has demonstrated that autistic children can present motor issues, including delays in eyeblink conditioning and vestibulo-ocular reflex (Piochon et al. 2015). Moreover, disruptions in various pathways associated with motor function such as sensorimotor deficits, anomalies in gaze fixation, oculomotor alterations, and abnormalities in maintaining balance and posture (Fatemi et al. 2012) have been highlighted in individuals with ASD. Precisely, the altered pathways involved in these mechanisms are: i) the sensorimotor circuit involving the cerebellum, basal ganglia, and motor and parietal cortices; the oculomotor circuit, which encompasses the pons, brainstem, superior colliculus, frontal eye field, and cerebellar vermis;

ii) the upper limb control circuit, comprising the neocortex, cerebellar cortex, and DCN; iii) the gait and postural control circuit involving the vermis and intermediate cerebellum; iv) and the motor learning circuits, where CFs from the IO reach the molecular layer of the cerebellar cortex, playing a crucial role (Mosconi et al. 2015). Overall, motor deficits could be viewed as a characteristic of ASD, and the relationship between cerebellar dysfunctions and autism could also be examined from a motor perspective (Piochon et al. 2015).

However, it has been established that the cerebellum is also involved in emotional and high-level cognitive processes. Indeed, Schmahmann and Sherman introduced the term "cerebellar cognitive affective syndrome" for the first time, based on various studies that have demonstrated impairments in non-motor functions as a result of cerebellar alterations (Schmahmann and Sherman 1998). These dysfunctions consist of impairments in concept formation and intellectual processing in individuals with olivopontocerebellar atrophy, errors in executive tasks in patients with cerebellar cortex atrophy, visual-spatial alterations in individuals who have undergone left cerebellar hemisphere removal, and language deficits in children with cerebellar lesions (Schmahmann and Sherman 1998). As a result, investigations on the potential role of the cerebellum in autism regarding cognitive and emotional characteristics has been recently intensified (Sydnor and Aldinger 2021). Using resting-state fMRI techniques, an underconnectivity in cerebellar circuits implicated in higher cognitive functions has been described in individuals with ASD (Mosconi et al. 2015). Additionally, fMRI studies have revealed that the cerebellum and amygdala are active during implicit processing of facial mimic and expression while in subjects with ASD they are inactive (D'Angelo and Casali 2012). Cerebellar alterations in autistic individuals can also result in the disruption of specific speech features (Fatemi et al. 2012). Furthermore, evidence has shown that attention-orienting deficits in individuals with autism may be associated with a decrease in volume of lobules VI-VII in the cerebellar vermis (Townsend et al. 1999). Disruptions in the posterior lobe of the vermis, which is connected to the anterior limbic system, have been linked to mild cognitive impairments, deficits in executive functions, language difficulties, and disinhibition in individuals with autism (Fatemi et al. 2012). The involvement of the cerebellum in ASDs is also strongly supported by anatomical abnormalities (Leroi et al. 2002). Specifically, post-mortem studies have revealed that cerebellar alterations are one of the

most prominent findings in autistic patients. An increase in both total brain and cerebellar volume have been reported (Stanfield et al. 2008). Specifically, alterations in the structure and form of the cerebellum, which includes underdevelopment of the vermis and malformation of the flocculus, have been described (Piochon et al. 2015). Another study has revealed a consistent loss of PCs in ASD subjects, particularly in the posterolateral neocerebellar cortex and in the adjacent archicerebellar cortex (Kemper and Bauman 1998; Vargas et al. 2005). Since PCs are cerebellar neurons that utilize GABA as a neurotransmitter and convey the sole output of the entire cerebellar cortex to DCN, a loss of them in ASD patients has a crucial impact on both the cerebellar GABAergic system and DCN functioning (Vargas et al. 2005; Whitney et al. 2009). Finally, the loss of PCs also leads to a retrograde loss of cells in the IO (Fatemi et al. 2012).

Undoubtedly, animal models have significantly contributed to understand the underlying mechanisms of autism and to confirm the involvement of the cerebellum in this disorder (for a deeper insight in animal models used for autism studies see Mapelli et al. 2022; Fig. 1.14). In particular, studies on FMR1 mutant mice, which exhibit the fragile X syndrome, have shown an increase in LTD of PF-PC synapses, leading to an imbalanced relationship between LTD and LTP in the molecular layer. This balance is critical for motor learning in the cerebellum, therefore, when disrupted, it can lead to altered eyeblink conditioning in FMR1 mutant mice (Koekkoek et al. 2005). At the same time, FMR1 knock-out mice exhibit cognitive and behavioural abnormalities that resemble those observed in autistic individuals (Koekkoek et al. 2005).

Another mouse model of ASD, with a selective loss of Tsc1 in PCs, has shown changes in social behaviour, repetitive behaviours, and a decrease in PCs excitability (Tsai et al. 2012). Additionally, a study investigating structural connectivity in this model found abnormalities in the network involving the cerebellar right Crus I and the inferior parietal lobe. This disrupted circuit leads to difficulties in integrating visuospatial and motor cognitive information, as well as a decrease in the ability to understand and imitate expressions and gestures (Stoodley et al. 2017). Furthermore, an intriguing study in PC-Tsc-1 mutant mice has shown that disruptions of the functional connection between the right Crus I and the contralateral mPFC lead to increased repetitive behaviours and decreased social preferences, thus confirming the

hypothesis of the critical role of connections between cerebellum and PFC in autism (E. Kelly et al. 2020).

In another study, the lack of gabr3 gene, which encodes for the β3 subunit of the $GABA_A$ receptors, has been reported to cause autistic-like behaviour in mice. The $gabr3^{-/-}$ mouse model displays hypoplasia of the cerebellar vermis lobules and behavioural changes, such as decreased social interactions, deficits in exploratory behaviours, and orientation-attention processes (DeLorey et al. 2008).

1.4.2 Prefrontal cortex and autism

The mPFC is connected to medial temporal regions generating a system that modulates emotional processing. Thus, lesions in the mPFC can cause abnormalities in social interactions and responsiveness, lack of social abilities, and altered fear-extinction in rodents (Rinaldi, Perrodin, and Markram 2008). Moreover, in ASD subjects, it is common to observe structural changes and PFC enlargement (Stoner et al. 2014). Specifically, significant changes have been reported in frontal regions in the laminar cytoarchitecture and cortical organization, as well as an increase in cell density, reduction in neuronal size, and decrease in dendritic spine density (Carper and Courchesne 2005). Moreover, autistic subjects exhibit a larger size of the frontal lobe compared to non-autistic ones, and this increase in volume has been positively associated with the typical symptoms of autism (Rogers et al. 2011). This enlargement can reach up to 13%, leading to an increase in cortical minicolumns and a decrease in the distance between them (Abrahams and Geschwind 2010). Furthermore, an increase in the E/I ratio may occur due to an enhanced activity of excitatory neurons or an impaired activity of inhibitory neurons (Polleux and Lauder 2004). Yizhar et al. (2011) propose that E/I dysregulation, which is linked to several autism-related genes responsible for the development, maintenance, and functioning of excitatory synapses, may result in an increased excitability in the main cortical regions typically associated with ASD. This increased excitability may cause seizure episodes in approximately 30% of autistic patients. Neuroimaging techniques have revealed that an underconnectivity exists between the medial/orbital prefrontal and temporoparietal regions during cognitive tasks, including problem-solving (Kana, Libero, and Moore 2011). Further fMRI studies examining various tasks such as language, problem-solving, social cognition, and working memory in individuals

with autism have also demonstrated a functional underconnectivity between different neocortical areas. Autistic adolescents experience difficulties with frontal lobe associated skills due to the failure of frontal circuitry to mature and develop normally (Minshew and Williams 2007). Notably, studies have found a correlation between the degree of alterations in the frontal cortex and abnormalities in the cerebellum (Rogers et al. 2011; Thomas C. Watson, Jones, and Apps 2009). Specifically, the cerebellar regions linked to autism are those connected with frontal areas. The posterior cerebellar hemispheres are associated with communication with the prefrontal cortex, while the lobules VI and VII of the cerebellar vermis are associated with the midfrontal regions in rodents, which correspond to the ACC in humans (S. S. H. Wang, Kloth, and Badura 2014). Additionally, autism may involve the cerebello-thalamo-cortical loops, which are responsible for cognitive, affective, and motor processing. Studies suggest that damage to the corticopontine projections originating from the neocortical layer 5 can cause disruptions in downstream signalling, resulting in autistic symptoms (S. S. H. Wang, Kloth, and Badura 2014). As a result, the prefrontal cortex has been strongly implicated in autism, explaining the impairments in higher functions such as cognition, language, sociability, and emotion that are typical of individuals with autism. However, the changes in prefrontal cortex microcircuitry related to autism have not yet been fully understood (Rinaldi, Perrodin, and Markram 2008).

Mouse models of prefrontal cortex (PFC) dysfunctions have been developed to investigate the molecular impairments associated with ASD (C. Watson, Paxinos, and Puelles 2011). In the mPFC of Mecp2-mutant mice, a model of Rett syndrome, researchers have observed a significant reduction in postsynaptic excitatory currents and a decrease in NMDA/AMPA currents, mainly due to a decrease in excitatory dendritic spines density (Sceniak et al. 2016). Another study also reported a shift in the E/I balance towards inhibition in Mecp2 mutant mice (Dani et al. 2005). In contrast to the previously mentioned evidence, hyper-connectivity and hyper-plasticity have been identified as predominant phenomena in a rat model of autism induced by valproic acid. Specifically, in this rat model, layer V pyramidal cells were found to form more synaptic connections with neighbouring neurons compared to the control group (Rinaldi, Perrodin, and Markram 2008). Similarly, a study of the Fmr1 KO mouse model for mental retardation and autism also demonstrated abnormal connectivity in the prefrontal cortex, with layer V pyramidal cells exhibiting hyper-connectivity with nearby pyramidal

neurons (Testa-Silva et al. 2012). According to Rinaldi, Perrodin, and Markram (2008), the indications suggest that the cause of several deficits associated with autism, such as altered sociability, attentional dysfunction, and repetitive behaviours, may be linked to a hyper-functioning cortex rather than a hypo-active neocortex. The Intense World Theory, which summarizes the most distinctive neurobiological aspects of autism, supports these considerations by demonstrating that hyper-plasticity and hyper-connectivity are the most prevalent and detectable events in the amygdala and neocortex of individuals with autism, as well as potentially in other areas of the brain (Markram and Markram 2010).

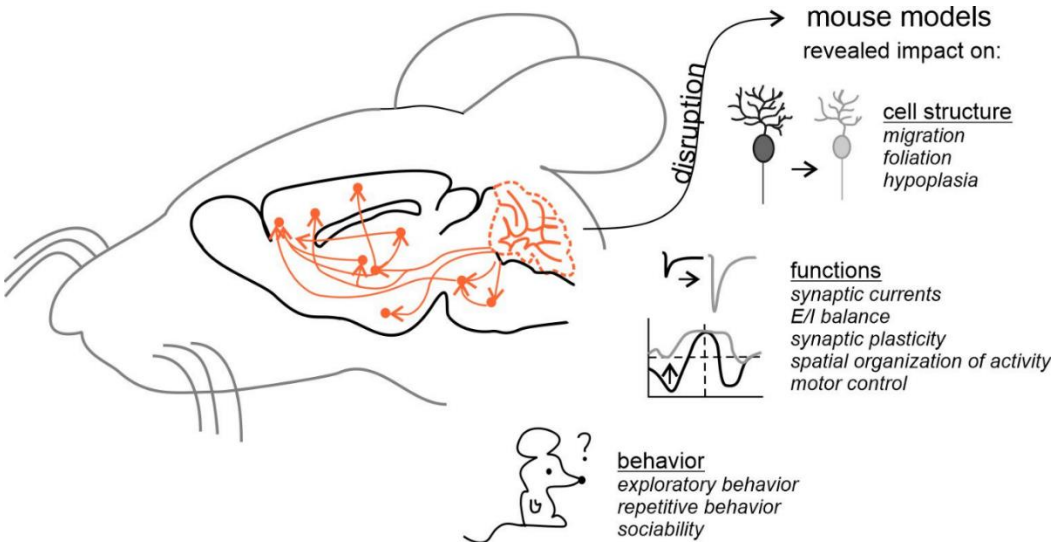

Figure 1.14| Mouse models are an invaluable tool to get insights into the molecular and cellular counterparts of the disease, acting on the specific genetic background generating ASD-like phenotype (L. Mapelli et al. 2022).

1.4.3 IB2 mouse model

One of the most recent mouse models of autism is the IB2 KO mouse. The chromosome 22q terminal region is a well-known locus associated with autism, and specifically, deletions in Chr22q13.3 are linked with both Phelan-McDermid syndrome and some cases of ASD in humans (Delahaye et al. 2009). The majority of patients with Phelan-McDermid syndrome have deletions that extend beyond SHANK3 by at least 0.8 Mb, and as a result, they also exhibit co-deletion of the closely linked MAPKIP2 gene, also known as IB2 or JIP2 (Durand et al. 2007). The gene named Islet Brain-2 (IB2) produces a protein with the same name, which is present in both neurons and pancreatic cells. Its primary function in pancreatic cells is

believed to be the modulation of the JNK signalling pathway (Negri et al. 2000). In the brain, the IB2 protein is mainly found in the postsynaptic densities (PSDs) of the cerebral and cerebellar cortices and, in particular, a high concentration of this protein has been found in the PSDs of cerebellar glomeruli (Giza et al. 2010). The human MAPKIP2 gene has an ortholog in mice located in chromosome 15 called Mapk8ip2 and led researchers to studying mice that lacked the IB2 gene (Giza et al. 2010). Mice lacking IB2 showed increased NMDA receptors-mediated currents, indicating that IB2 plays a crucial role in glutamatergic synaptic neurotransmission. In terms of structure, mice without IB2 had abnormalities in the morphology of their PCs. In terms of behaviour, the lack of IB2 mostly resulted in reduced exploration of new environments and worsened motor, social, and cognitive functions, therefore showing autistic-like phenotype (Giza et al. 2010). The anatomical, functional, and behavioural changes observed in IB2-deficient mice, combined with the fact that the orthologous gene is deleted in most human cases of Phelan-McDermid syndrome and some cases of ASD, make these mice a promising new model for studying autism (Soda et al. 2019). As the cerebellum has been increasingly recognized as a key factor in the development of autism, and the IB2 protein is found in high concentrations in the PSDs of granular layer glomeruli, researchers have started to investigate molecular changes in the cerebellar cortex using the IB2 KO mouse model (Giza et al. 2010). Specifically, the cerebellar granular layer, which represent the input stage of cerebellar cortical processing, was studied in this mutant mouse. The findings showed an abnormal increase in granule cells intrinsic excitability and NMDA receptor-mediated currents, leading to an increase in the E/I ratio. Increased LTP has been also reported. Additionally, changes in the centre-surround organization of the granular layer have been identified, characterized by an enhanced excitation core and reduced inhibition in the surround (Soda et al. 2019).

All this evidence supports the IB2 KO mouse as a suitable model for studying molecular changes in the cerebellum related to autism. However, as the PFC plays a significant role in the development of ASD and has strong connections with the cerebellar cortex, it is important to also investigate the PFC, and its indirect inputs from the cerebellum, using this mouse model. Such investigations could provide valuable insights into the molecular alterations underlying ASD in the brain and should therefore be considered an important avenue of research.

Chapter 2

MATERIALS AND METHODS

Electrophysiological recordings were performed on 30-40 days old mice (either C57BL/6 or IB2 WT and KO) of either sex. During the housing period the animals followed a 12-hours day-night cycle, food and water were always available. Animal maintenance and experimental procedures were performed according to the international guidelines of the European Union Directive 2010/63/EU on the ethical use of animals and were approved by the local ethical committee of the University of Pavia and by the Italian Ministry of Health (authorization n. 638/2017-PR). All experiments were performed on head fixed urethane anesthetized mice. The comparison between neuronal activity of male and female did not show any statistical difference meaning that the oestrus cycle did not affect the data shown in this thesis.

2.1 Animal preparation

The mice used for the experimental procedures were anesthetized with intraperitoneal injection of urethane. After the first injection (initial dose: 1.3 g / kg urethane dissolved in 0.9% NaCl solution; Sigma Aldrich), 3-4 booster injections (10% of the injection dose) were given every 30 minutes to achieve a deep state of anaesthesia in the mice. The level of anaesthesia was monitored by testing the absence of spontaneous facial whisking and the paw retraction reflex after pinching. The choice of urethane was determined by the minimal effects it causes on the main neurotransmission systems: 10% decrease in N-methyl-D-aspartate receptor (NMDAR)-mediated current, 18% decrease in α-amino-3-hydroxy-5-methyl-4-isoxazol-propionic receptor (AMPAR)-mediated current, 23% increase in γ-aminobutyric acid (GABA)-mediated current. The mouse was then positioned on a stereotaxic table covered with a heating plate (HP-1M: RTD/157, Physitemp Instruments Inc, Clifton, NJ, USA) and a feedback temperature controller connected to a rectal probe allowed to maintain body temperature at around 36°C (TCAT-2LV controller, Physitemp Instruments Inc, Clifton, NJ, USA). After reduction of cutaneous reflexes by subcutaneous application of lidocaine (0.2ml; Astrazeneca), skin and muscles were removed to expose the skull. The head was fixed over the Bregma to a metal bar connected to a custom-built stereotaxic table. Two craniotomies were performed, one at the level of the cerebellum, to gain access to the DN,

the other to expose the mPFC in order to position the recording electrodes (from Bregma: DN: -5.8 AP, +2.25 ML, +2.35 DV; PrL: +2.8 AP, 0.25 ML, +0.6 DV).

2.2 Extracellular recordings

Extracellular electrodes can detect action potentials produced by currents flowing in the extracellular space of an active neuron. At the resting state, the neuronal membrane potential (the difference between the intracellular and extracellular space) is usually around -70 mV. Thanks to the volume conductor theory (Heinricher 2004; Lorente de No 1947; Rall 1962)it is possible to model the extracellular current flowing around the axon of an active neuron. The easiest case is to visualize the axon surrounded by an extracellular saline bath, known as "volume conductor". At the axon resting state, no current flows and the membrane potential is uniform along the entirety of its length (Fig. 2.1A). When an action potential is generated in the initial segment of the axon, that spot of the membrane is depolarized, leading to an inward current flow, called "sink". Regions near or distant to the sink will serve as "source" of the current for the active region (Fig. 2.1B). An electrode near the sink will record a negative potential; on the other hand, an electrode near the source will record a positive potential (with respect to a distant indifferent electrode).

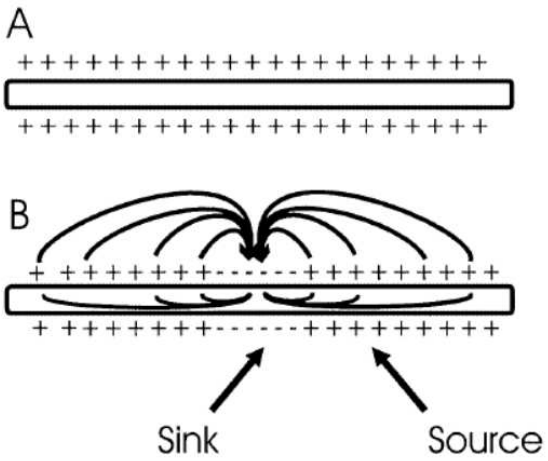

Figure 2.1| Volume conductor theory. (A) At the axon resting state, the membrane potential is uniform and there's no current flow. **(B)** When a segment of the membrane is depolarized current will start flowing (Heinricher 2004).

According to the model of sink and source, when an electrode is near an axon conducting an action potential it will record a triphasic signal composed of a small positive flection, which represent the positive potential of the membrane not affected by the depolarization, followed by a prominent negative deflection, reflecting the action potential that reaches the membrane under the electrode, and finally another small positive flection meaning that the action potential has passed along the membrane, which acts again as a source. The two positive flections are smaller than the negative one since distal regions to the origin site of the action potential have lower density current (Heinricher 2004) (Fig. 2.2).

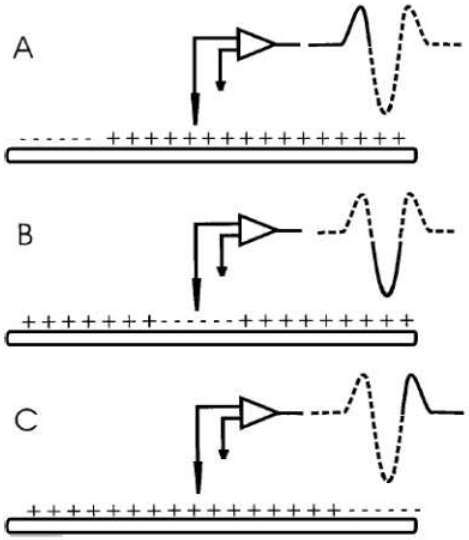

Figure 2.2| Example of a triphasic extracellular signal recorded by an electrode near the axon propagating an action potential, following the rules of source and sink based on the volume conductor theory (Heinricher 2004).

Interestingly, intracellular and extracellular potentials simultaneously recorded during antidromic activation of a motoneuron in the ventral horn of a cat revealed that the negative deflection of the extracellular spike corresponds to the intracellular depolarization, whereas the last extracellular positive flection corresponds to the intracellular repolarization phase (Heinricher 2004) (Fig. 2.3).

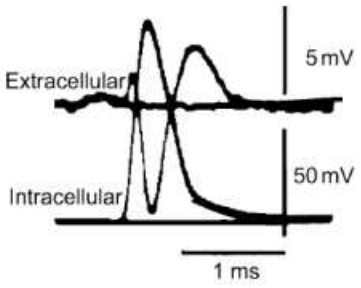

Figure 2.3| Intracellular and extracellular potential recorded simultaneously during antidromic activation of a motoneuron in the ventral horn of the cat. The negative extracellular deflection coincides with the intracellular depolarization, whilst the positive extracellular deflection coincides with the intracellular repolarization phase (Heinricher 2004).

Moreover, spikes can be generated at the level of soma or dendrites. In both cases the model predicts a biphasic signal in which the initial negative component is followed by a positive phase (Fig. 2.4). Nevertheless, in real conditions the geometry of the dendrites and the distribution of the conductance among the membrane changes between neurons. Also, the position of the electrode with respect to the cell influence the recorded signal, complicating the picture of the simplified model based on the volume conductor theory.

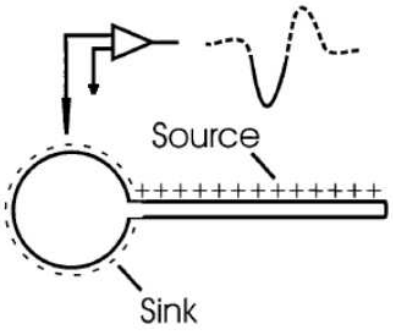

Figure 2.4| Action potential generated at the soma. The sink corresponds to the initial negative component which is followed by the late positive phase corresponding to the source (Heinricher 2004).

In *in vivo* extracellular recordings, it is possible to derive the extracellular spikes generated by currents that flow through the neuronal membrane into the extracellular space. Both single units (SU) and population potentials (Local field potentials, LFP) can be derived, to study neuronal physiology and connectivity in a functional context. Neurons are known to use two

different strategies to decode information, the first is called “rate coding” and uses the firing rate, the second is the “time coding”, which considers the temporal latency of individual spikes.

However, this technique has some limitation. Indeed, extracellular recordings are not informative of both neuronal intrinsic electrophysiological properties and intracellular events that can occur during neuronal activity.

2.3 In vivo extracellular recordings from PrL in mice.

Extracellular recordings can be performed with different types of electrodes, depending on experimental needs and to ensure a good signal-to-noise ratio. In this work, we used quartz-coated platinum/tungsten fibre microelectrodes (1-5MΩ; Thomas Recording, GmbH, Germany) mounted in a 16-channel multi-electrode array (MEA) system (system Eckhorn microdrive, Thomas Recording GmbH, Germany; Fig. 2.5).

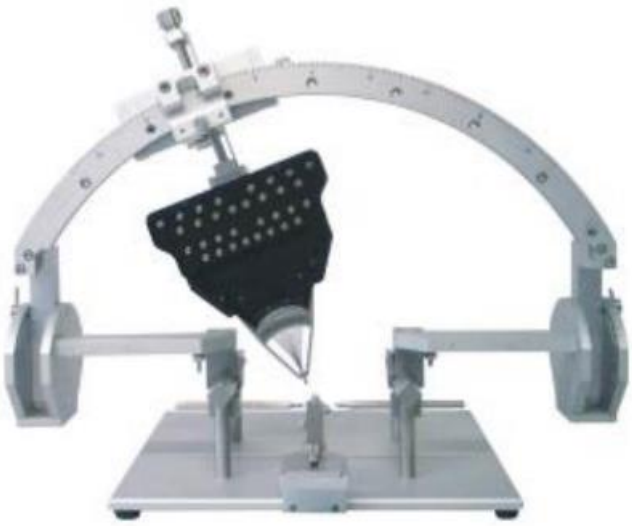

Figure 2.5| Eckhorn Matrix. Multi-electrode array system mounting up to 16 independent electrodes in a matrix 4x4 with inter-electrode distance of 100 µm.

Microelectrodes were placed in a 4x4 matrix with inter-electrode distance of 100 µm, allowing the independent and simultaneous insertion of each of the 16 electrodes into the exposed brain surface.

The electrophysiological detection and acquisition of the signals were performed using OpenEx software (Tucker-Davis Technologies, Alachua, FL, USA), then digitalized at 25 kHz using a band-pass filter, and amplified and stored with a RZ5D processor multi-channel workstation (Tucker-Davis Technologies, Alachua, FL, USA).

Single unit recordings were obtained from the PrL region of mPFC of head restrained urethane anesthetized mice. The activity of the single units was recorded during electrical stimulation of the DN. Spontaneous activity of PrL neurons was recorded for about 5 minutes, then electrical stimulation of DN (21 pulses, 100 Hz, 100 µA) was performed every 5 seconds using a co-axial platinum bipolar tungsten electrode, to evoke neuronal responses into the PrL area. Then 4 subsets of experiments were performed:

1. Superfusion of GABA-A receptor antagonist (SR-95531) onto the PrL surface.
2. Superfusion of NMDA and AMPA receptor antagonists (NBQX, D-APV and 7Cl-kynurenate) onto the PrL surface.
3. Co-superfusion of D1-like and D2-like receptor antagonists (SCH23390 hydrochloride, selective D1- like antagonist; (S)-(-)-Sulpiride, selective D2-like antagonist) onto the PrL surface.
4. Subsequent superfusion of D1/D2-like receptor antagonist followed by GABA-A receptor antagonist onto the PrL surface.

In this condition, 5 minutes recording of spontaneous activity was followed by DN electrical stimulation, delivered every 5 seconds for 20 minutes as control period. The same stimulation protocol was delivered after drug perfusion. All drugs were applied using a micropipette after the control period and maintained through the rest of the recording (30 minutes).

2.4 Histological confirmation

Histological analysis was performed to confirm the location of the electrodes at the level of DN and PrL. At the end of each experiment, electrical lesions were made by applying a 20 µA-20s current pulse through the recording electrode connected to a stimulus isolator and a stimulation unit. After the electrical lesions, a transcardiac perfusion with Phosphate-buffered saline (PBS) followed by 4% paraformaldehyde (Sigma Aldrich) was performed. The removed fixated brain was then dehydrated using a 30% sucrose solution in PBS, embedded in OCT (Cryostat embedding medium, Killik, Bio-Optica) and stored at -80°C.

Brains were cut with a cryostat to obtain 20 µm thick sections that were stained with toluidine blue. Finally histological confirmation of both registration (PrL) and stimulation (DN) sites was obtained by microscopic observation of the stained sections.

2.5 Data analysis

Each recording was analysed offline using SpikeTrain (Neurasmus B.V., Rotterdam the Netherlands) running under MATLAB environment (Mathworks, MA, USA), and Excel. The units recorded from each electrode were sorted to isolate the spikes from background noise or stimulus artifacts. The spike detection procedure consisted in manually positioning a threshold, in order to detect the events and assign a marker. Then, Peri-Stimulus Time Histograms (PSTHs) were constructed using 100 and 20 ms bin widths. The responses of PrL units to DN stimulation were analysed on 100 ms bin width PSTHs, while 20 ms bin width PSTHs were used to analyse the duration and latency of the response. To study the changes of PrL neurons firing frequency induced by DN stimulation, the spontaneous firing rate of each unit was compared to that measured during the stimulation period. A change in bin amplitude (i.e., firing frequency) in the PSTH after the stimulus was considered statistically significant when it exceeded once the value of the mean standard deviation of pre-stimulus bin amplitudes. To measure the regularity of firing, the coefficient of variation of the inter-spike interval (CV2) was calculated

Statistical comparisons were carried out using paired or unpaired Student's *t-test*. All data in the text are reported as mean ± SEM (standard error of the mean). Data were fitted using routines written in OriginPro8 (OriginLac co., MA, USA).

Chapter 3

AIM OF THE THESIS

We conducted a study to explore the potential contribution of the cerebellum to neocortical processing, building on existing evidence demonstrating the interconnection between the cerebellum and cerebral associative areas of the brain, including the mPFC. A comprehensive tractographic reconstruction of human cerebellar projections, which originate from the DCN and pass through the superior cerebellar peduncle, demonstrated a strong cerebello-prefrontal cortex connection (Palesi et al. 2015). This finding was supported by *in vivo* electrophysiological studies in rodents, which also reported a bidirectional functional connection between these brain regions (Thomas C. Watson et al. 2014; Thomas C. Watson, Jones, and Apps 2009). In addition, clinical studies have provided support for the hypothesis of a cerebellar role in cognitive functions, as cerebellar abnormalities have been linked to various cognitive dysfunctions.

Despite the increasing attention towards the cerebello-prefrontal cortex connections, however, most of the recent investigations still overlook the potential impact of the cerebellum on the functioning of the mPFC (Laubach et al. 2018). To this end, we characterized single unit firing changes in mPFC neurons of the prelimbic subdivision (PrL) following electrical stimulation of the contralateral dentate nucleus, both in healthy mice (C57BL/6) and in a pathological model of ASD (IB2 WT and KO mice).

As already mentioned in chapter 1.3, the cerebellum is connected to the mPFC via a dopaminergic pathway passing through the VTA, and a glutamatergic pathway passing through the thalamus (Mittleman et al. 2008). We attempted at discriminating cerebellar modulation of PrL activity through these two pathways using pharmacological approaches, and investigated whether and how specific neuromodulators or neurotransmitters affect PrL neurons responses to cerebellar stimulation. Specifically, we evaluated the GABAergic, dopaminergic, and glutamatergic contribution using specific antagonists perfused on the PrL surface whilst stimulating the DN.

This work could open new perspectives on cerebellar contribution to cognitive function and dysfunction, highlighting how the impact of the cerebellum over the correct functioning of the cerebral cortex might be more relevant than previously thought.

Chapter 4

Dopaminergic Modulation of Prefrontal Cortex Inhibition

Danila Di Domenico and Lisa Mapelli

Review. Biomedicines, 11(5), 1276; doi: 10.3390/biomedicines11051276. April 2023

biomedicines

MDPI

Review

Dopaminergic Modulation of Prefrontal Cortex Inhibition

Danila Di Domenico and Lisa Mapelli *

Department of Brain and Behavioral Sciences, University of Pavia, 27100 Pavia, Italy
* Correspondence: lisa.mapelli@unipv.it

Abstract: The prefrontal cortex is the highest stage of integration in the mammalian brain. Its functions vary greatly, from working memory to decision-making, and are primarily related to higher cognitive functions. This explains the considerable effort devoted to investigating this area, revealing the complex molecular, cellular, and network organization, and the essential role of various regulatory controls. In particular, the dopaminergic modulation and the impact of local interneurons activity are critical for prefrontal cortex functioning, controlling the excitatory/inhibitory balance and the overall network processing. Though often studied separately, the dopaminergic and GABAergic systems are deeply intertwined in influencing prefrontal network processing. This mini review will focus on the dopaminergic modulation of GABAergic inhibition, which plays a significant role in shaping prefrontal cortex activity.

Keywords: prefrontal cortex; dopaminergic system; GABAergic system

Citation: Di Domenico, D.; Mapelli, L. Dopaminergic Modulation of Prefrontal Cortex Inhibition. *Biomedicines* **2023**, *11*, 1276. https://doi.org/10.3390/biomedicines11051276

Academic Editor: Marc Ekker

Received: 31 March 2023
Revised: 21 April 2023
Accepted: 23 April 2023
Published: 25 April 2023

1. The Prefrontal Cortex

The prefrontal cortex (PFC) is thought to be the highest association area in the mammalian cortex and is required for proper executive control. Task flexibility and planning [1], selective attention, attentional set-shifting, rule learning, strategy switching, and goal-directed behavior [2–4] are just some of the many PFC functions. This considered, it is not surprising that PFC alterations have been associated with a variety of psychiatric conditions. For example, several investigations reported PFC-related impaired working memory [5–8] and altered network oscillations [9,10] in schizophrenia. Though rodent PFC is less complex than that of primates, it exerts similar functions in the executive domain [11]. For this reason, the rodent represents a valuable model to investigate how PFC functions are determined at the molecular, cellular, and network levels. However, investigations in rodents are complicated by the lack of a univocal and unambiguous nomenclature of PFC subdivisions. Due to its recent evolution and inter-species variability, it is challenging to identify proper structural and functional criteria to define PFC regions [12,13]. This has been the subject of many studies aiming at characterizing differences and similarities of mammalian PFC [14]. Ref [15] introduced a hodological criterium based on the assumption that the mediodorsal thalamic nucleus (MD) is the primary site of projections toward the PFC. Therefore, according to this definition, the mammalian PFC could be identified based on the connectivity with the MD. Following this perspective, the effective existence in rats of two prefrontal cortex areas receiving projections from the MD, indicated as medial and orbitofrontal, was demonstrated [16]. Clearly, this definition bears some limitations. Indeed, other criteria were then adopted. For example, other researchers proposed a cytoarchitectural criterion, though this method was deemed valid only for closely related species [12]. To date, the best way to define PFC parcellation is proposed to be a combination of four criteria: function, architecture, connectivity, and topography [17,18]. In particular, the relevance of the connectivity aspect grew over time. Recent works have described the organization of cortical interconnectivity into modules along the whole brain [18,19] and identified a prefrontal cortical module. The areas within the prefrontal module show dense interconnections [20,21] and are believed to be devoted to similar functions [22].

The regions recognized as a component of the prefrontal module are the prelimbic area, the infralimbic area, the anterior cingulate area, the frontal pole cerebral cortex, and the orbital areas. Another widely used distinction, mainly based on connectivity mapping including thalamocortical, corticothalamic, corticostriatal, and corticocortical projections, recognizes three broad PFC subdivisions: the dorsomedial PFC (dmPFC), ventromedial PFC (vmPFC), and ventrolateral PFC (vlPFC). Considering the complex scenario of rodent PFC nomenclature and the absence of a standard reference for the different studies available in the literature, it is not surprising that many studies focusing on the PFC report vague indications of the subregion actually subjected to analysis. In particular, most investigations on the highest-level cognitive functioning in rodents target the so-called medial PFC (mPFC), comprising the infralimbic, prelimbic, and anterior cingulate areas [2,13]. It is worth specifying that there is no direct anatomical equivalence between human and rodent PFC. However, the rodent mPFC is anatomically located in correspondence with the anterior cingulate cortex (ACC) in humans (see [13] for a detailed review of the comparison between rodent and human PFC). Here, we will mainly refer to rodent reports on the mPFC, which is the most commonly addressed PFC area. The cytoarchitecture and the connectivity patterns are similar in rodents and humans, with the significant difference represented by the lack of the granular layer (layer IV) in rodent PFC. In both cases, the PFC is mainly composed of pyramidal neurons (PN, 80–90%) and inhibitory interneurons (IN, 10–20%) [23]. The main excitatory output is provided by the PNs, which are strongly interconnected to form a local network that projects to other cortical and subcortical areas. PN activity is modulated by a strong network of GABAergic INs [24,25], which proved to be essential for controlling PN firing and generating neuronal network oscillations [26–28]. The interplay between PNs and INs modulates PFC activity and is crucial to maintain proper cognitive functions.

2. Dopamine Receptors in the PFC

Dopamine (DA) is released in the mPFC by projections originating from the midbrain nuclei of the ventral tegmental area (VTA) and substantia nigra pars compacta [29,30]. Once released, DA interacts with five different receptors subtypes (D1, D2, D3, D4, D5) subdivided into two families: D1-like receptors comprising D1 and D5, and D2-like receptors comprising D2, D3, and D4 [29,31,32]. Receptors belonging to the D1-like family are more abundant than those of the D2-like family and are expressed in all PFC layers. On the other hand, receptors of the D2-like family are primarily expressed in deeper layers (mainly layer V) [33], and their affinity is 10–100 times higher than that of D1-like receptors [34]. Both DA receptor families are expressed on pyramidal and non-pyramidal neurons, thus modulating excitation and inhibition [29,33]. Finally, these two receptor classes differ in the intracellular signaling pathway mediating their effects. Since DA receptors are G-protein coupled receptors (GPCRs), they all activate heteromeric G-proteins, but the second messenger and the effector proteins activated are usually different for different receptors and, in most cases, mediate opposite responses.

In particular, D1-like receptors activation is coupled with the G-proteins $G\alpha_s$ and $G\alpha_{olf}$ which, in turn, are associated with adenylyl cyclase (AC) that, once activated, increases the level of cyclic adenosine monophosphate (cAMP) leading to the activation of protein kinase A (PKA). PKA modulates most D1-like functions by phosphorylating many substrates including voltage-gated K^+, Na^+, and Ca^{2+} channels, GABA receptors, and NMDA receptors [32,35]. One of the main PKA targets is the DA and cAMP-regulated phosphoprotein DARPP-32, which is crucial in regulating downstream signaling pathways. When phosphorylated, DARPP-32 inhibits the protein phosphatase 1 (PP1) that opposes PKA action, eventually amplifying PKA signaling. On the other hand, the activation of D2-like receptors leads to the opposite effect. When activated, these receptors couple with $G\alpha_i$ and $G\alpha_o$ that inhibit the activation of AC, thus limiting PKA signaling. Moreover, the activation of D2-like receptors determines the activation of the calmodulin-dependent protein phosphatase (PP2B), which turns DARPP-32 into a strong inhibitor of PKA signaling [32]. Thus,

DARPP-32 can bidirectionally modulate PKA activity. Besides their regulation through PKA pathways, ion channels can also be modulated directly via binding the Gβγ subunit or indirectly via activation of the phospholipase C (PLC) by both D1-like and D2-like receptors (Figure 1). The latter is most common for modulating Ca^{2+} conductance, determining a decrease in $Ca_V2.2$ (N-type) and Ca_V1 (L-type) currents. PLC can also be activated through coupling with $G\alpha_q$, though limited to cells expressing D5 and D1/D2 heterodimers [36,37]. Lastly, D1-like and D2-like receptors can modulate NMDA and GABA receptors through direct protein–protein interactions or PKA/IP3 signaling [35]. The mechanism by which D2-like receptors, particularly D4, regulate GABA receptors involves a pathway comprising the dephosphorylation of cofilin (an actin depolymerizing factor) via PP1 activation. This leads to the loss of actin stability, with a consequent interruption of myosin motor-mediated transport of GABA receptor-containing vesicles in the membrane, resulting in a reduced GABA receptor-mediated current [38].

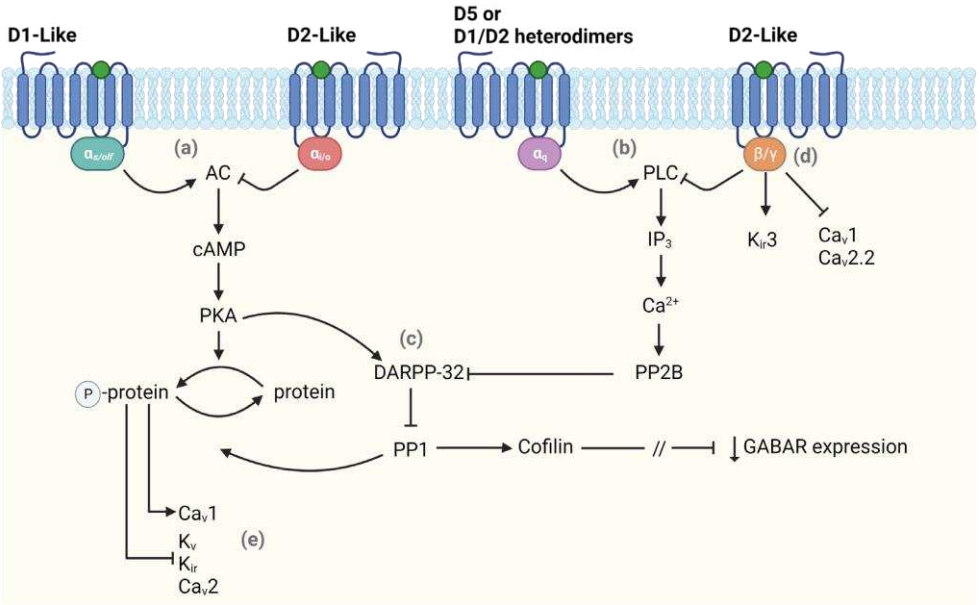

Figure 1. Main intracellular pathways activated by dopamine receptors. The scheme shows different pathways in which dopamine (DA) affects the modulation of intracellular signaling. DA can regulate the activation state of (**a**) adenylyl cyclase (AC) or (**b**) phospholipase C (PLC) binding either D1-like or D2-like receptors. (**c**) Both pathways lead to a modulation (either positive or negative) of DARPP-32 which regulates the expression of GABA receptors. DA also affects neuronal excitability by modulating voltage-dependent ion channels via activation of (**d**) β/γ subunit or (**e**) AC pathway. The forward and stop arrows indicate activation or inhibition of the next element in the chain, respectively. This figure was created with BioRender.com.

3. Dopamine Modulation of GABAergic Inhibition

3.1. On Pyramidal Neurons (PN)

As nicely reviewed by [29], the net effect of DA release onto the PFC also depends on cell type, synaptic properties, and interactions with other neurotransmitters. One of the critical DA roles in the PFC is the modulation of the GABAergic system. This modulation contributes to setting the proper excitation/inhibition (E/I) balance in the PFC, which requires fine-tuning to ensure correct network activity. Indeed, the E/I ratio is disrupted in a broad range of psychiatric disorders [39–41]. Many studies focused on the role of D4 receptors in preserving the correct E/I balance. D4 receptors are enriched in the PFC and are usually expressed in dendritic processes [42–44], while D1 receptors are most prominent at PN dendritic spines [45]. In particular, D4 receptors are mainly expressed nearby $GABA_A$ receptors in PFC PNs [46]. Experimental evidence showed that D2/D4 receptor agonists decrease the inhibitory post-synaptic currents (IPSCs) of layer V PN in rodent PFC, while a

D1 receptor agonist increases IPSCs amplitude in the same neurons [46–48]. When D1- and D2-like receptors activation combines, an initial downregulation of the IPSCs mediated by D2-like receptors is followed by a D1-like receptors-dependent IPSCs increase. This suggests the biphasic nature of DA modulation of GABAergic responses in PFC PNs [29,47].

DA is reported to regulate inhibition through different intracellular mechanisms. In particular, high DA concentrations increase spontaneous inhibitory postsynaptic potentials (sIPSP) in PFC layer II/III [49] and layer V-VI PNs [50], revealing DA-mediated enhancement of GABA release. On the other hand, DA can depress evoked IPSP (eIPSP) in layer V-VI PNs [47,51,52]. This evidence shows that DA can modulate spontaneous and evoked IPSPs affecting GABA release mechanisms, hence regulating the presynaptic machinery [29]. This effect was also described in IN-PN pair recordings [53]. A possible explanation of the different DA impact on spontaneous and evoked IPSCs is proposed by [29]. The authors highlighted that the eIPSCs derive from activating a specific fiber through electrical stimulation, while sIPSCs derive from multiple diverse inputs. Therefore, the effect of DA on IPSCs may depend on the neuronal type generating the IPSC and the different neurons originating the GABAergic terminals impinging on that same neuron [29]. The heterogeneity of DA modulation reported in different studies might also depend on the recording sites. Indeed, D1- and D2-like receptors have different expression patterns: while D1-like receptors mRNA are also expressed in superficial layers, D2-like receptors are restricted to deeper layers such as layer V [33] (Figure 2).

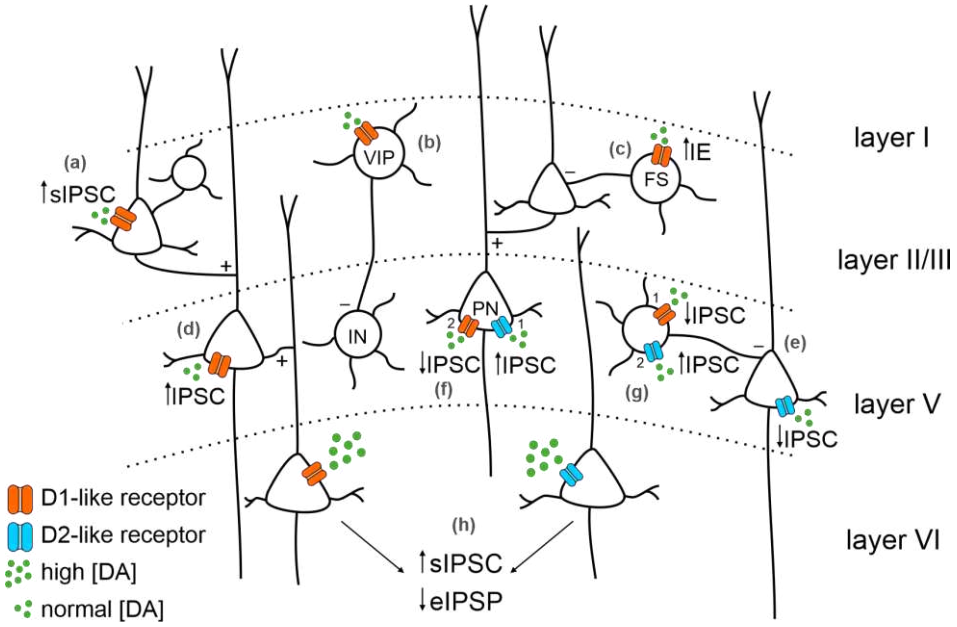

Figure 2. Dopaminergic receptors distribution in the PFC and main effects on inhibition. The distribution of dopamine (DA) receptors among PFC layers and their expression on different neuronal types can variably affect inhibition. In layer II/III, DA (green dots) binding D1-like receptors (orange) on pyramidal neurons (PNs, (**a**)) increases spontaneous IPSC (sIPSC); (**b**) on vasoactive intestinal peptide (VIP) neurons, it starts internal loops inhibiting deeper layers' inhibitory interneurons (INs); and (**c**) on fast-spiking interneurons (FS) increases intrinsic excitability. DA binding D1-like receptor expressed in layer V PNs (**d**) increases the IPSC. DA binding D2-like receptors (blue) expressed in layer V PNs (**e**) decreases the IPSC. Expression of both D1-like and D2-like receptors in layer V PNs (**f**) increases the IPSC mediated by D2-like receptor activation (1) followed by a IPSC decrease mediated by D1-like receptor activation (2). On INs (**g**), the decrease in the IPSC mediated by D1-like receptors (1) is followed by an increased IPSC mediated by D2-like receptors (2). (**h**) In layer VI PNs, the activation of DA receptors by high DA concentration leads to an increase in sIPSC and a decrease in evoked IPSC (eIPSC).

3.2. On Inhibitory Interneurons (IN)

DA receptors are expressed in a wide array of GABAergic interneurons and, therefore, DA release onto the PFC affects IN activity, too [33,54,55]. DA is known to induce an increase in intrinsic excitability favoring depolarization in fast-spiking interneurons (FS) via a D1-like receptor-dependent mechanism [56,57]. Moreover, the effect of D1-like and D2-like receptors on PFC GABAergic INs may differ on a temporal scale. The activation of D1-like receptors induces both a depolarization and an increase in the neuronal excitability of FS. Different mechanisms mediate these two effects. The DA-induced depolarization lasts less than the increased excitability, meaning that DA can act through the same receptors to modulate different ionic currents at different time scales [56]. Interestingly, the activation of D2-like receptors at the peak of D1-like mediated IPSC determines a decrease in the IPSC amplitude [47,56]. Consistent with the biphasic hypothesis of DA modulation of the GABAergic system, D2-like receptors mediate a reduction in inhibition, and D1-like receptors mediate an increase in inhibition on PFC PNs, influencing IN activity (Figure 2). Lastly, D1-like receptors in superficial layers are often associated with vasoactive intestinal peptide (VIP) GABAergic INs and inhibit deeper INs via internal loops and interactions [58]. This supports the D1-like receptor role in determining circuit disinhibition, which is fundamental to appropriately modulating the PFC range of activity.

3.3. Evidence In Vivo

Several studies showed that DA exerts a predominantly inhibitory effect on PFC PN in vivo, primarily suppressing spontaneous firing [59–61]. Importantly, microdialysis data in vivo revealed a tonic level of DA in the PFC [62,63]. Most studies reported here were performed on anesthetized animals, where little VTA activity is presumably present at rest. Nevertheless, the stimulation of fiber bundles at the medial forebrain, or direct VTA stimulation, effectively increased DA levels in the PFC. It should also be considered that the absence of not experimentally evoked DA release is an advantage in characterizing transient DA effects on PFC neurons. For these reasons, these studies are considered suitable to address the consequences of DA release on the PFC in vivo. Indeed, VTA stimulation induces a fast EPSP-IPSP sequence in PFC PNs, with the IPSP consistent with $GABA_A$ receptors activation [60]. Interestingly, the inhibitory component is eliminated not only by $GABA_A$ receptor antagonists [64] but also by D2-like receptor antagonists, which tonically inhibit neuronal excitability [65–67]. When the D2-like receptor tone is abolished, the entire network physiology changes: neurons increase their firing, and the inhibition produced by VTA stimulation is occluded [29]. Overall, these studies show that DA released from dopaminergic terminals in the PFC, as well as exogenous DA, modulates spontaneous firing in vivo through complex mechanisms depending on the endogenous DA tone, the amount of DA released, and the activated receptor subtype. This effect was also confirmed by a computational model in which increasing DA concentrations elicited the facilitation of FS activity, with consequent suppression of pyramidal neurons firing. Moreover, enhancing basal DA levels rescues the initial condition, through the downregulation of the GABAergic tone, with consequent hyperactivity of PN firing [68]. Interestingly, computational models primarily based on in vivo studies have proposed a dual mechanism by which D1-like receptors can modulate working memory. First, the spontaneous activity of PN is decreased by upregulating inhibitory GABA currents; then, high-activity states are induced by upregulating excitatory NMDA currents [69,70]. This effect is believed to be mediated by D1-like receptors, which might induce inhibition by amplifying IPSCs in PNs [71], or an excitatory effect by enhancing NMDA receptor-mediated responses [72,73]. The same computational model was also used to implement D2-like receptors modulation of PFC activity. It was proposed that D2-like receptors activation decreases inhibitory currents in PNs while increasing IN excitability to maintain E/I balance [74].

Taken together, these findings provide evidence for a delicate homeostatic interplay between dopaminergic and GABAergic systems necessary to maintain PFC network stability and output selectivity.

3.4. Comments on PFC Regional Specificity

As pointed out in the first section, the PFC can be subdivided into several regions. It might then be of interest to consider whether a regional specificity has been observed in dopaminergic and GABAergic interplay. However, the intricate PFC subregions identification and nomenclature complicate the picture. Considering the literature reviewed here and mentioning to whatever extent the interaction between dopaminergic and GABAergic systems, it is not possible to infer a region specificity. Indeed, out of 24 studies, 14 reported to be generally on the mPFC (10) or PFC (4), 8 addressed the prelimbic or prelimbic/infralimbic region (without discrimination), and 2 specified the anterior cingulate cortex and the shoulder region or Fr2 region of the frontal cortex (without discrimination). Therefore, it is not possible to extrapolate differences in dopaminergic–GABAergic interaction among the mPFC subdivisions. Indeed, the prelimbic region seems to be the preferred target of most studies.

However, searching for a regional distinction might be pointless. Accumulating evidence suggests that current subdivisions might not reflect actual PFC functioning segregation. Recently, besides the cytoarchitecture and connectivity distinction criteria, the PFC gene expression profile has also been reported [75]. Interestingly, this study did not identify distinct subregions, but the genetic profile was, in fact, common to the multiple regions composing the PFC. Therefore, the PFC subdivisions based on connectivity or cytoarchitecture criteria, already not matching one another, are not confirmed by gene expression. This is of particular interest since it highlights a crucial aspect when considering PFC functions. The scenario that is emerging suggests that assigning different functions to the different PFC subdivisions is indeed deeply misleading. Based on connectivity alone, some distinctions seem to emerge, at least among the three main subdivisions (dmPFC, vmPFC, and vlPFC), which show different densities of specific connections. Nevertheless, their connectivity is not entirely differentiated, and the connections are shared but differ quantitatively [18]. Further based on this evidence, the dmPFC is often studied for sensorimotor behavior, the vmPFC is often associated with emotions and memory, while the vlPFC, though much less studied than the other two subdivisions, is often correlated to reward-related information and addictive behavior. However, this might reflect the common practice of the researchers rather than actual functional segregation. Several behavioral studies suggested that the perturbation of any PFC subdivision is sufficient to disrupt behavior and the whole cortical activity, independent of the type of task at hand (see [18] for an extensive discussion on this topic). Therefore, despite the different supposed roles of each subdivision, it is most likely that the PFC processes higher cognitive functions as a whole and cannot be assigned to a specific subregion [76].

4. Clinical Relevance

Given the evidence summarized so far, it is not surprising that several PFC-related pathologies involve alterations in both the dopaminergic and GABAergic systems. In the following paragraphs, we will briefly summarize the involvement of the dopaminergic and GABAergic systems in the main pathologies with a prominent PFC component, in particular schizophrenia and autism spectrum disorders.

Schizophrenia is one of the most studied cognitive pathologies, with a renowned involvement of the dopaminergic system, which is responsible for maintaining the proper E/I balance [77]. The “revised dopamine hypothesis” proposes that schizophrenic patients have hyperactive dopamine transmission in mesolimbic areas and hypoactive dopamine transmission in PFC [78]. The positive symptoms of schizophrenia include hallucinations and delusion due to an augmented dopamine release in subcortical areas, leading to an increase in D2-like receptors activation [79], and are thought to be caused by disrupted

cortical pathways through the nucleus accumbens [80]. On the other hand, negative symptoms, such as anhedonia, lack of motivation, and speech impairments, result from reduced D1-like receptors activation in the PFC [79]. As computational models highlighted, the imbalance between D1-like and D2-like receptor activity might explain the positive and negative symptoms and the cognitive alterations in schizophrenia [81]. Interestingly, besides other players recently found involved (as the glutamatergic system and the NMDA receptors, [82,83]), the GABAergic system has been reported to be altered. In particular, a reduction in GABAergic inhibition is often reported (e.g., a reduced expression of GAD67, GAT1, and $GABA_A$ receptors; a decreased number of inhibitory interneurons; reduced inhibitory currents; [84] for details). The investigations on GABAergic disruption in schizophrenia are complicated since the alterations differ depending on the specific targeted PFC region [85]. In any case, GABAergic signaling alterations will contribute to the E/I balance disruption associated with this disease, both in humans and animal models. Alterations in GABA release have been correlated with impaired gamma oscillations and, as such, to the cognitive symptoms of the disease [86]. Interestingly, the GABAergic system deficit in the PFC has been proposed to result from the altered dopaminergic tone in the striatum in a mouse model with striatal D2 receptors overexpression [87]. Though the idea that the GABAergic and dopaminergic systems influence each other and collaborate in determining the pathological alterations in schizophrenia is not new [88,89], further research on this interaction might reveal critical to disentangle the complex pathophysiology of the disease. This would have a relevant impact from the clinical perspective. Independent of where the primary alteration occurred, a clinical intervention might need to impact both systems to regain a proper balance in PFC network activity. Moreover, a complete view of such a complex pathology will need to integrate the alterations seen in other neurotransmitter systems (such as the glutamatergic one) and the impact on the E/I balance of the glutamate/GABA interplay [77].

Autism spectrum disorders (ASD) are neurodevelopmental disorders characterized by deficits in social cognition, repetitive and stereotyped behavior, and restricted interests. The investigation of the pathophysiology of ASD is complicated by the incredibly heterogeneous genetic and phenotypic profiles that can be found in humans and the several animal models of the disease [90,91]. Nevertheless, the diverse molecular, cellular, and network alterations reported in literature seem to converge on a common outcome characterized by altered E/I balance (in favor of excitation), network hyperexcitability, and hyperresponsivity, often accompanied by altered long-range connectivity [92–94]. The GABAergic system is considered central for ASD research, and its interplay with the glutamatergic one to determine the E/I balance is one of the most studied topics in this field [95]. The most common alteration reported is a decrease inhibition efficiency, ultimately leading to the complex cognitive dysfunctions reported and the comorbidity with anxiety and other disorders [84]. The involvement of the dopaminergic system in ASD is supported by significant evidence in humans and animal models [96] and confirmed by the contribution of alterations in genes related to DA neurotransmission and its modulation [97]. The prefrontal cortex and striatum are considered the most affected brain regions. Given the role of the dopaminergic system in fine-tuning network transmission and signal-to-noise ratio during behavior, alterations in this system are considered causal for the reduced sociability and increased repetitive behavior that characterize ASD phenotype in mice and, most likely, in humans [98,99]. Therefore, ASD physiopathology could be the ideal ground to study the correlation between DA and GABAergic system alterations.

Affective disorders, such as major depression and bipolar disorder, and **anxiety disorders** are commonly associated with altered serotoninergic tone and glutamate/GABA systems imbalance. Nevertheless, many symptoms are considered to rely on dopaminergic miscontrol leading, for example, to a lack of motivation and anhedonia in depression [100,101]. In particular, many forms of depression have been correlated with PFC hyperactivity, and acting on the systems controlling the E/I balance in this region is the primary treatment approach to date [100]. The circuits responsible for the stress response, including the

hippocampus and amygdala, are also involved in the altered PFC-related communication found in these disorders [100,102]. Altered DA signaling is also reported in post-traumatic stress disorder [103]. Moreover, the involvement of the dopaminergic system in pain modulation and **chronic pain** can be considered related to the previous disorders [104,105]. Interestingly, the increased mPFC output observed in neuropathic pain conditions has been correlated with altered VTA-mediated DA control over the prelimbic region in rats, associated with impaired integration of GABAergic inhibition [106].

5. Conclusions

The dopaminergic system modulates the PFC network activity state, finely tuning the signal-to-noise ratio and the E/I balance. These effects are partially exerted influencing the GABAergic system through complex intracellular pathways that modify GABA receptors expression and activity, and modulate GABA release by INs. DA control of the PFC activity state and responsiveness modulates the gain of signal transmission modifying the tonic DA level and regulates the timing of neuronal responses through its complex phasic component. The PFC is one of the most integrative areas in the brain, and the interplay between the dopaminergic and GABAergic systems is one of the critical features that influence input integration by this network and therefore deserves special attention. Further effort should also be devoted to exploring the reciprocal influence of these two systems in PFC-related neuropathologies. More often than not, the alterations in DA and GABAergic systems and their impact on the clinical perspective are studied separately. This is undoubtedly due to the intrinsic difficulty in disentangling the relative contribution of the two systems to the alterations observed and to the limitations of using animal models for addressing cognitive phenotype. Nevertheless, the data summarized in this mini review strongly support the idea that the interplay between these two systems significantly contributes to originate the unbalance seen in pathological models, possibly with a primarily affected system causing the impairment of the other. The recent technological advancements and the application of computational models could boost the research in this field and allow us to address this issue with a renewed effort.

Author Contributions: Conceptualization, L.M.; writing—original draft preparation, D.D.D. and L.M.; writing—review and editing, L.M.; visualization, D.D.D.; supervision, L.M. All authors have read and agreed to the published version of the manuscript.

Funding: This research received no external funding.

Institutional Review Board Statement: Not applicable.

Informed Consent Statement: Not applicable.

Data Availability Statement: No new data were created or analyzed in this study. Data sharing is not applicable to this article.

Conflicts of Interest: The authors declare no conflict of interest.

Abbreviations

AC	adenylyl cyclase
ACC	anterior cingulate cortex
ASD	autism spectrum disorders
cAMP	cyclic adenosine monophosphate
DA	dopamine
DARPP-32	DA and cAMP-regulated phosphoprotein
dmPFC	dorsomedial prefrontal cortex
eIPSP	evoked inhibitory postsynaptic potential
EPSP	excitatory postsynaptic potential
E/I	excitation/inhibition

FS	fast-spiking interneurons
GAD67	glutamate decarboxylase 67
GAT1	GABA transporter type 1
IN	inhibitory interneuron
IP3	inositol triphosphate
IPSP	inhibitory postsynaptic potential
mPFC	medial prefrontal cortex
PFC	prefrontal cortex
PN	pyramidal neuron
VTA	ventral tegmental area
GPCR	G-protein coupled receptor
IPSC	inhibitory post-synaptic current
PKA	protein kinase A
PLC	phospholipase C
PP1	protein phosphatase 1
PP2B	calmodulin-dependent protein phosphatase
sIPSP	spontaneous inhibitory postsynaptic potential
VIP	vasoactive intestinal peptide
vlPFC	ventrolateral prefrontal cortex
vmPFC	ventromedial prefrontal cortex

References

1. Elliott, R. Executive Functions and Their Disorders. *Br. Med. Bull.* **2003**, *65*, 49–59. [CrossRef] [PubMed]
2. Huang, Y.Y.; Simpson, E.; Kellendonk, C.; Kandel, E.R. Genetic Evidence for the Bidirectional Modulation of Synaptic Plasticity in the Prefrontal Cortex by D1 Receptors. *Proc. Natl. Acad. Sci. USA* **2004**, *101*, 3236–3241. [CrossRef] [PubMed]
3. Aron, A.R.; Robbins, T.W.; Poldrack, R.A. Inhibition and the Right Inferior Frontal Cortex. *Trends Cogn. Sci.* **2004**, *8*, 170–177. [CrossRef] [PubMed]
4. Buschman, T.J.; Miller, E.K. Top-down versus bottom-up control of attention in the prefrontal and posterior parietal cortices. *Science* **2007**, *315*, 1860–1862. [CrossRef]
5. Goldman-Rakic, P.S. The Cortical Dopamine System: Role in Memory and Cognition. *Adv. Pharmacol.* **1997**, *42*, 707–711. [CrossRef]
6. Goldman-Rakic, P.S. Cellular Basis of Working Memory. *Neuron* **1995**, *14*, 477–485. [CrossRef]
7. Goldman-Rakic, P.S. The Physiological Approach: Functional Architecture of Working Memory and Disordered Cognition in Schizophrenia. *Biol. Psychiatry* **1999**, *46*, 650–661. [CrossRef]
8. Kesner, R.P.; Churchwell, J.C. An Analysis of Rat Prefrontal Cortex in Mediating Executive Function. *Neurobiol. Learn. Mem.* **2011**, *96*, 417–431. [CrossRef]
9. Arnsten, A.F.T.; Wang, M.J.; Paspalas, C.D. Neuromodulation of Thought: Flexibilities and Vulnerabilities in Prefrontal Cortical Network Synapses. *Neuron* **2012**, *76*, 223–239. [CrossRef]
10. Volk, D.; Lewis, D. GABA Targets for the Treatment of Cognitive Dysfunction in Schizophrenia. *Curr. Neuropharmacol.* **2005**, *3*, 45–62. [CrossRef]
11. Seamans, J.K.; Lapish, C.C.; Durstewitz, D. Comparing the Prefrontal Cortex of Rats and Primates: Insights from Electrophysiology. *Neurotox. Res.* **2008**, *14*, 249–262. [CrossRef] [PubMed]
12. Carlén, M. What Constitutes the Prefrontal Cortex? *Science* **2017**, *358*, 478–482. [CrossRef]
13. Laubach, M.; Amarante, L.M.; Swanson, K.; White, S.R. What, If Anything, Is Rodent Prefrontal Cortex? *eNeuro* **2018**, *5*, ENEURO.0315-18.2018. [CrossRef] [PubMed]
14. Fuster, J.M. The Prefrontal Cortex—An Update: Time Is of the Essence. *Neuron* **2001**, *30*, 319–333. [CrossRef]
15. Rose, J.E.; Woolsey, C.N. The Orbitofrontal Cortex and Its Connections with the Mediodorsal Nucleus in Rabbit, Sheep and Cat. *Res. Publ. Assoc. Res. Nerv. Ment. Dis.* **1948**, *27*, 210–232.
16. Otani, S. (Ed.) *Prefrontal Cortex: From Synaptic Plasticity to Cognition*; Springer Science & Business Media: Berlin/Heidelberg, Germany, 2004.
17. Van Essen, D.C.; Glasser, M.F. Parcellating Cerebral Cortex: How Invasive Animal Studies Inform Noninvasive Mapmaking in Humans. *Neuron* **2018**, *99*, 640–663. [CrossRef] [PubMed]
18. Le Merre, P.; Ährlund-Richter, S.; Carlén, M. The Mouse Prefrontal Cortex: Unity in Diversity. *Neuron* **2021**, *109*, 1925–1944. [CrossRef]

19. Harris, J.A.; Mihalas, S.; Hirokawa, K.E.; Whitesell, J.D.; Choi, H.; Bernard, A.; Bohn, P.; Caldejon, S.; Casal, L.; Cho, A.; et al. Hierarchical Organization of Cortical and Thalamic Connectivity. *Nature* **2019**, *575*, 195–202. [CrossRef]
20. Ercsey-Ravasz, M.; Markov, N.T.; Lamy, C.; VanEssen, D.C.; Knoblauch, K.; Toroczkai, Z.; Kennedy, H. A Predictive Network Model of Cerebral Cortical Connectivity Based on a Distance Rule. *Neuron* **2013**, *80*, 184–197. [CrossRef]
21. Gămănuț, R.; Kennedy, H.; Toroczkai, Z.; Ercsey-Ravasz, M.; Van Essen, D.C.; Knoblauch, K.; Burkhalter, A. The Mouse Cortical Connectome, Characterized by an Ultra-Dense Cortical Graph, Maintains Specificity by Distinct Connectivity Profiles. *Neuron* **2018**, *97*, 698–715.e10. [CrossRef]
22. Bullmore, E.; Sporns, O. Complex Brain Networks: Graph Theoretical Analysis of Structural and Functional Systems. *Nat. Rev. Neurosci.* **2009**, *10*, 186–198. [CrossRef] [PubMed]
23. Riga, D.; Matos, M.R.; Glas, A.; Smit, A.B.; Spijker, S.; Van den Oever, M.C. Optogenetic Dissection of Medial Prefrontal Cortex Circuitry. *Front. Syst. Neurosci.* **2014**, *8*, 230. [CrossRef] [PubMed]
24. Palmer, L.; Murayama, M.; Larkum, M. Inhibitory Regulation of Dendritic Activity in Vivo. *Front. Neural Circuits* **2012**, *6*, 26. [CrossRef]
25. Anastasiades, P.G.; Carter, A.G. Circuit Organization of the Rodent Medial Prefrontal Cortex. *Trends Neurosci.* **2021**, *44*, 550–563. [CrossRef] [PubMed]
26. Whittington, M.A.; Traub, R.D. Interneuron Diversity Series: Inhibitory Interneurons and Network Oscillations in Vitro. *Trends Neurosci.* **2003**, *26*, 676–682. [CrossRef] [PubMed]
27. Kvitsiani, D.; Ranade, S.; Hangya, B.; Taniguchi, H.; Huang, J.Z.; Kepecs, A. Distinct Behavioural and Network Correlates of Two Interneuron Types in Prefrontal Cortex. *Nature* **2013**, *498*, 363–366. [CrossRef]
28. Cobb, S.R.; Buhl, E.H.; Halasy, K.; Paulsen, O.; Somogyi, P. Synchronization of Neuronal Activity in Hippocampus by Individual GABAergic Interneurons. *Nature* **1995**, *378*, 75–78. [CrossRef]
29. Seamans, J.K.; Yang, C.R. The Principal Features and Mechanisms of Dopamine Modulation in the Prefrontal Cortex. *Prog. Neurobiol.* **2004**, *74*, 1–58. [CrossRef]
30. Puig, M.V.; Rose, J.; Schmidt, R.; Freund, N. Dopamine Modulation of Learning and Memory in the Prefrontal Cortex: Insights from Studies in Primates, Rodents, and Birds. *Front. Neural Circuits* **2014**, *8*, 93. [CrossRef]
31. Ott, T.; Nieder, A. Dopamine and Cognitive Control in Prefrontal Cortex. *Trends Cogn. Sci.* **2019**, *23*, 213–234. [CrossRef]
32. Tritsch, N.X.; Sabatini, B.L. Dopaminergic Modulation of Synaptic Transmission in Cortex and Striatum. *Neuron* **2012**, *76*, 33–50. [CrossRef] [PubMed]
33. Santana, N.; Mengod, G.; Artigas, F. Quantitative Analysis of the Expression of Dopamine D1 and D2 Receptors in Pyramidal and GABAergic Neurons of the Rat Prefrontal Cortex. *Cereb. Cortex* **2009**, *19*, 849–860. [CrossRef] [PubMed]
34. Beaulieu, J.M.; Gainetdinov, R.R. The Physiology, Signaling, and Pharmacology of Dopamine Receptors. *Pharmacol. Rev.* **2011**, *63*, 182–217. [CrossRef]
35. Huang, S.; Borgland, S.L.; Zamponi, G.W. Dopaminergic Modulation of Pain Signals in the Medial Prefrontal Cortex: Challenges and Perspectives. *Neurosci. Lett.* **2019**, *702*, 71–76. [CrossRef] [PubMed]
36. Lee, S.P.; So, C.H.; Rashid, A.J.; Varghese, G.; Cheng, R.; Lança, A.J.; O'Dowd, B.F.; George, S.R. Dopamine D1 and D2 Receptor Co-Activation Generates a Novel Phospholipase C-Mediated Calcium Signal. *J. Biol. Chem.* **2004**, *279*, 35671–35678. [CrossRef]
37. Sahu, A.; Tyeryar, K.R.; Vongtau, H.O.; Sibley, D.R.; Undieh, A.S. D 5 Dopamine Receptors Are Required for Dopaminergic Activation of Phospholipase C. *Mol. Pharmacol.* **2009**, *75*, 447–453. [CrossRef]
38. Graziane, N.M.; Yuen, E.Y.; Yan, Z. Dopamine D4 Receptors Regulate GABAA Receptor Trafficking via an Actin/Cofilin/Myosin-Dependent Mechanism. *J. Biol. Chem.* **2009**, *284*, 8329–8336. [CrossRef]
39. Lewis, D.A.; Gonzalez-Burgos, G. Pathophysiologically Based Treatment Interventions in Schizophrenia. *Nat. Med.* **2006**, *12*, 1016–1022. [CrossRef]
40. O'Donnell, P. Adolescent Onset of Cortical Disinhibition in Schizophrenia: Insights from Animal Models. *Schizophr. Bull.* **2011**, *37*, 484–492. [CrossRef]
41. Tseng, K.Y.; Chambers, R.A.; Lipska, B.K. The Neonatal Ventral Hippocampal Lesion as a Heuristic Neurodevelopmental Model of Schizophrenia. *Behav. Brain Res.* **2009**, *204*, 295–305. [CrossRef]
42. Mrzljak, L.; Bergson, C.; Pappy, M.; Huff, R.; Levenson, R.; Goldman-Rakic, P.S. Localization of Dopamine D4 Receptors in GABAergic Neurons of the Primate Brain. *Nature* **1996**, *381*, 245–248. [CrossRef] [PubMed]
43. Ariano, M.A.; Wang, J.; Noblett, K.L.; Larson, E.R.; Sibley, D.R. Cellular Distribution of the Rat D4 Dopamine Receptor Protein in the CNS Using Anti-Receptor Antisera. *Brain Res.* **1997**, *752*, 26–34. [CrossRef] [PubMed]
44. Wędzony, K.; Chocyk, A.; Maćkowiak, M.; Fijał, K.; Czyrak, A. Cortical Localization of Dopamine D4 Receptors in the Rat Brain—Immunocytochemical Study. *J. Physiol. Pharmacol.* **2000**, *51*, 205–221. [PubMed]
45. Smiley, J.F.; Levey, A.I.; Ciliax, B.J.; Goldman-Rakic, P.S. D1 Dopamine Receptor Immunoreactivity in Human and Monkey Cerebral Cortex: Predominant and Extrasynaptic Localization in Dendritic Spines. *Proc. Natl. Acad. Sci. USA* **1994**, *91*, 5720–5724. [CrossRef] [PubMed]
46. Wang, X.; Zhong, P.; Yan, Z. Dopamine D4 Modulate GABAergic Signaling in Pyramidal Neurons. *J. Neurosci.* **2002**, *22*, 9185–9193. [CrossRef]

47. Seamans, J.K.; Gorelova, N.; Durstewitz, D.; Yang, C.R. Bidirectional Dopamine Modulation of GABAergic Inhibition in Prefrontal Cortical Pyramidal Neurons. *J. Neurosci.* **2001**, *21*, 3628–3638. [CrossRef]
48. Chiu, C.Q.; Puente, N.; Grandes, P.; Castillo, P.E. Dopaminergic Modulation of Endocannabinoid-Mediated Plasticity at GABAergic Synapses in the Prefrontal Cortex. *J. Neurosci.* **2010**, *30*, 7236–7248. [CrossRef]
49. Zhou, F.M.; Hablitz, J.J. Dopamine Modulation of Membrane and Synaptic Properties of Interneurons in Rat Cerebral Cortex. *J. Neurophysiol.* **1999**, *81*, 967–976. [CrossRef]
50. Penit-Soria, J.; Audinat, E.; Crepel, F. Excitation of Rat Prefrontal Cortical Neurons by Dopamine: An in Vitro Electrophysiological Study. *Brain Res.* **1987**, *425*, 263–274. [CrossRef]
51. Law-Tho, D.; Desce, J.M.; Crepel, F. Dopamine Favours the Emergence of Long-Term Depression versus Long-Term Potentiation in Slices of Rat Prefrontal Cortex. *Neurosci. Lett.* **1995**, *188*, 125–128. [CrossRef]
52. Gonzalez-Islas, C.; Hablitz, J.J. Dopamine Inhibition of Evoked IPSCs in Rat Prefrontal Cortex. *J. Neurophysiol.* **2001**, *86*, 2911–2918. [CrossRef] [PubMed]
53. Gao, W.J.; Goldman-Rakic, P.S. Selective Modulation of Excitatory and Inhibitory Microcircuits by Dopamine. *Proc. Natl. Acad. Sci. USA* **2003**, *100*, 2836–2841. [CrossRef] [PubMed]
54. Chris Muly, E.; Szigeti, K.; Goldman-Rakic, P.S. D1 Receptor in Interneurons of Macaque Prefrontal Cortex: Distribution and Subcellular Localization. *J. Neurosci.* **1998**, *18*, 10553–10565. [CrossRef] [PubMed]
55. Glausier, J.R.; Khan, Z.U.; Muly, E.C. Dopamine D1 and D5 Receptors Are Localized to Discrete Populations of Interneurons in Primate Prefrontal Cortex. *Cereb. Cortex* **2009**, *19*, 1820–1834. [CrossRef] [PubMed]
56. Gorelova, N.; Seamans, J.K.; Yang, C.R. Mechanisms of Dopamine Activation of Fast-Spiking Interneurons That Exert Inhibition in Rat Prefrontal Cortex. *J. Neurophysiol.* **2002**, *88*, 3150–3166. [CrossRef] [PubMed]
57. Tseng, K.Y.; O'Donnell, P. Dopamine Modulation of Prefrontal Cortical Interneurons Changes during Adolescence. *Cereb. Cortex* **2007**, *17*, 1235–1240. [CrossRef] [PubMed]
58. Anastasiades, P.G.; Boada, C.; Carter, A.G. Cell-Type-Specific D1 Dopamine Receptor Modulation of Projection Neurons and Interneurons in the Prefrontal Cortex. *Cereb. Cortex* **2019**, *29*, 3224–3242. [CrossRef] [PubMed]
59. Ferron, A.; Thierry, A.M.; Le Douarin, C.; Glowinski, J. Inhibitory Influence of the Mesocortical Dopaminergic System on Spontaneous Activity or Excitatory Response Induced from the Thalamic Mediodorsal Nucleus in the Rat Medial Prefrontal Cortex. *Brain Res.* **1984**, *302*, 257–265. [CrossRef]
60. Lewis, B.L.; O'Donnell, P. Ventral Tegmental Area Afferents to the Prefrontal Cortex Maintain Membrane Potential "up" States in Pyramidal Neurons via D1 Dopamine Receptors. *Cereb. Cortex* **2000**, *10*, 1168–1175. [CrossRef]
61. Tseng, K.Y.; Mallet, N.; Toreson, K.L.; Le Moine, C.; Gonon, F.; O'Donnell, P. Excitatory Response of Prefrontal Cortical Fast-Spiking Interneurons to Ventral Tegmental Area Stimulation in Vivo. *Synapse* **2006**, *59*, 412–417. [CrossRef]
62. Garris, P.A.; Collins, L.B.; Jones, S.R.; Wightman, R.M. Evoked Extracellular Dopamine In Vivo in the Medial Prefrontal Cortex. *J. Neurochem.* **1993**, *61*, 637–647. [CrossRef] [PubMed]
63. Garris, P.A.; Wightman, R.M. Different Kinetics Govern Dopaminergic Transmission in the Amygdala, Prefrontal Cortex, and Striatum: An in Vivo Voltammetric Study. *J. Neurosci.* **1994**, *14*, 442–450. [CrossRef] [PubMed]
64. Pirot, S.; Godbout, R.; Mantz, J.; Tassin, J.P.; Glowinski, J.; Thierry, A.M. Inhibitory Effects of Ventral Tegmental Area Stimulation on the Activity of Prefrontal Cortical Neurons: Evidence for the Involvement of Both Dopaminergic and GABAergic Components. *Neuroscience* **1992**, *49*, 857–865. [CrossRef] [PubMed]
65. West, A.R.; Grace, A.A. Opposite Influences of Endogenous Dopamine D1 and D2 Receptor Activation on Activity States and Electrophysiological Properties of Striatal Neurons: Studies Combining in Vivo Intracellular Recordings and Reverse Microdialysis. *J. Neurosci.* **2002**, *22*, 294–304. [CrossRef] [PubMed]
66. Rubinstein, M.; Cepeda, C.; Hurst, R.S.; Flores-Hernandez, J.; Ariano, M.A.; Falzone, T.L.; Kozell, L.B.; Meshul, C.K.; Bunzow, J.R.; Low, M.J.; et al. Dopamine D4 Receptor-Deficient Mice Display Cortical Hyperexcitability. *J. Neurosci.* **2001**, *21*, 3756–3763. [CrossRef]
67. Wang, X.; Zhong, P.; Gu, Z.; Yan, Z. Regulation of NMDA Receptors by Dopamine D4 Signaling in Prefrontal Cortex. *J. Neurosci.* **2003**, *23*, 9852–9861. [CrossRef]
68. Lew, S.E.; Tseng, K.Y. Dopamine Modulation of GABAergic Function Enables Network Stability and Input Selectivity for Sustaining Working Memory in a Computational Model of the Prefrontal Cortex. *Neuropsychopharmacology* **2014**, *39*, 3067–3076. [CrossRef] [PubMed]
69. Durstewitz, D.; Seamans, J.K. The Computational Role of Dopamine D1 Receptors in Working Memory. *Neural Networks* **2002**, *15*, 561–572. [CrossRef]
70. Brunel, N.; Sup, E.N.; Wang, X. Effects of Neuromodulation in a Cortical Network Model of Object Working. *J. Comput. Neurosci.* **2001**, *11*, 63–85. [CrossRef]
71. Trantham-Davidson, H.; Neely, L.C.; Lavin, A.; Seamans, J.K. Mechanisms Underlying Differential D1 versus D2 Dopamine Receptor Regulation of Inhibition in Prefrontal Cortex. *J. Neurosci.* **2004**, *24*, 10652–10659. [CrossRef]
72. Seamans, J.K.; Durstewitz, D.; Christie, B.R.; Stevens, C.F.; Sejnowski, T.J. Dopamine D1/D5 Receptor Modulation of Excitatory Synaptic Inputs to Layer V Prefrontal Cortex Neurons. *Proc. Natl. Acad. Sci. USA* **2001**, *98*, 301–306. [CrossRef]

73. Tseng, K.Y.; O'Donnell, P. Dopamine-Glutamate Interactions Controlling Prefrontal Cortical Pyramidal Cell Excitability Involve Multiple Signaling Mechanisms. *J. Neurosci.* **2004**, *24*, 5131–5139. [CrossRef]
74. Ott, T.; Nieder, A. Dopamine D2 Receptors Enhance Population Dynamics in Primate Prefrontal Working Memory Circuits. *Cereb. Cortex* **2017**, *27*, 4423–4435. [CrossRef] [PubMed]
75. Ortiz, C.; Navarro, J.F.; Jurek, A.; Märtin, A.; Lundeberg, J.; Meletis, K. Molecular Atlas of the Adult Mouse Brain. *Sci. Adv.* **2020**, *6*, eabb3446. [CrossRef]
76. Wilson, C.R.E.; Gaffan, D.; Browning, P.G.F.; Baxter, M.G. Functional Localization within the Prefrontal Cortex: Missing the Forest for the Trees? *Trends Neurosci.* **2010**, *33*, 533–540. [CrossRef] [PubMed]
77. Liu, Y.; Ouyang, P.; Zheng, Y.; Mi, L.; Zhao, J.; Ning, Y.; Guo, W. A Selective Review of the Excitatory-Inhibitory Imbalance in Schizophrenia: Underlying Biology, Genetics, Microcircuits, and Symptoms. *Front. Cell Dev. Biol.* **2021**, *9*, 2917. [CrossRef] [PubMed]
78. da Silva Alves, F.; Figee, M.; van Avamelsvoort, T.; Veltman, D.; de Haan, L. The Revised Dopamine Hypothesis of Schizophrenia: Evidence from Pharmacological MRI Studies with Atypical Antipsychotic Medication. *Psychopharmacol. Bull.* **2008**, *41*, 121–132.
79. Shen, L.H.; Liao, M.H.; Tseng, Y.C. Recent Advances in Imaging of Dopaminergic Neurons for Evaluation of Neuropsychiatric Disorders. *J. Biomed. Biotechnol.* **2012**, *2012*, 259349. [CrossRef]
80. O'Donnell, P.; Grace, A.A. Dysfunctions in Multiple Interrelated Systems as the Neurobiological Bases of Schizophrenic Symptom Clusters. *Schizophr. Bull.* **1998**, *24*, 267–283. [CrossRef]
81. Durstewitz, D.; Seamans, J.K. The Dual-State Theory of Prefrontal Cortex Dopamine Function with Relevance to Catechol-O-Methyltransferase Genotypes and Schizophrenia. *Biol. Psychiatry* **2008**, *64*, 739–749. [CrossRef]
82. Nakazawa, K.; Sapkota, K. The Origin of NMDA Receptor Hypofunction in Schizophrenia. *Pharmacol. Ther.* **2020**, *205*, 107426. [CrossRef]
83. Kruse, A.O.; Bustillo, J.R. Glutamatergic Dysfunction in Schizophrenia. *Transl. Psychiatry* **2022**, *12*, 500. [CrossRef]
84. Zhang, W.; Xiong, B.R.; Zhang, L.Q.; Huang, X.; Yuan, X.; Tian, Y.K.; Tian, X.B. The Role of the GABAergic System in Diseases of the Central Nervous System. *Neuroscience* **2021**, *470*, 88–99. [CrossRef] [PubMed]
85. Benes, F.M. The GABA System in Schizophrenia: Cells, Molecules and Microcircuitry. *Schizophr. Res.* **2015**, *167*, 1–3. [CrossRef]
86. Crabtree, G.W.; Park, A.J.; Gordon, J.A.; Gogos, J.A. Cytosolic Accumulation of L-Proline Disrupts GABA-Ergic Transmission through GAD Blockade. *Cell Rep.* **2016**, *17*, 570–582. [CrossRef] [PubMed]
87. Li, Y.C.; Kellendonk, C.; Simpson, E.H.; Kandel, E.R.; Gao, W.J. D2 Receptor Overexpression in the Striatum Leads to a Deficit in Inhibitory Transmission and Dopamine Sensitivity in Mouse Prefrontal Cortex. *Proc. Natl. Acad. Sci. USA* **2011**, *108*, 12107–12112. [CrossRef] [PubMed]
88. Garbutt, J.C.; Van Kammen, D.P. The Interaction between GABA and Dopamine: Implications for Schizophrenia. *Schizophr. Bull.* **1983**, *9*, 336–353. [CrossRef]
89. Benes, F.M. The Role of Stress and Dopamine-GABA Interactions in the Vulnerability for Schizophrenia. *J. Psychiatr. Res.* **1997**, *31*, 257–275. [CrossRef]
90. Bey, A.; Jiang, Y.H. Overview of mouse models of autism spectrum disorders. *Curr Protoc Pharmacol.* **2014**, *66*, 1–26. [CrossRef]
91. Mapelli, L.; Soda, T.; D'Angelo, E.; Prestori, F. The Cerebellar Involvement in Autism Spectrum Disorders: From the Social Brain to Mouse Models. *Int. J. Mol. Sci.* **2022**, *23*, 3894. [CrossRef]
92. Uzunova, G.; Pallanti, S.; Hollander, E. Excitatory/Inhibitory Imbalance in Autism Spectrum Disorders: Implications for Interventions and Therapeutics. *World J. Biol. Psychiatry* **2016**, *17*, 174–186. [CrossRef] [PubMed]
93. Rinaldi, T.; Perrodin, C.; Markram, H. Hyper-Connectivity and Hyper-Plasticity in the Medial Prefrontal Cortex in the Valproic Acid Animal Model of Autism. *Front. Neural Circuits* **2008**, *2*, 4. [CrossRef]
94. Soda, T.; Mapelli, L.; Locatelli, F.; Botta, L.; Goldfarb, M.; Prestori, F.; D'Angelo, E.U. Hyperexcitability and Hyperplasticity Disrupt Cerebellar Signal Transfer in the Ib2 Ko Mouse Model of Autism. *J. Neurosci.* **2019**, *39*, 2383–2397, Erratum in *J. Neurosci.* **2019**, *39*, 7029. [CrossRef] [PubMed]
95. Antoine, M.W.; Langberg, T.; Schnepel, P.; Feldman, D.E. Increased Excitation-Inhibition Ratio Stabilizes Synapse and Circuit Excitability in Four Autism Mouse Models. *Neuron* **2019**, *101*, 648–661.e4. [CrossRef] [PubMed]
96. Kosillo, P.; Bateup, H.S. Dopaminergic Dysregulation in Syndromic Autism Spectrum Disorders: Insights From Genetic Mouse Models. *Front. Neural Circuits* **2021**, *15*, 700968. [CrossRef]
97. Nguyen, M.; Roth, A.; Kyzar, E.J.; Poudel, M.K.; Wong, K.; Stewart, A.M.; Kalueff, A.V. Decoding the Contribution of Dopaminergic Genes and Pathways to Autism Spectrum Disorder (ASD). *Neurochem. Int.* **2014**, *66*, 15–26. [CrossRef] [PubMed]
98. Gunaydin, L.A.; Grosenick, L.; Finkelstein, J.C.; Kauvar, I.V.; Fenno, L.E.; Adhikari, A.; Lammel, S.; Mirzabekov, J.J.; Airan, R.D.; Zalocusky, K.A.; et al. Natural Neural Projection Dynamics Underlying Social Behavior. *Cell* **2014**, *157*, 1535–1551. [CrossRef]
99. Lee, Y.; Kim, H.; Kim, J.E.; Park, J.Y.; Choi, J.; Lee, J.E.; Lee, E.H.; Han, P.L. Excessive D1 Dopamine Receptor Activation in the Dorsal Striatum Promotes Autistic-Like Behaviors. *Mol. Neurobiol.* **2018**, *55*, 5658–5671. [CrossRef]
100. Grace, A.A. Dysregulation of the Dopamine System in the Pathophysiology of Schizophrenia and Depression. *Nat. Rev. Neurosci.* **2016**, *17*, 524–532. [CrossRef]
101. Wise, R.A. Dopamine and Reward: The Anhedonia Hypothesis 30 Years On. *Neurotox. Res.* **2008**, *14*, 169–183. [CrossRef]
102. McKlveen, J.M.; Moloney, R.D.; Scheimann, J.R.; Myers, B.; Herman, J.P. "Braking" the Prefrontal Cortex: The Role of Glucocorticoids and Interneurons in Stress Adaptation and Pathology. *Biol. Psychiatry* **2019**, *86*, 669–681. [CrossRef]

103. Yan, R.; Wang, T.; Zhou, Q. Elevated Dopamine Signaling from Ventral Tegmental Area to Prefrontal Cortical Parvalbumin Neurons Drives Conditioned Inhibition. *Proc. Natl. Acad. Sci. USA* **2019**, *116*, 13077–13086. [CrossRef] [PubMed]
104. Kummer, K.K.; Mitrić, M.; Kalpachidou, T.; Kress, M. The Medial Prefrontal Cortex as a Central Hub for Mental Comorbidities Associated with Chronic Pain. *Int. J. Mol. Sci.* **2020**, *21*, 3440. [CrossRef] [PubMed]
105. Bushnell, M.C.; Čeko, M.; Low, L.A. Cognitive and Emotional Control of Pain and Its Disruption in Chronic Pain. *Nat. Rev. Neurosci.* **2013**, *14*, 502–511. [CrossRef] [PubMed]
106. Huang, S.; Zhang, Z.; Gambeta, E.; Xu, S.C.; Thomas, C.; Godfrey, N.; Chen, L.; M'Dahoma, S.; Borgland, S.L.; Zamponi, G.W. Dopamine Inputs from the Ventral Tegmental Area into the Medial Prefrontal Cortex Modulate Neuropathic Pain-Associated Behaviors in Mice. *Cell Rep.* **2020**, *31*, 107812. [CrossRef] [PubMed]

Chapter 5

In-vivo characterization of cerebellar modulation over prefrontal cortex activity in anesthetized mice.

In preparation

In collaboration with:

Ileana Montagna, Letizia Moscato, Simona Tritto, Egidio D'Angelo and Lisa Mapelli

Author contribution: DDD performed the entire set of recordings using subsequent D1/D2 like receptor antagonists and gabazine, and the entire set with glutamate receptors antagonists, histology, data analysis and wrote the manuscript; IM performed recordings using D1/D2-like receptor antagonists, the entire set of recordings with gabazine; LeM performed pharmacology with selective D1/D2-like receptor antagonist, and data analysis; ST performed histology and image analysis; LiM and ED coordinated the work, wrote the manuscript, and approved the final version of the manuscript.

Abstract

Alterations in cerebello-prefrontal cortex (mPFC) connections characterize several cognitive dysfunctions (such as schizophrenia), suggesting that the cerebellum has a crucial impact on mPFC functioning. The cerebellum might regulate mPFC activity through a dopaminergic pathway relayed by the ventral tegmental area (VTA), and a glutamatergic pathway relayed by the mediodorsal and ventrolateral nuclei of the thalamus. At present, the mechanisms of cerebellar regulation of mPFC are still largely unknown. To get insight into the process of cerebellum-mPFC communication, we used single-unit recordings *in vivo* in the prelimbic area (PrL) of the mPFC in anesthetized mice. Electrical stimulation of the contralateral cerebellar dentate nucleus elicited a pause in PrL neurons firing, sometimes followed by an excitation rebound. To investigate the nature of PrL responses, we applied a $GABA_A$ receptor antagonist (gabazine), D1-like and D2-like dopamine receptor antagonists (SCH23390 and Sulpiride, respectively), and NMDA and AMPA glutamate receptors antagonists (NBQX, D-APV and 7Cl-kynurenate). Gabazine perfusion confirmed the inhibitory nature of the pause, while the

blockade of dopaminergic transmission modulated PrL neurons spontaneous firing without abolishing pause responses. Glutamate receptor antagonists almost completely abolished the basal discharge of PrL neurons. Our data show that cerebellar activation transiently decreases PrL activity engaging local inhibitory circuits (probably activated by thalamic projections), while dopaminergic receptors regulate PrL basal discharge. Thus, the combined effect of the two pathways tunes PrL activity modifying the signal-to-noise ratio and modulating neuronal discharge. Overall, these findings provide evidence for a complex cerebellar functional control over the PrL.

5.1 Introduction

Despite the commonly held belief that the cerebellum primarily plays a role in sensorimotor integration, multiple studies suggest that the cerebellum also plays a critical role in cognitive functions. Human anatomical MRI tracing studies have identified prominent interconnecting tracts between the cerebellum and neocortical areas involved in cognition, such as the medial prefrontal cortex (mPFC) (Palesi et al. 2015), providing evidence for the cerebellar involvement in cognitive processes. Studies in rodents have used axonal tracing to identify the cerebellar connections to the mediodorsal thalamus (MD), and beyond, to the mPFC (Pisano et al. 2021). In recent years, an increasing number of studies have focused on understanding the nature and importance of the cerebellum-prefrontal connection. Several cognitive disorders, including schizophrenia and autism spectrum disorders, have been associated with abnormal functioning of the prefrontal-cerebellar pathway (Andreasen et al. 1996; Andreasen and Pierson 2008; Fatemi et al. 2012; Whitney et al. 2008), highlighting the potential relevance of this connection in cognitive processes. These findings present new perspectives for comprehending the neuronal mechanisms that underlie various pathologies. Studies have observed structural and functional changes, such as a reduced number of Purkinje cells, cerebellar hypoplasia, and an increased volume of the frontal lobe cortex, that positively correlate with symptoms of autism (Palmen et al. 2004; Vargas et al. 2005; Whitney et al. 2008). Conversely, abnormalities in the cerebellar vermis (Henze et al. 2011; Lawyer et al. 2009; Okugawa et al. 2008)and a decrease in cerebellar projections within the cerebellar peduncles have been linked to schizophrenia (Kyriakopoulos et al. 2008). These observations

shed new light on the potential underlying causes of these disorders. Research conducted on rodents uncovered the presence of a bidirectional connection between the cerebellum and mPFC, as shown through electrophysiological and amperometric studies conducted *in vivo* (Thomas C. Watson et al. 2014; Thomas C. Watson, Jones, and Apps 2009). Specifically, it has been observed that electrical stimulation of the fastigial nucleus (FN) results in responses in the prelimbic subdivision (PrL) of the mPFC (Thomas C. Watson et al. 2014), indicating a functional interplay between these two regions.

Similarly, electrical stimulation of the PrL has been shown to evoke field potential responses in Purkinje cells (PCs) located in the cerebellar vermis, as well as in the paravermal and lateral cerebellar cortex, albeit with smaller amplitude (Thomas C. Watson, Jones, and Apps 2009). Moreover, studies have shown that stimulation of the dentate nucleus (DN) in urethane-anesthetized mice can lead to dopamine release in the mPFC via cerebellum-activated ventral tegmental area (VTA) projections or glutamatergic projections from thalamic nuclei, indicating the involvement of multiple brain regions in this interconnection (Rogers et al. 2011).

Additionally, recent research has shown that activating cerebellar terminals over the VTA in freely moving mice does not generate enough dopamine release in the mPFC to encourage prosocial behaviour (Carta et al. 2019). Therefore, the presumed cognitive functions associated with cerebellar stimulation of mPFC activity cannot be solely attributed to the dopaminergic pathway.

The MD is responsible for most thalamocortical projections to the mPFC (Ferguson and Gao 2018). These projections from the MD contain glutamatergic neurons that contact both pyramidal neurons in layer V and interneurons in layers III and V of the mPFC. This results in the formation of inhibitory synapses with pyramidal excitatory neurons, which then regulate their discharge patterns (Povysheva et al. 2006; Rotaru, Barrionuevo, and Sesack 2005). Indeed, mPFC interneurons play a critical role in maintaining the balance between excitatory and inhibitory signals that regulate pyramidal neuron firing in the mPFC. This is achieved through feedforward inhibition and gain control activity (Ferguson and Gao 2018).

Hence, the cerebellum may influence mPFC activity through various pathways, although the underlying mechanisms are not well understood. On one hand, dopamine has both opposing

and mixed effects on pyramidal cells and local interneurons in mPFC. These effects involve various classes and subtypes of dopamine receptors (mainly D1- or D2-like), which are also distributed heterogeneously among prefrontal neurons (Di Domenico and Mapelli 2023; Floresco et al. 2006; Floresco and Magyar 2006). Indeed, pyramidal neurons usually express just one receptor type (either D1-like or D2-like) and the co-expression of both types is rare (Gaspar, Bloch, and Le Moine 1995). Furthermore, research has demonstrated that dopamine can modulate mPFC neurons by either reducing spontaneous and evoked activity (Gulledge and Jaffe 1998) or increasing neuronal excitability (Buchta et al. 2017; Otani, Bai, and Blot 2015; Trantham-Davidson, Kröner, and Seamans 2008).

On the other hand, thalamic projections target various layers in the mPFC, generating different effects on cortical activity. Given the complexity of the mPFC circuitry, it is challenging to determine whether the cerebello-thalamo-cortical pathway directly stimulates mPFC pyramidal neurons or indirectly modulates them through local interneurons.

Herein, we characterized PrL neurons responses following electrical stimulation of contralateral cerebellar DN in mice *in vivo*. Cerebellar nuclei stimulation elicited a pause in PrL neurons spontaneous activity, that in some cases was followed by a burst. Moreover, the involvement of the three major neurotransmitter pathways was investigated. First, $GABA_A$ receptors blockade almost completely abolished PrL neurons response to cerebellar stimulation, revealing a possible role of GABAergic system in local synaptic inhibition. Secondly, the blockade of the principal dopamine receptors revealed a modulatory role of the dopamine (DA) on PrL neurons excitability. Thirdly, we also investigated the glutamatergic contribution, by blocking NMDA and AMPA receptors, revealing that PrL neurons spontaneous activity requires glutamatergic synaptic inputs. Finally, we also evaluated the interplay between the dopaminergic and GABAergic systems, which is necessary to maintain a good E/I balance and ensure a proper PFC functioning. Taken together, these results demonstrate the functional interaction between the cerebellum and the PrL, offering new insight into the nature of this functional interplay. Specifically, our results reveal that the influence of the cerebellum on the mPFC extends beyond dopamine-mediated control, highlighting the existence of more intricate mechanisms through which the cerebellum may affect mPFC activity.

5.2 Materials and methods

Multiple single/units recordings were performed in the PrL of C57BL/6 mice of both sexes (30.0±0.2 days old; n=55) under urethane anaesthesia. No significant difference was detected in the neuronal properties and responsivity between males and females (a group of 32 males and 23 females; unpaired Student's *t* test yielded p=0.1 for spontaneous frequency, p=0.3 for response amplitude as pause depth, and p=0.2 for percent change after pharmacological treatment). As such, the outcomes reported in this study were deemed to be gender-unrelated. Additionally, the anaesthesia employed, urethane, has minimal effects on glutamatergic and GABAergic receptors (Hara and Harris 2002), making it unlikely to impact stimulus-evoked responses in mPFC neurons during our recordings.

5.2.1 Surgical procedures

Urethane was dissolved in a saline solution (1.3g/kg urethane in 0.9% NaCl, Sigma Aldrich) and was administrated to mice through intraperitoneal injections. Thirty minutes after the first injection, 3-4 booster injections (10% of the induction dose) were administered to maintain deep anaesthesia. To ensure the depth of anaesthesia, the leg withdrawal reflex after pinching and the presence of spontaneous whisking were tested. Mice were then placed on a custom-built stereotaxic table covered with a heating plate to maintain the body temperature at 36°C. Lidocaine (0.2ml; Astrazeneca) was subcutaneously applied to reduce cutaneous reflexes.

The skull was then exposed, and the mouse head was fixed to a metal bar connected to a pedestal anchored to the stereotaxic table. The skin and muscles were removed surgically, and craniotomy was performed over the cerebellum and mPFC to expose their surface and place electrodes. The coordinates used for electrode placement were as follows: for cerebellum (from Bregma, DN: -5.8 AP, +2.5 ML, +2.4 DV); for mPFC (PrL: +2.8 AP, 0.25 ML, +0.6 DV). The dura mater was carefully removed, and the surface was perfused with saline solution (NaCl 0.9%; Sigma Aldrich) to prevent drying.

5.2.2 Electrophysiological recordings

The quartz-coated platinum/tungsten electrodes (1-5MΩ; Thomas Recording GmBh, Giessen, Germany), were arranged in a 4x4 Eckhorn Matrix (100µm inter-electrode distance) and placed over the exposed mPFC area, contralateral to the stimulus source. Each recording

electrode was independently moved and inserted to reach the PrL at the average depth of 826.05±29.21 µm (n=119). Electrophysiological signals were recorded at 25 kHz, amplified, and digitized with a 300-5000 Hz band-pass filter using a RZ5D processor multi-channel workstation (Tucker-Davis Technologies, Alachua, FL, USA). At the end of each experiment, the exact location of the electrodes in PrL and DN was identified through histological tissue processing after electric lesions.

5.2.3 Electrical stimulation

Electrical stimulation of the DN was performed applying 21 pulses at 100Hz and 100 µA, repeated every 5 s, using a bipolar tungsten electrode (0.5 MΩ; World Precision Instruments Inc, Sarasota, FL, USA) connected to a stimulator unit through a stimulus isolator. The protocol was modified from Watson et al. (2014), who used 100 pulses at 100Hz. Additionally, high-frequency cerebellar stimulation (100 pulses, 50 Hz) has been associated with dopamine efflux in the mPFC (Mittleman et al. 2008). Based on these reports, a similar stimulation protocol was developed, which was efficient in evoking cortical neuron responses and is likely to elicit dopamine release in the mPFC (Mittleman et al. 2008). The stimulating electrode was mounted on a Patch-star micromanipulator (Scientifica, Ltd) and precisely lowered into the cerebellum to a depth of 2600 µm from the surface to stimulate DN. Once a PrL neuron was detected, spontaneous activity was recorded for 5 minutes, followed by control recording during cerebellar stimulation for approximately 8 minutes to characterize the evoked response patterns in PrL neurons. Out of 119 neurons recorded, the effect of DN stimulation on PrL was detected and characterized in 88 units. In 31 units, no significant response to stimulation was observed.

5.2.4 Pharmacology

All drugs were added to a Krebs solution with the following composition (in mM): 120 NaCl, 2 KCl, 1.2 $MgSO_4$, 26 $NaHCO_3$, 1.2 KH_2PO_4, 2 $CaCl_2$, and 11 glucose. This solution was perfused onto the PrL surface through a micropipette and was equilibrated with 95% O2-5% CO2 to maintain a pH of 7.4.

To assess the GABAergic contribution to PrL responses detected following DN stimulation, the selective $GABA_A$ receptor antagonist gabazine (SR-95531, Abcam, 3 mM; Kurt et al., 2006) was perfused onto the mPFC surface immediately after control recordings. PrL neuron activity was

then recorded for 30 minutes after drug perfusion, during which the same pattern of electrical stimuli was delivered to the DN.

Then a second subset of experiments was performed to evaluate the glutamatergic contribution. As with the $GABA_A$ receptor antagonist, NMDA and AMPA receptors antagonists (NBQX, D-APV and 7Cl-kynurenate, 10mM) were applied to the mPFC surface and unit activity was recorded for 50 minutes.

To evaluate the dopaminergic contribution, selective dopamine receptor antagonists SCH23390 hydrochloride (selective D1-like receptor antagonist, 44 mM; Abcam) and (S)-Sulpiride (selective D2-like receptor antagonist, 36 mM; Abcam), were co-perfused onto the PrL surface. The effects of these selective antagonists on PrL response pattern during DN stimulation were monitored for at least 20 minutes.

Finally, a fourth subset of experiments was performed by combining the third and the first subsets. After control recordings, selective dopamine receptors antagonists SCH23390 hydrochloride (selective D1-like receptor antagonist, 44 mM; Abcam) and (S)-Sulpiride (selective D2-like receptor antagonist, 36 mM; Abcam) were co-perfused onto the PrL surface, followed by the perfusion of the selective $GABA_A$ receptor antagonist gabazine (SR-95531, Abcam, 3 mM). The effects of the antagonists on PrL neurons firing and responses to DN stimulation were monitored for at least 20 minutes.

5.2.5 Histology

Histological examination was used to confirm the exact placement of the recording and stimulating electrodes in PrL and DN, respectively. After each experiment, a 20 μA current was applied for 20 seconds through the same electrodes used for electrophysiological recordings in the PrL to create an electric lesion. The stimulating electrode in the DN produced a discernible electrical signature to the tissue due to the current injection (100 μA) during experimental procedures. Following transcardial perfusion of Phosphate-Buffered Saline (PBS) solution and 4% formaldehyde, the mouse brains were fixed and cryopreserved. Histological sections of 20μm thickness were obtained and stained with toluidine blue. The correct location of the recording and stimulation sites was determined through histological analysis using an optical microscope (Fig. 5.2).

5.2.6 Data analysis

The electrophysiological signals from PrL neurons were acquired using OpenEx software (Tucker-Davis Technologies) and then analysed offline using SpikeTrain (Neurasmus BV, Rotterdam, Netherlands) running under MATLAB (MathWorks, MA, USA). To analyse PrL responses to DN stimulation, peri-stimulus time histograms (PSTHs) with a 100 ms bin width were constructed. These histograms demonstrated that PrL response patterns consistently exhibited a pause, sometimes followed by bursts emerging from the background activity.

PSTHs with 20ms bin width were used to estimate response latency and duration. PrL responses were identified as pauses or peaks in PSTHs when bin values exceeded once the standard deviation of the basal frequency measured in the pre-stimulus period.

To evaluate the effects of selective antagonists on the detected responses, changes in pause amplitude and area in PSTHs were compared with respect to control. Response parameters were measured over 10, 20, and 30 minutes after drugs perfusion. Antagonist-mediated increase or decrease in neuronal responsiveness to cerebellar stimulation were detected as positive or negative changes compared to control, respectively. To test whether selective antagonists influenced the spontaneous firing rate and coefficient of variation of the inter-spike interval (CV2, which provides information about the spiking regularity), firing rate and CV2 were measured after antagonist perfusion and compared to control measurements. Data were fitted using OriginPro8 (OriginLac co., MA, USA), and statistical analysis was performed using paired or unpaired Student's *t* test. All data are reported as mean ± SEM (standard error of the mean).

5.3 Results

The single units recorded in the PrL (n = 119) showed a spontaneous activity with a mean basal frequency of 0.95 ± 0.11 Hz (Fig. 5.1). This observation is in agreement with previous reports of PrL neurons spontaneous firing in urethane anesthetized rodents (Watson et al. 2014).

Figure 5.1| Example of a spontaneous PrL neuron firing obtained with extracellular in vivo recording. Both the registration and electrical stimulation sites were confirmed by histological analysis (Fig. 5.2).

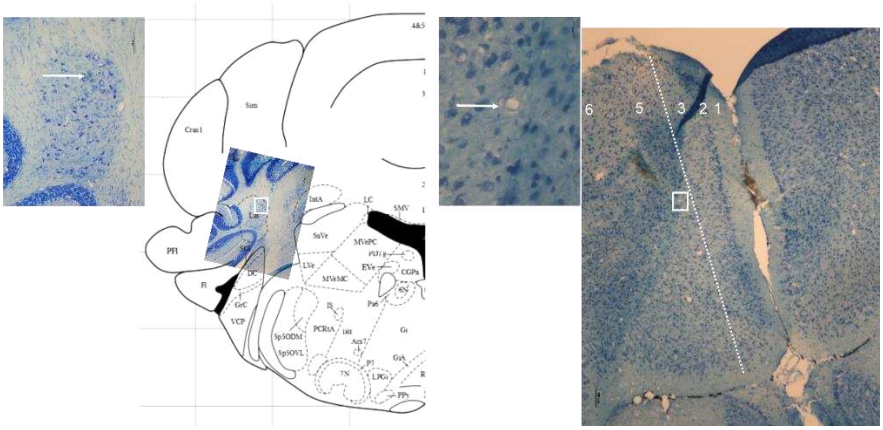

Figure 5.2| Histological identification of stimulation site in the DN and of recording site in PrL. *At left*) Toluidine blue stained coronal section of the cerebellum. The region in the rectangle is magnified on top left; the white arrow indicates the electrical lesion made by the stimulating electrode at the level of DN. *At right*) Toluidine blue stained coronal section of PrL region. The white arrow indicates the lesion made through the electrode used for recordings of PrL neurons. The lesion indicates that the recording site was located in layers V of the PrL.

5.3.1 Impact of DN stimulation on PrL neurons activity

The responsive units recorded (n = 88) showed a spontaneous activity with a discharge rate of 0.85 ± 0.09 Hz. In addition, one response pattern has been identified within the PSTH, characterized by a brief pause after the stimulus which sometimes was followed by a burst, evident as a peak in the PSTH (Fig 5.3A). In these cases, the PSTH peak amplitude negatively

correlated with the pause depth (Fig.5.3B), strongly suggesting that these peaks might reflect rebound bursts.

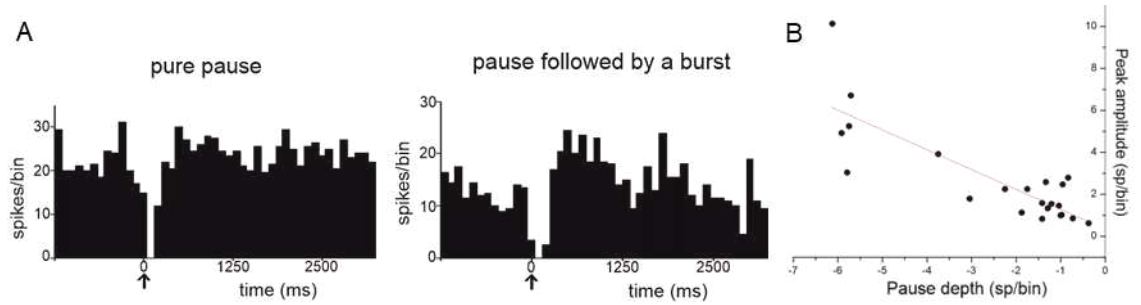

Figure 5.3| characterization of the PrL responses to DN stimulation. (A) Examples of PSTHs obtained from PrL neurons showing a pause following DN stimulation, followed by a burst in the PSTH *at right*. The black arrow indicates the stimulus onset. **(B)** When the burst was present, a negative correlation was found between pause depth and peak amplitude ($R2=0.67$, $p(F)=9.5x10^{-7}$).

The responses showing pure inhibition were characterized by a pause with a latency of 15 ± 3 ms and a duration of 195.06 ± 9.83 ms. When a peak followed the pause, the pause latency was 21.6 ± 7.8 ms and duration was 155 ± 13.8 ms (latency and duration did not differ significantly; p=0.08 and p=0.06, respectively). DN stimulation did not evoke responses in 26% of the recorded PrL neurons (n = 31), considering the analysis criteria adopted.

5.3.2 Effect of GABAA-receptor antagonist on evoked PrL responses

At first, we investigated the inhibitory nature of the PrL response to DN stimulation . The depth of PrL neurons responses was measured before and after the perfusion over the PrL of the selective $GABA_A$ antagonist gabazine (SR-95531, 3 mM). PrL neurons responses to DN stimulation was recorded for 20 minutes in control and for 30 minutes after gabazine perfusion on the surface of the mPFC. Out of the 16 recorded units, 6 were not responsive. The response changes following gabazine perfusion was assessed after 20 minutes from drug perfusion. Gabazine determined an increase in the spontaneous activity in all the recorded units (n=10, 315±128%, p = 0.041) and a reduction of the pause in all the recorded units (-100 ± 0.00%, p = 0.0001; Figure 5.4).

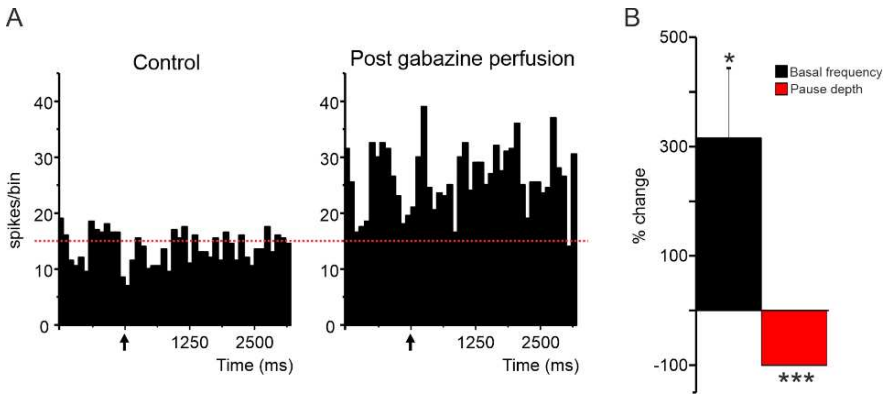

Figure 5.4| Average PSTHs of PrL responses before and 20 min after gabazine perfusion. A) The PSTHs show that inhibitory responses in PrL neurons were significantly reduced whilst basal frequency notably increased following gabazine perfusion (n=10). B) The histograms show the % changes in basal frequency and pause depth. *(* p<0.05; *** p<0.0001)*

5.3.3 Effect of NMDA and AMPA receptors block on evoked PrL response.

Given the possible network activating the local interneurons (afferent excitatory fibres impinging on local inhibitory interneurons, which are the actual responsible for the inhibitory response of PrL recorded neurons), we blocked the glutamatergic transmission to further characterize the pathway involved.

The experimental setting was similar to the previous one. After recording the activity of the PrL neurons following the stimulation of the DN for 20 minutes, glutamate receptor antagonists (NBQX, D-APV, and 7Cl-kynurenate, 10mM) were perfused on the surface of the mPFC, recording the activity of the single units for a further 50 minutes. We recorded 18 units which all responded to the DN stimulation with a pause. After the perfusion of the glutamate receptor antagonists, basal activity is already decreased after 5 minutes and almost completely stopped after 20 minutes (Fig. 5.5).

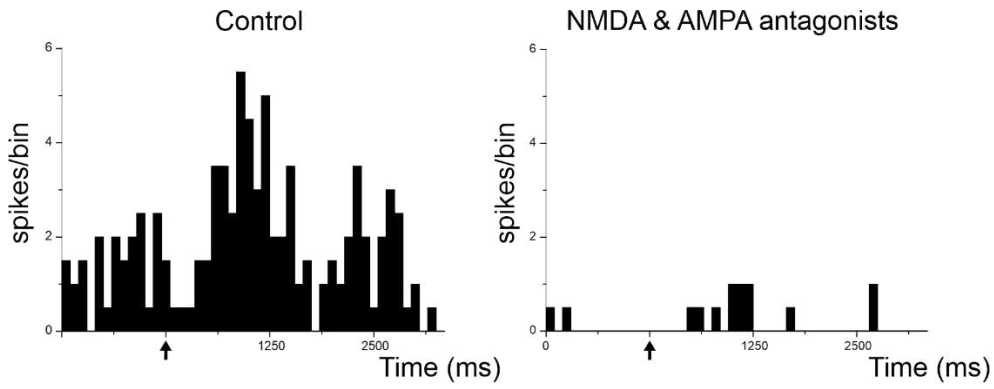

Figure 5.5|Example PSTH of PrL response before and 30 minutes after NMDA and AMPA antagonists perfusion. The PSTHs show that the basal activity of the PrL unit is almost completely abolished after 30 minutes from the perfusion of NMDA and AMPA antagonists with respect to the control condition.

Basal activity reached a plateau at 30 minutes after drug perfusion as shown in Figure 5.6 (-87.8% ± 9.8%, n=18). Given that basal firing was almost suppressed, it was not possible to detect any further downregulating effect of DN stimulation on PrL units firing (see Fig. 5.5).

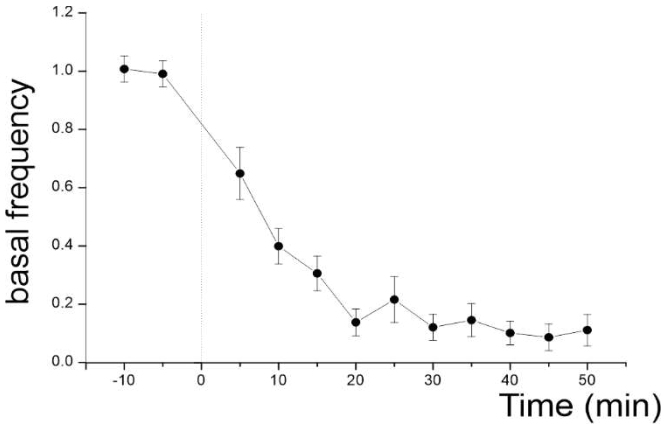

Figure 5.6|Average time course of the basal frequency before and after glutamatergic transmission blockers. Notice that basal frequency almost immediately starts to decrease and reaches a plateau around 30 minutes after antagonists perfusion.

5.3.4 Effect of D1-like and D2-like receptors antagonists on evoked PrL response.

In order to evaluate the involvement of the dopaminergic pathway between the cerebellum and the mPFC in our conditions, the effect of selective antagonists for dopaminergic receptors was investigated. The experiments were carried out using the same procedures described previously. The activity of the recorded units was monitored for 20 minutes and subsequently D1-like, and D2-like receptors antagonists (SCH23390 hydrochloride 44mM, (S)-Sulpiride 36 mM) were co-perfused on the PrL surface. The activity of single units was recorded for an additional 40 minutes. In 11 out of 26 PrL units, D1-like and D2-like dopamine receptors blockade induced a significant increase in spontaneous activity (after 20 min from drugs perfusion: +88.1±14.2 %, p=0.0015). Conversely, in 15 out of 26 PrL neurons, D1-like and D2-like antagonists perfusion caused a decrease in spontaneous firing (-62.11±6.07%, p=0.007). This might reflect the different distribution of D1-like and D2-like receptors among PrL

neuronal subpopulations. The evoked inhibitory responses in PrL were not abolished by the selective dopamine receptors antagonists (Fig.5.7)

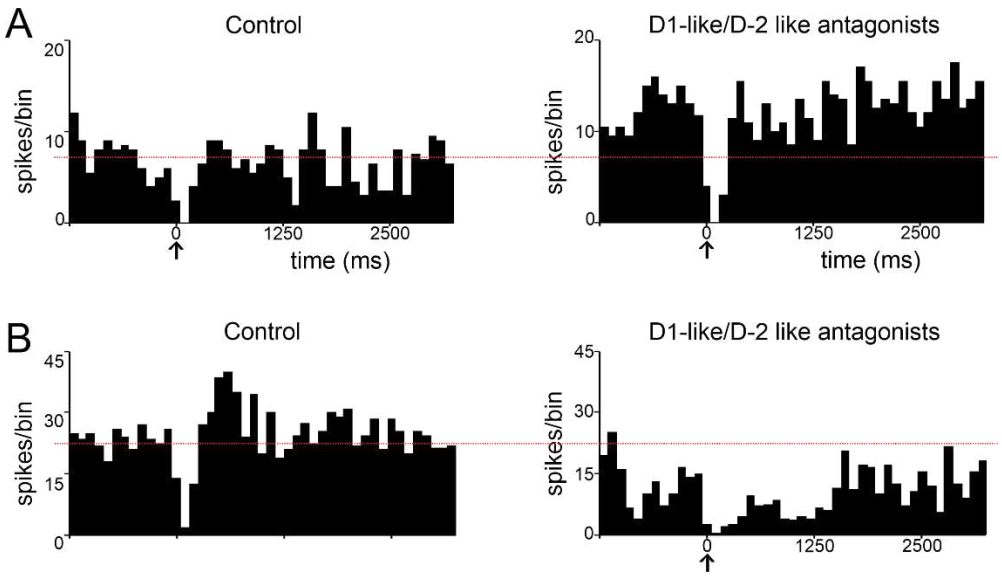

Figure 5.7| Comparative examples of PSTHs of PrL responses before and 20 minutes after D1-like and D2-like receptors antagonists perfusion. The PSTHs show that evoked inhibitory responses are not abolished by drugs application while basal frequency is either increased **(A)** or decreased **(B).**

The changes in the basal frequency brought about a parallel change in the pause depth (Fig. 5.8A) as evident by a strong linear correlation between the two parameters, as shown in Fig. 5.8B.

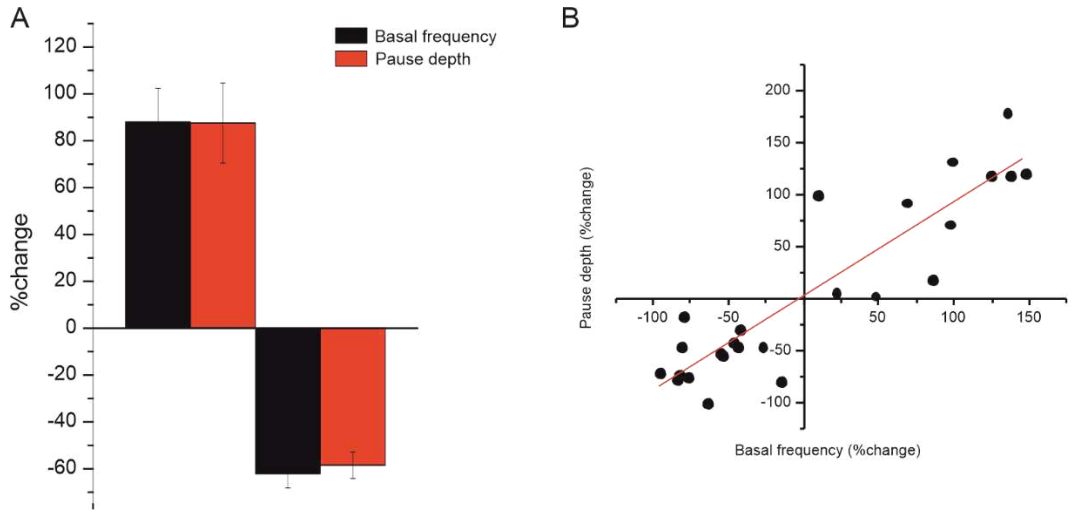

Figure 5.8| Basal frequency changes following D1-like and D2-like antagonists perfusion. A) The histograms show the % changes in basal frequency and pause depth for increases (*left*) and decreases (*right*). **B)** The plot shows the positive correlation between changes in PrL neurons basal frequencies and response amplitude following D1-like and D2-like antagonists perfusion (R^2=0.8195, n=26).

To evaluate whether DN stimulation evoked a transient dopaminergic effect in the PrL, not evident during the pause response due to the suppressed firing, we carefully checked the unit basal frequency immediately before and after DN stimulation during the control period (before dopaminergic receptors blocker perfusion; see B1 and B2 time windows in Fig. 5.9 box). The B2/B1 ratio is expected to reflect a possible change induced by cerebellum-dependent dopamine release. This ratio in then compared to the changes in the basal frequency of the same unit determined by dopamine receptor antagonists. The normalized changes of B2/B1 ratio and basal frequency after dopamine receptors blockade is reported in Figure 5.9, both for units showing a basal frequency increase and for units showing a basal frequency decrease (increase n=10, p=0.002; decrease n=14, p=0.02). As expected, if DN stimulation evoked dopamine release, the units showing an increase in basal firing after dopaminergic block were characterized by a B2<B1 ratio. That is, dopamine release determines a decrease in basal firing, confirmed by the increase obtained after blocking dopaminergic receptors. This effect was more evident for increases than for decreases, probably reflecting the different D1-like and D2-like receptors affinity (see Discussion). Considering the significant change in basal frequency before and after DN stimulation and the comparison with the effect of dopaminergic block, our data strongly stand for dopamine release during cerebellar stimulation in our experimental conditions.

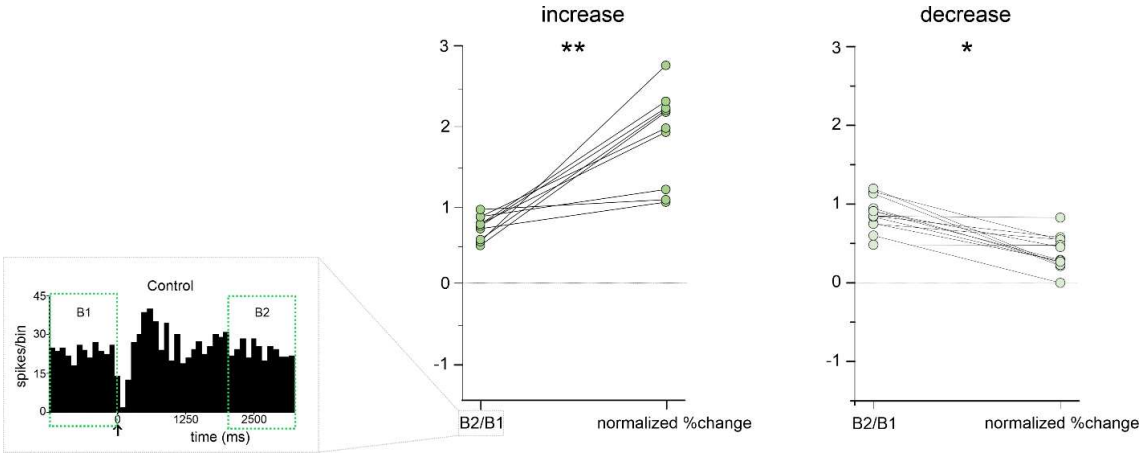

Figure 5.9| Correlation between B2/B1 ratio and the normalized percent change of basal frequency after blocking D1/D2 receptors for both the increase (*left*) and decrease (*right*) groups. The the box shows how B1 and B2 were calculated. * p<0.05; ** p<0.01.

5.3.5 Effect of subsequent D1/D2-like receptors antagonists and $GABA_A$-receptor antagonist on evoked PrL responses

Lastly, we investigated whether the dopaminergic-mediated effectscan influence the GABAergic contribution to the PrL units responses after DN stimulation. Indeed, the two systems are strictly interconneted to maintain the correct E/I balance in the mPFC (Di Domenico and Mapelli 2023). To this end, the activity of the PrL units were recorded for 20 minutes whilst stimulating the DN. Then D1-like and D2-like receptor antagonists were co-perfused onto the PrL surface and the activity of the neurons was recorded for 40 minutes. Finally gabazine was perfused on the PrL surface and the activity of the units was recorded for other 30 minutes. The combined effect of D1/D2-like receptor antagonists and gabazine was evaluated in 21 units. As evident in figure 5.10A, the pause suppression and the increase of firing, characterizing the effect of gabazine perfusion alone, did not occur when gabazine perfusion was preceeded by the blockade of D1-D2-like receptors. In particular, our results show that the effect of GABA-A receptor block on the pause was correlated with that of D1-D2 receptor block on background frequency (Fig. 5.10B).

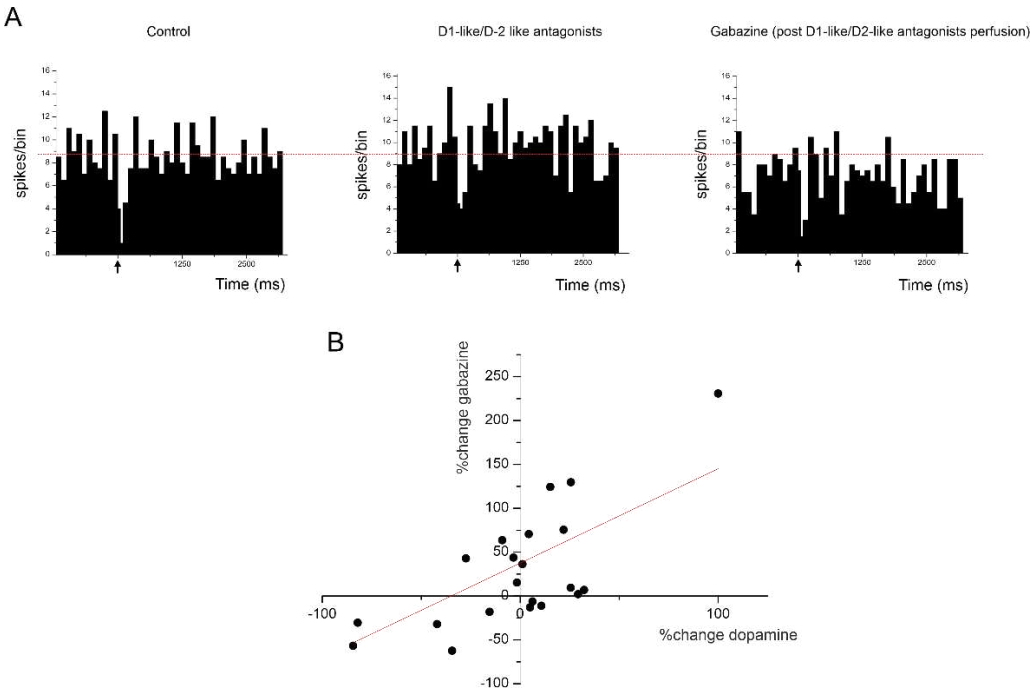

Figure 5.10|Responses after subsequent superfusion of D1/D2 like receptors antagonist and gabazine. A) examples of PSTHs responses in control condition, after 20 minutes of dopamine receptors antagonists superfusion and $GABA_A$ receptor antagonist (gabazine) perfusion. The pause, which was abolished in gabazine only condition, is still present when blocking $GABA_A$ receptor after dopamine receptors blockade. B) correlation plot of % change of basal frequency after blocking dopamine receptors (% change dopamine) and $GABA_A$ receptor (% change gabazine) (R^2=0.56, p(f)=0.003)

5.4 Discussion

The units recorded in the PrL showed spontaneous activity and responded to the electrical stimulation of the DN. Every responding unit showed a decrease or suppression of the basal firing, evident as a pause in the PSTH. Some units also showed a burst following the pause, which had a rebound nature unveiled by the positive correlation between the pause depth and peak amplitude. Pyramidal cells represent the 80-90% of the total neuronal population in the mPFC, whilst the remaining 10–20% consists of inhibitory GABAergic interneurons (Ascoli et al. 2008; Defelipe et al. 2013; Riga et al. 2014). Following these considerations, and taking into account the smaller soma of interneurons, recording electrodes lowered into the PrL had a much higher probability to detect pyramidal neurons activity rather than that of local interneurons.

The nature of the response was investigated pharmacologically by using antagonists of GABA-A, glutamatergic AMPA and NMDA, D1-like and D2-like dopaminergic receptors. This approach considered the thalamic and dopaminergic pathways connecting the cerebellum and the mPFC, and local inhibition. Our results revealed that cerebellar stimulation negatively modulates PrL firing, most likely acting through local inhibitory circuit, and influences dopamine release thus affecting the signal-to-noise ratio of signal transmission in the cortical network. Moreover, the dopaminergic system influences PrL neurons response to GABAergic inhibition, unravelling a complex interplay between these two systems that relies on the dopaminergic receptor subtype expressed.

5.4.1 Nature of PrL neuron responses to DN stimulation

According to previous electrophysiological studies conducted in rodents *in vivo* (Watson et al. 2014), neuronal responses to DN stimulation occurred with a latency of about 13 ms. This estimate is compatible with the main pathways involved in cerebellum-mPFC connectivity. The primary targets of cerebellar projections include many subcortical regions such as the VTA and thalamic nuclei, which send connections to the mPFC. Other studies have shown the interconnection between the cerebellum and the basal ganglia, whose projections also reach the mPFC (Middleton and Strick 1994). Therefore, the existence of multiple pathways acting on the mPFC and involving projections deriving from the cerebellum could explain the different pharmacological effects observed in this study.

5.4.2 Inhibitory component in PrL neurons responses

The blockade of GABA-A receptors revealed the inhibitory nature of PrL response to DN stimulation. In particular, gabazine perfusion determined an almost complete suppression of the response and an increase in neuronal basal frequency, as expected if the response was mediated by local inhibition and a local inhibitory tone down-regulated PrL neurons basal discharge. Indeed, it has been reported that GABAergic synaptic inhibition within the PrL is mediated by thalamic projections activated by DN stimulation (Rogers et al. 2011). In particular, the MD thalamus is reported as the major contributor to glutamatergic projections reaching the mPFC and contacting inhibitory interneurons in cortical Layers III/V (Ferguson and Gao 2018). Though part of the glutamatergic fibres from the MD thalamus is also reported to directly excite pyramidal neurons in Layer V (Ferguson and Gao 2018), we never observed a burst response in the recorded units. The burst that sometimes followed the pause disappeared after gabazine perfusion, confirming its rebound nature. Our data support the impact of inhibitory interneurons on overall cortical activity, which is prominent in determining the E/I balance through feedforward inhibition and gain control on pyramidal neurons firing (Ferguson and Gao 2018).

Herein, the activation of cortical inhibitory interneurons via the cerebello-thalamic pathway might provide a plausible explanation to the inhibitory response detected in PrL following DN stimulation. Therefore, a reasonable explanation of our data is that the impact of cerebellar activation on PrL activity is mainly exerted through the activation of inhibitory cells regulating pyramidal neurons activity.

5.4.3 Glutamatergic component of PrL activity

We then tested the influence on PrL responses exerted by the glutamatergic system. Considering the probable role of excitatory inputs to PrL interneurons to drive pyramidal neurons inhibitory response, we expected that AMPA and NMDA receptors blockade could impact on, or directly abolish, PrL responses to DN stimulation.

However, our results show that PrL neuronal basal firing depends on the glutamatergic input and the blockade of glutamatergic receptors caused an almost suppression of the firing. Therefore, it was not possible to evaluate a specific effect on the response to DN stimulation. However, these data are in agreement with previous reports of decreased spontaneous

activity in PFC pyramidal cells when NMDA and AMPA receptors are blocked (Rotaru et al. 2011). Our results support the hypothesis that the glutamatergic input is needed to generate spontaneous firing in pyramidal cells. Overall, the glutamatergic connection seems to have a dual contribution: an indirect one, determining the activation of inhibitory interneurons inducing the pause of pyramidal cells basal frequency; and a direct one, being needed to spontaneous activity generation in pyramidal cells.

5.4.4 Dopaminergic modulation of PrL activity and response to DN stimulation.

In urethane anesthetized mice, the electrical stimulation of the DN exerts a modulatory action on mPFC neurons, mediated by the release of dopamine through the VTA-mediated pathway (Rogers et al. 2011). Dopamine plays its role in neuromodulation by influencing both intrinsic excitability and membrane input resistance. In this way, the spontaneous and evoked activity of PrL neurons is facilitated or suppressed, affecting the signal-to-noise ratio of synaptic transmission at these relays.

Our results suggest that most of the dopaminergic contribution to the activity of PrL leads to substantial changes in the basal firing of responsive neurons. In particular, an increase or a decrease in the basal firing rate was observed in all recorded units. This is in agreement with dopamine impact on intrinsic cellular excitability. Co-perfusion of both D1-like and D2-like receptor antagonist drugs did not abolish the responses of recorded neurons, supporting the hypothesis that dopamine released at the PrL level may modulate neuronal responses evoked by DN stimulation, probably acting on intrinsic excitability. Our data are also compatible with a transient dopamine release during DN stimulation.

Many studies conducted *in vivo* indicate that the increase or decrease in the activity of pyramidal neurons and local inhibitory interneurons in the PrL is determined by the involvement of multiple receptor classes and subtypes, including dopaminergic D1-like and D2- like receptors, heterogeneously distributed at the level of cortical neuron subpopulations (Gulledge and Jaffe 1998; Parfitt, Gratton, and Bickford-Wimer 1990; Seamans, Durstewitz, et al. 2001; Sesack and Bunney 1989)). These two receptor sub-families usually mediate opposite effects on neuronal activity, explaining the diverse effects of dopaminergic receptors antagonists on PrL neurons reported in our study.

5.4.5 Effect of combined dopaminergic and GABAergic systems on PrL neurons response to cerebellar stimulation.

As well reviewed in Di Domenico and Mapelli (2023) (chapter 4) the interplay between the dopaminergic and GABAergic system plays an important role in keeping the correct E/I balance in the mPFC. We investigated whether these two systems were influencing each other in our experimental setting. Our results show that, when blocking $GABA_A$ receptor after blocking D1-like and D2-like receptors, the effect is not the same as perfusing gabazine alone. Indeed, the pause does not completely disappear, and the basal frequency does not always increase, but the effect of gabazine depend on that obtained after blocking D1/D2-like receptors. Our results confirm the interplay between the dopaminergic and GABAergic system, and are in agreement with a prominent role of the dopaminergic receptor subtype in determining the final outcome of inhibition. In particular, D1-like receptors blockade triggers an intracellular pathway leading to a decrease in GABA release, thus a reduction in inhibitory post-synaptic currents (IPSC) generation and a consequent increase of the basal frequency of PrL pyramidal neurons (Seamans, Gorelova, et al. 2001; Seamans and Yang 2004). On the other hand, the blockade of D2-like receptors induces an increase in GABA release, leading to an IPSC increase and a reduction of the basal frequency of PrL pyramidal neurons (Chiu et al. 2010; Seamans, Gorelova, et al. 2001; Seamans and Yang 2004). These two effects are evident in the correlation plot in Fig. 5.10B, where the percent change of the basal frequency of recorded neurons is compared in the two conditions (i.e., the blockade of dopaminergic receptors and GABA receptors). Indeed, the top-right section of the plot can be attributed to the blockade of D1-like receptors leading to a reduction of GABA release. Thus, a further block of $GABA_A$ receptors would enhance the IPSC decrease. On the other hand, at the bottom-left section of the plot, we can speculate that gabazine cannot overcome the inhibition enhancement induced by the blockade of D2-like receptors.

5.4.6 Possible pathways involved in DN modulation of PrL

The cerebellum affects neuronal activity in the mPFC through different pathways (Fig. 5.11) mainly involving the VTA or the thalamus (Rogers et al. 2011; Schmahmann 1996). The inhibitory responses recorded in PrL neurons following DN stimulation might be evoked via the thalamic pathway indirectly promoting pyramidal neurons inhibition through local inhibitory interneurons activation. This pathway could also directly affect pyramidal neurons

regulating their firing via glutamatergic transmission, though this was not evident in our recordings.

Dopamine release in the mPFC following cerebellar activation mainly derives from the VTA pathway (Rogers et al. 2011). Interestingly, both the electrical stimulation of the VTA and local perfusion of dopamine were reported to inhibit spontaneous activity in most mPFC neurons (Pirot et al. 1992). This observation is compatible with the case of increases in PrL neurons firing following blockade of D1-like and D2-like receptors observed in our recordings. Nevertheless, we also observed a decrease of PrL neurons basal firing in the same conditions, probably reflecting the different distribution of dopaminergic receptors among PrL neurons.

DN connection with both VTA and MD thalamus, then projecting to the mPFC, suggests that these pathways are most likely involved in cognitive functions. In particular, the prominent MD innervations over the mPFC play a fundamental role in cognitive processes (Parnaudeau, Bolkan, and Kellendonk 2018). Remarkably, reduction of E/I balance in mPFC due to the increase in cortical interneurons excitability is reported to impair working memory, cognitive flexibility and social interaction (Ferguson and Gao 2018).

Since our data support the hypothesis that cerebellar stimulation provides inhibition of PrL neurons activity, it is reasonable to consider the cerebellum as involved in the regulation of the E/I balance in the cortical network. Hence, the functional role of the cerebellum in cognition gains a prominent value considering the global effects exerted by inhibitory pathways over mPFC correct functioning.

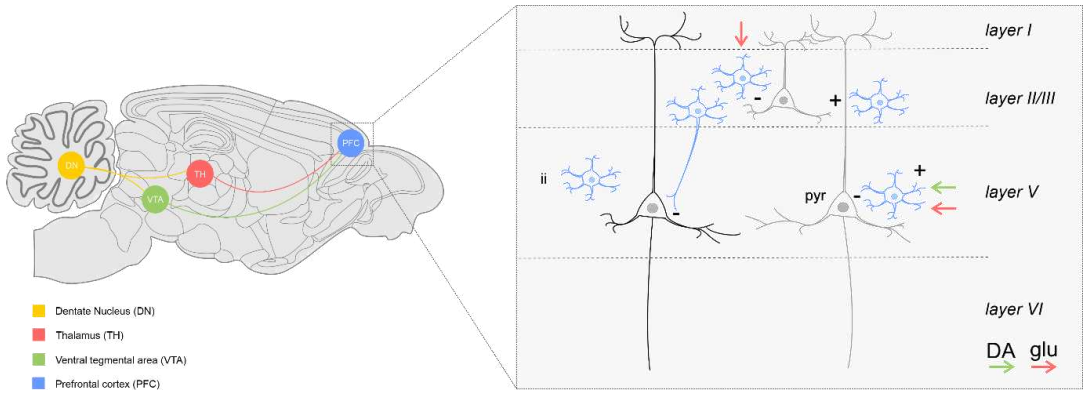

Figure 5.11| Possible pathways involved in the DN modulation of PrL. The DN is connected to the PrL via two pathways. The glutamatergic one (*red arrows*), passing through the thalamus, contacts both the inhibitory interneuron (ii), inducing the pause response in the recorded units of the PrL, and the pyramidal neurons (pyr), contributing to their spontaneous firing. The dopaminergic pathway (*green arrow*), passing through the ventral tegmental area (VTA) has a neuromodulatory effect on the PrL pyramidal neurons increasing or decreasing their basal frequency.

5.5 Conclusions and future perspectives

The present study shows that the cerebellum may have indeed a prominent role in regulating activity of cortical areas involved in cognitive functions and provides new insights for understanding neuronal mechanisms underlying cognitive processes related to cerebello-prefrontal interactions. However, although electrical stimulation is widely employed in brain research, it has to be considered that it might lack specificity, due to current spread and *en passant* fibre activation, and its effect might be associated with either modification in local neural activity as well as changes spreading within the entire neural network (Trevathan et al. 2021). For these reasons, the next step in the characterization of cerebello-prefrontal physiological interaction should include optogenetics. The virally driven expression of light-sensitive ionic channels specifically onto cerebellar projections to MD thalamus or VTA, would allow the selective activation of separate cerebellar pathways involved in modulation of mPFC activity, thus giving a better characterization of the cerebellar role in cognitive processes and overall brain functioning.

Chapter 6

Hyperexcitability and altered functional connectivity in a mouse model of autism: focus on the cerebello-prefrontal cortex interaction.

In preparation

In collaboration with:

Eleonora Pali, Maria Conforti, Ileana Montagna, Simona Tritto, Egidio D'Angelo, Francesca Prestori and Lisa Mapelli

Author contribution: DDD performed *in vivo* data analysis, wrote the manuscript, and prepared the figures; EP performed patch-clamp recordings and analysis; MC performed part of the *in vivo* data analysis; IM performed *in vivo* experiments; ST performed histology, image analysis, and genotyping; ED and FP coordinated the work; LM performed VSDi experiments, coordinated the work, and wrote the manuscript.

6.1 Introduction

Autism spectrum disorders (ASDs) are developmental disorders characterized by impaired social interactions and by the presence of repetitive behaviour. Since this disorder is a spectrum, it covers a long range of clinical conditions, varying from hypofunctional to hyperfunctional, and it is also associated to alterations at different brain areas. The prefrontal cortex (PFC) is commonly associated to ASDs but several evidence hint for a cerebellar the involvement (Amaral 2011; Betancur 2011; Ellegood et al. 2015). Indeed, cerebellar impairment has been linked to various ASDs forms, such as Phelan–McDermid, Fragile X, Tuberous Sclerosis, and Rett syndrome (for review, see Allen 2006; D'Angelo and Casali 2012; Hampson and Blatt 2015; Ito 2008; Mosconi et al. 2015; Schmahmann 2004; Zeidán-Chuliá et al. 2016).

ASDs are often associated with microcircuits alterations, caused by mutations in gene coding for synaptic proteins (Banerjee, Riordan, and Bhat 2014; Kim, Lim, and Kaang 2016; Qiu, Aldinger, and Levitt 2012; De Rubeis and Buxbaum 2015). This leads to hyper-reactivity to

stimulation, accompanied by altered neuronal excitability and synaptic plasticity, related to increased glutamatergic transmission (Markram et al. 2008; Markram and Markram 2010; Rinaldi, Perrodin, and Markram 2008); dysregulation of the excitation (E)/inhibition (I) balance related to various alterations at excitatory and inhibitory synapses (Gogolla et al. 2009; Rubenstein and Merzenich 2003; Uzunova, Pallanti, and Hollander 2016); and altered modular organization of microcircuits (Casanova 2003, 2006; Hutsler and Casanova 2016; Soda et al. 2019) related to reduced lateral inhibition, bringing about changes in the spatial organization of neuronal activation and synaptic plasticity in the neocortex. In particular, the altered spatial organization of activity reported by Casanova's group consists in a shift of the E/I balance from the classical Mexican hat profile (excitation in the centre, surrounded by lateral inhibition) to the so-called stovepipe hat shape (larger cores of excitation with little or no inhibition in the surrounds (Casanova, 2003, 2006; Soda et al., 2019).

In particular, an important role in synaptic and microcircuit dysregulation has been attributed to NMDA receptor hyperfunction (Rinaldi et al. 2007). One of the autistic mouse models that present an increase in NMDA mediated currents in cerebellar granule cells (GrCs) is the IB2 KO mouse model. The IB2 gene codes for a protein present in both neurons and pancreatic cells. In the brain, the IB2 protein is mainly found in the postsynaptic densities (PSDs) of the cerebral and cerebellar cortices and, in particular, a high concentration of this protein has been found in the PSDs of cerebellar glomeruli (Giza et al. 2010). Mice lacking IB2 showed increased NMDA receptors-mediated currents, indicating that IB2 plays a crucial role in glutamatergic synaptic neurotransmission.

Moreover, these mice display autistic-like behavioural deficits, and the IB2 gene is co-deleted with Shank3 in almost all the cases of Phelan–McDermid syndrome (Kolevzon et al. 2014; Manning et al. 2004; Phelan 2008; Soorya et al. 2013), a disease in which autistic symptoms are associated to cerebellar deficits such as impaired motor performance and learning (Giza et al. 2010). Patch clamp recordings and voltage sensitive dye imaging (VSDi) have shown that the granular layer of IB2 KO mice is characterized by hyperexcitability and hyperplasticity leading to an increase in the E/I balance and an altered shape of the centre/surround structures emerging in the granular layer after mossy fibres stimulation (Soda et al. 2019).

Recently, the connections between the PFC and the cerebellum gained attention in ASD research. The cerebellum can influence the PFC via two main pathways, one passing through

the VTA, and the other passing through the thalamus. Recent findings have highlighted that the stimulation of the cerebellar dentate nucleus (DN) in C57BL/6 mice has an impact of mPFC neurons activity, specifically inhibiting the spontaneous activity of the recorded neurons (Di Domenico et al. in preparation, chapter 5).

Herein, we characterized IB2 KO mice PrL neurons, compared to those of WT littermates, using various techniques. First, we used voltage sensitive dye imaging on acute brain slices to assess the E/I balance in response to electrical stimulation of the cortical inputs. Then, we used patch clamp to assess the electrophysiological properties and responsiveness of layer V pyramidal neurons. Finally, we used *in vivo* single unit recordings of PrL pyramidal neurons whilst electrically stimulating the DN to assess the cerebellar contribution to the PrL activity.

6.2 Materials and methods

All procedures were conducted in accordance with European Guidelines for the Care and Use of Laboratory Animals (Council Directive 2010/63/ EU) and approved by the Ethical Committee of Italian Ministry of Health (637/2017-PR and 577/2018-PR)).

6.2.1 Genotyping and maintenance of IB2 KO mice.

Experiments were conducted on IB2 $^{+/+}$ [wild-type (WT)] and IB2 $^{-/-}$ (KO) mice obtained by crossing IB2 $^{+/-}$ parents, since IB2 KO are poor breeders, possibly reflecting the social deficit associated with IB2 deletion (Giza et al. 2010; Soda et al. 2019). The genotyping was conducted through PCR using four primers to detect wild-type and null alleles, as previously described (Giza et al. 2010; Soda et al. 2019).

6.2.2 Slice preparation and solutions.

Both the VSDi and the patch clamp recordings have been conducted on 17- to 24-days-old (postnatal day 0 = day of birth) WT and IB2 KO mice of either sex. Mice were anesthetized with halothane (Sigma-Aldrich) and killed by decapitation to remove the brain for acute slice preparation. Coronal sections (270 µm) containing the prelimbic mPFC (PrL) were cut in ice-cold Krebs' solution bubbled with carbogen gas (95% O_2/5% CO_2) containing the following (in mM): 120 NaCl, 2 KCl, 1.2 $MgSO_4$, 26 $NaHCO_3$, 1.2 KH_2PO_4, 2 $CaCl_2$, and 11 glucose. Slices were allowed to recover at room temperature for at least 1 h, before being transferred to a recording chamber mounted on the stage of an upright microscope (Olympus). The slices

were perfused with oxygenated Krebs' solution and maintained at 32°C with a Peltier feedback device (catalogue #TC-324B, Warner Instruments). The $GABA_A$ receptor antagonist gabazine (10μM, Abcam) was added to the Krebs' solution in certain experiments, as specified.

6.2.3 Voltage Sensitive Dye imaging (VSDi).

The stock solution for voltage-sensitive dye imaging (VSDi) contained the dye Di-4- ANEPPS (Invitrogen) dissolved in a solution based on Krebs' solution containing 50% ethanol (Sigma-Aldrich) and 5% Cremophor EL (Sigma-Aldrich). Slices for optical recordings were incubated for 30 min in oxygenated Krebs' solution added to a 3% Di-4-ANEPPS stock solution and mixed with an equal volume of foetal bovine serum (Invitrogen) to reach a final dye concentration of 2 mM (Soda et al. 2019; Vranesic et al. 1994). After incubation, the slices were rinsed with Krebs' solution to wash out the dye that was not incorporated by the tissue, before being transferred to the recording chamber installed on an upright epifluorescence microscope (SliceScope, Scientifica), equipped with a 4x objective (XLFluor4x/340, 0.28 numerical aperture, water-immersion; Olympus). The light generated by a halogen lamp (10 V, 150 W; model LM150, MORITEX) was controlled by an electronic shutter (Newport), and then passed through an excitation filter (λ=535±20 nm), projected onto a dichroic mirror (λ= 565 nm), and reflected toward the objective lens to illuminate the specimen. Fluorescence generated by the tissue was transmitted through an absorption filter (λ>580 nm) to the CCD camera (MICAM01, SciMedia/Brain Vision). The whole imaging system was connected through an input/output interface (Brain Vision) to a PC controlling illumination, stimulation, and data acquisition. The final pixel size was 21.4 x 21.4 μm with a 4x objective. Full-frame image acquisition was performed at 0.5 kHz. Data were acquired and displayed using Brain Vision software, and signals were analysed using custom made routines written in MATLAB (MathWorks). At the beginning of recordings, a calibration procedure was adopted to ensure homogeneity across experiments. The dynamic range of the CCD camera was calibrated by measuring background fluorescence and setting the average light intensity in the absence of stimulation to 50% of the saturation level. The background fluorescence was sampled for 50 ms before triggering electrical stimulation and was used to measure the initial fluorescence intensity (F_0). The relative fluorescence change ($\Delta F/F_0$) was then calculated for each time frame. The signal-to-noise ratio was improved by averaging 80 consecutive trials. The

electrical stimulation was performed with a bipolar tungsten electrode positioned on the white matter bundle below layer VI and connected to a stimulator unit through a stimulus isolation unit. The stimulation protocol consisted of 5 pulses delivered at 50 Hz and repeated every 10s.

6.2.4 VSDi data analysis.

Fluorescence data collected by Brain Vision acquisition software were filtered using both a cubic filter (3x3) and a spatial filter (3x3) embedded in the software, and then were exported and processed in MATLAB. The resulting files were a series of matrices each representing a temporal frame of the acquired trace. Using appropriate MATLAB routines written ad hoc, single matrices representing the signal area during the stimulation were obtained for all the cortical layers. For the analysis of the E/I balance and spatial distribution of excitation and inhibition in the PrL, the stimulation of the white matter bundle below layer VI was repeated in control and during gabazine perfusion. This approach allowed reconstructing the map of regions with prevailing E compared to regions showing prevailing I (Gandolfi et al. 2014; J. Mapelli and D'Angelo 2007; Soda et al. 2019). In this case, the E map was constructed on the control responses (where the response is available only in the regions where excitation prevails over inhibition), while the I map was constructed subtracting the maps after gabazine perfusion to the control maps (unveiling the regions where, before gabazine perfusion, excitation was prevented by inhibition). Both E and I maps were normalized to 1, and the E/I balance maps were obtained as (E-I)/E. The average E/I map was constructed using 5 WT and 6 KO slices, aligning the single maps starting from layer I. Data are reported as mean $\pm$ SEM (standard error of the mean) and statistical significance was assessed using paired or unpaired Student's *t* test.

6.2.5 Whole cell patch clamp recordings.

Whole-cell patch clamp recordings were performed with Multiclamp 700B amplifier [3 dB; cut-off frequency (fc),10 kHz], sampled with Digidata 1440A interface, and analysed off-line with pClamp10 software (Molecular Devices). Patch pipettes were pulled from borosilicate glass capillaries (Sutter Instruments) and filled with an intracellular solution containing (mM): 145 potassium gluconate, 5 KCl, 10 HEPES, 0.2 EGTA, 4.6 MgCl2,4 ATP-Na_2, and 0.4 GTP-Na_2, adjusted at pH 7.3 with KOH. In each recording, the current transients elicited by 10 mV

hyperpolarizing pulses from the holding potential of -70 mV in voltage-clamp mode returned a biexponential relaxation, with a major component related to a somatodendritic charging. The major component was analysed to extract basic parameters useful to evaluate the recording conditions and to compare different cell groups. Membrane capacitance (Cm) was measured from the capacitive charge (the area underlying current transients), and Rs was calculated as Rs = τ_{vc} /Cm; τ= voltage-clamp time constant. The membrane resistance (Rm) was computed from the steady-state current flowing after termination of the transient. The 3 dB fc of the electrode-cell system was calculated as voltage-clamp cut-off frequency (f_{vc}) = $(2\pi \times \tau_{vc})^{-1}$. The data are reported in Table 6.1.

	WT (n=7)	KO (n=8)
C_m (pF)	112.72 ± 9.55	100.81 ± 9.84
R_s (MOhm)	2.91 ± 0.93	2.87 ± 0.33
R_{input} (MOhm)	139.99 ± 27.31	158.15 ± 22.90
f_{vc} (KHz)	0.54 ± 0.05	0.62 ± 0.06

Table 6.1| Electrophysiological properties of layer V pyramidal neurons. The data were obtained using K-gluconate intracellular solution and analysing current transient elicited by 10 mV voltage clamp steps delivered from the holding potential of -70 mV. No significant differences were found between IB2 WT and KO layer V pyramidal neurons (unpaired Student's *t* test).

6.2.6 Layer V pyramidal neurons excitability.

Patch pipettes had 3-5 MΩ resistance before seal formation. Just after obtaining the cell attached configuration, electrode capacitance was carefully cancelled to allow for electronic compensation of pipette charging. At the beginning of each recording, a series of depolarizing steps was applied in voltage clamp to measure the total voltage-dependent current of the pyramidal neurons. Leakage and capacitance were subtracted using hyperpolarizing pulses delivered before the test pulse (P/4 protocol). After switching to current clamp, intrinsic excitability was investigated by setting resting membrane potential at -80 mV and injecting 1 s current steps (starting at -50 pA with 25 pA increment every 5s). The membrane potential during current steps was estimated as the average value between 800 and 1000 ms. Action potential frequency was measured by dividing the number of spikes by step duration.

6.2.7 In-vivo electrophysiological recordings.

Multiple single units recording was performed in the PrL of IB2 WT and KO mice of both sexes (30.0±0.2 days old; WT n=6; KO n=9) under urethane anaesthesia. In particular, urethane has minimal effects on glutamatergic and GABAergic receptors (Hara and Harris 2002), making it unlikely to impact stimulus-evoked responses in mPFC neurons during our recordings.

6.2.8 Surgical procedures

Urethane was dissolved in saline solution (1.3g/kg urethane in 0.9% NaCl, Sigma Aldrich) and was administrated through intraperitoneal injections. Thirty minutes after the first injection, 3-4 booster injections (10% of the induction dose) were administered to maintain deep anaesthesia. To ensure the correct anaesthesia, the leg withdrawal reflex after pinching and the presence of spontaneous whisking were tested. The mice were then placed on a custom-built stereotaxic table covered with a heating plate to maintain the body temperature at 36°C. Lidocaine (0.2ml; AstraZeneca) was subcutaneously applied to reduce cutaneous reflexes.

Then, the skull was exposed, and the mouse head was fixed to a metal bar connected to a pedestal anchored to the stereotaxic table. The skin and muscles were removed surgically, and craniotomy was performed over the cerebellum and mPFC to expose their surface and place the electrodes. The coordinates used for the electrode placement were as follows: for cerebellum (from Bregma, DN: -5.8 AP, +2.5 ML, +2.4 DV); for mPFC (PrL: +2.8 AP, 0.25 ML, +0.6 DV). The dura mater was carefully removed, and the surface was perfused with a saline solution (NaCl 0.9%; Sigma Aldrich) to prevent drying.

6.2.9 In vivo electrophysiological recordings

Quartz-coated platinum/tungsten electrodes (1-5MΩ; Thomas Recording GmBh, Giessen, Germany) were arranged in a 4x4 Eckhorn Matrix and placed over the exposed mPFC area, contralaterally to the stimulus source. Each recording electrode was independently moved and inserted to reach the PrL at a depth of 703. 6 ± 135.4 µm. The electrophysiological signals were recorded at 25 kHz, amplified, and digitized with a 300-5000 Hz band-pass filter using a RZ5D processor multi-channel workstation (Tucker-Davis Technologies, Alachua, FL, USA). At the end of each experiment, the exact location of the electrodes in PrL and DN was identified through histological tissue processing after electric lesions.

6.2.10 Electrical stimulation

Electrical stimulation of DN was performed by applying 21 pulses at 100Hz and 100 µA, repeated every 5 s, using a bipolar tungsten electrode (0.5 MΩ; World Precision Instruments Inc, Sarasota, FL, USA) connected to a stimulator unit through a stimulus isolator. The stimulating electrode was mounted on a Patch-star micromanipulator (Scientifica, Ltd) and precisely lowered into the cerebellum to a depth of 2600 µm from the surface to stimulate the DN. Once a PrL neuron was detected, spontaneous activity was recorded for 5 minutes, followed by control recording during cerebellar stimulation to characterize the evoked response patterns in PrL neurons.

6.2.11 Pharmacology

All drugs were added to a Krebs' solution with the following composition (in mM): 120 NaCl, 2 KCl, 1.2 $MgSO_4$, 26 $NaHCO_3$, 1.2 KH_2PO_4, 2 $CaCl_2$, and 11 glucose. This solution was perfused onto the PrL surface through a micropipette and was equilibrated with 95% O2-5% CO2 to maintain a pH of 7.4.

The pharmacological protocol was performed as follow: after 20 minutes of control recordings, selective dopamine receptor antagonists SCH23390 hydrochloride (selective D1-like receptor antagonist, 44 mM; Abcam) and (S)-Sulpiride (selective D2-like receptor antagonist, 36 mM; Abcam), were co-perfused onto the PrL surface. The effects of these selective antagonists on PrL response pattern during DN stimulation were monitored for at least 20 minutes during which the same pattern of electrical stimuli was delivered to the DN. Then, the selective $GABA_A$ receptor antagonist gabazine (SR-95531, Abcam, 3 mM; Kurt et al., 2006) was perfused onto the mPFC surface immediately after control recordings. PrL neuron activity was then recorded for 30 minutes after drug perfusion, during which the same pattern of electrical stimulation was delivered to the DN.

6.2.12 Histology

Histological examination was used to confirm the exact placement of the recording and stimulating electrodes in PrL and DN, respectively. After each experiment, a 20 µA current was applied for 20 seconds through the same electrodes used for electrophysiological recordings in the PrL to create an electric lesion. The stimulating electrode, positioned at the

level of DN, produced a discernible electrical signature to the tissue due to the current injection (100 µA) during experimental procedures. Following transcardial perfusion of Phosphate-Buffered Saline (PBS) solution and 4% formaldehyde, the mouse brains were fixed and cryopreserved. Histological sections of 20-µm thickness were obtained and stained with toluidine blue. The correct localization of the recording and stimulation sites was determined through histological analysis using an optical microscope.

6.2.13 Data Analysis

The electrophysiological signals from PrL neurons were acquired using OpenEx software (Tucker-Davis Technologies) and then analysed offline using SpikeTrain (Neurasmus BV, Rotterdam, Netherlands) running under MATLAB (MathWorks, MA, USA). To analyse PrL responses to DN stimulation, peri-stimulus time histograms (PSTHs) with 100 ms bin width were constructed. PSTH analysis revealed that the PrL response to DN stimulation reliably consisted in a pause, sometimes followed by bursts emerging from the background activity.

Latency and duration of the detected responses were estimated using 20ms bin width PSTHs. PrL responses were identified as pauses or peaks in PSTHs when values exceeded once the standard deviation of the basal frequency measured in the pre-stimulus period.

To evaluate the effects of selective antagonists on the detected responses, changes in pause amplitude in PSTHs with respect to control were compared. The effect of drug perfusion on PrL neuronal activity and responses was measured 30 minutes after drugs perfusion. Antagonist-mediated changes in neuronal responsiveness to cerebellar stimulation were detected as positive or negative changes compared to control. To test whether selective antagonists influenced the spontaneous firing rate and coefficient of variation of the inter-spike interval (CV2, which provides information about the spiking regularity), firing rate, inter-spike interval (ISI), and CV2 were measured after antagonist perfusion and compared to control measurements. Data were fitted using OriginPro8 (OriginLac co., MA, USA), and statistical analysis was performed using paired or unpaired Student's *t* test. All data are reported as mean ± SEM.

6.3 Results

6.3.1 Altered columnar organization of KO mice PrL

PrL network responses to electrical stimulation of input fibres was investigated using voltage sensitive dye imaging (VSDi) on acute brain slices from WT and KO IB2 mice. In particular, the distribution of excitation and inhibition in the network was evaluated by subtracting network activity in control and after blocking GABAergic inhibition through 10µM gabazine perfusion (see Methods for details). The stimulation of the white matter bundle below layer VI activated a columnar area covering all PrL layers. In particular, the excitatory/inhibitory (E/I) maps were characterized by a centre with prevailing excitation with lateral inhibition, shaping a columnar organization with the canonical Mexican hat profile (Fig. 6.1A). The reconstruction of the E/I maps in WT and KO PrL revealed an increased E/I ratio in KO PrL, characterized by an enhanced E in the centre and reduced lateral inhibition (Fig. 6.1A). Interestingly, the spatial profile shifted from the Mexican hat to the stovepipe hat shape (Fig. 6.1B), as predicted by anatomical observations of post-mortem ASDs brains (Casanova et al., 2006). In particular, the size of the central core of excitation of the cortical column doubled in KO compared to WT littermates (246±28µm n=5, and 399±41 µm n=6, in WT and KO, respectively; unpaired Student's t test p=0.025). The ratio between the area showing excitation and the area showing inhibition within the column was 2.30±1.05 in WT and 0.57±0.23 in KO (p=0.048). The altered E/I balance was most prominent in layer V, the main output layer of the mouse mPFC.

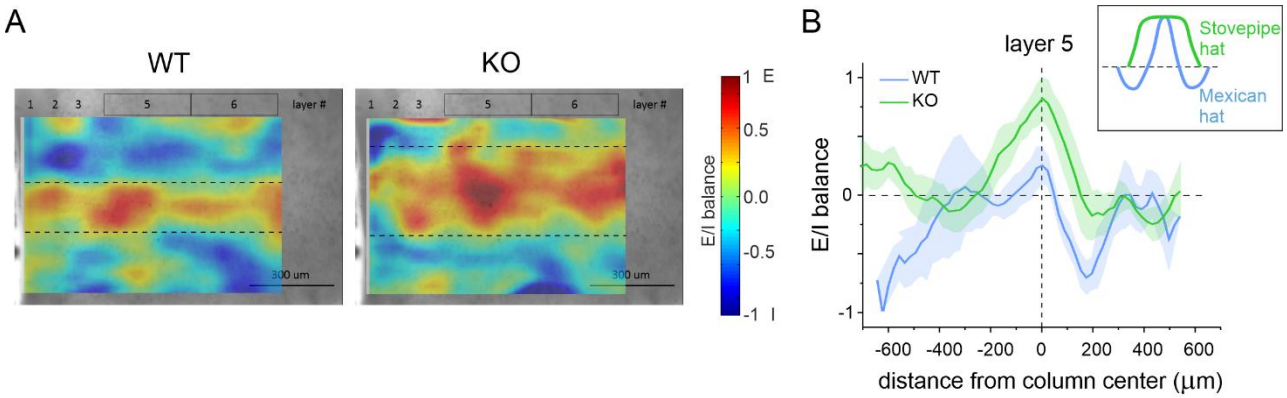

Figure 6.1| Excitatory/inhibitory balance and columnar organization in the granular layer. A) VSDi normalized maps showing the spatial distribution of excitation and inhibition in WT and IB2 KO prelimbic cortex (PrL). B) The plot shows the E/I balance as a function of distance from the centre for the maps shown in A. Note that in the IB2 KO PrL the excitation core is broader, while the inhibited surround is reduced, compared with the WT. This tends to shift from the typical Mexican hat shape in controls to the stovepipe hat shape in IB2 KO mice (inset).

6.3.2 Patch-clamp recordings

Considering the results described above, whole-cell patch-clamp recordings were performed on pyramidal neurons in layer V.

In whole-cell current clamp recordings, both IB2 WT and KO layer V pyramidal cells were silent at rest and responded to depolarizing current steps (from -50 pA with a 25 pA of increment) with spike discharges that increased their frequencies linearly with stimulus intensity.

IB2 KO layer 5 pyramidal neurons showed a larger increase of spike discharge compared to their WT littermates at both low current injection (200 pA: WT=4.7±2.2 Hz, n=6; KO=11.2±1.2 Hz, n=5; p=0.039) and high current injection (475 pA: WT=22.5±3.4 Hz, n=6; KO=33.2±3.8 Hz, n=5; p=0.041) shifting the frequency-intensity plot upward (Fig. 6.2A,B).

In the same experiments, whole-cell currents elicited by depolarizing voltage steps were recorded. The transient inward current density was significantly larger in IB2 KO with respect to the WT pyramidal neurons (WT=88.1±16.4 pA/pF, n=7; KO=152.2±21.5, n=8; p=0.037). On the other hand, the transient (A-type; WT=35.6±5.4 pA/pF, n=7; KO=37.0±3.9 pA/pF, n=8; p=0.83) and persistent outward (delayed rectifier; WT=25.4±5.2 pA/pF, n=7; KO=31.4±4.2 pA/pF, n=8; p=0.37) currents did not show any significant difference between the IB2 KO and their WT littermates (Fig. 6.2C).

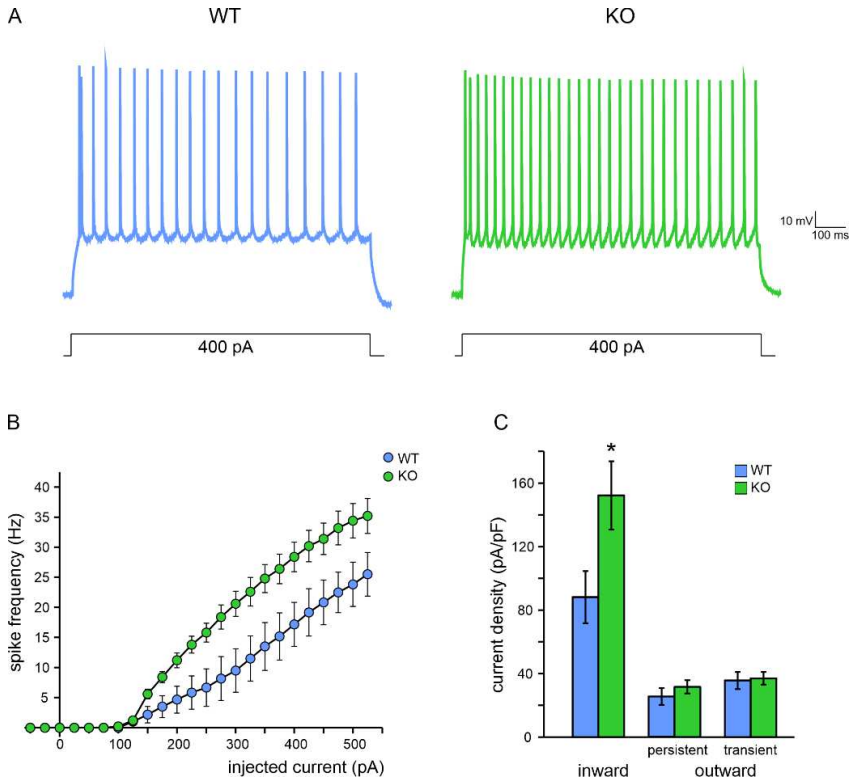

Figure 6.2|Layer V pyramidal cells electroresponsiveness. (A) Sample traces of two spike discharges related to IB2 WT (left) and KO (right) layer V pyramidal cells are represented. Voltage-responses were elicited from -80 mV using step current injection. **(B)** The plot shows the relationships between average spike frequency over 1 s and the injected current for IB2 WT (*blue*) and KO (*green*) layer V pyramidal cells. The average spike frequency was computed over 1s steps of injected current. Data are reported as mean ± SEM. **(C)** Voltage-activated inward and outward currents in layer V pyramidal cells of IB2 WT (*blue*) and KO (*green*). The histogram compares inward and outward current density normalized by membrane capacitance (Cm), measured at -40mV and +20mV in IB2 WT (*blue*) and KO (*green*).

6.3.3 In vivo single unit extracellular recordings

We recorded single units from PrL layer III/V of both IB2 WT (n=15) and KO (n=13) mice. The units recorded from the PrL of the WT group displayed a spontaneous activity of 1.11 ± 0.13 Hz, whilst the ones recorded from the KO group showed a spontaneous activity of 0.71 ± 0.11 Hz. KO units basal frequency was significantly lower than that of WT littermates (p=0.0376). Concerning PrL unit response to DN stimulation, the WT group showed a pause of -3.50±0.39 spikes/bin whilst the KO group responded with a pause of -2.53±0.34 spikes/bin (Fig. 6.3). Though KO PrL responses seemed consistently smaller, the difference was not statistically significant (p=0.06). This difference might be attributed to the lower basal firing of the KO group. The duration and latency of the response was not statistically different in WT and KO recordings. In particular, in the WT group the duration of the response was 180 ± 22 ms and

appeared with a latency of 13.8 ± 6.1 ms, whilst the KO group showed a response of 158 ± 26 ms duration that appeared after 21.3 ± 7.2 (unpaired Student's *t* test p=0.55; p=0.44, respectively).

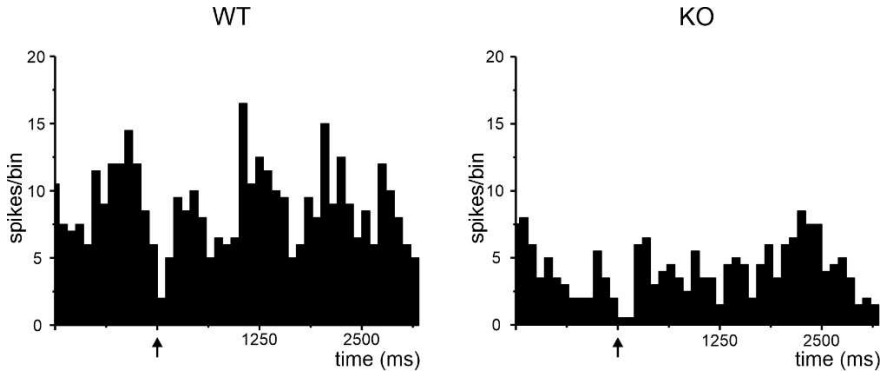

Figure 6.3| Examples of PSTHs of PrL response in IB2 WT (*left*) and KO (*right*) after DN stimulation. Notice the decrease of the basal frequency in response to DN stimulation and the decreased basal frequency in KO compared to WT neurons.

6.3.4 Effect of D1-like and D2-like receptors antagonists on IB2 WT and KO PrL.

Since the cerebellum is functionally connected to the PrL through a dopaminergic pathway, we investigated possible alterations of the dopaminergic modulation of the PrL in IB2 KO mice. To do so, PrL units activity and responses to DN stimulation were monitored for 20 minutes, before the co-perfusion on the PrL surface of D1-like, and D2-like receptors antagonists (SCH23390 hydrochloride, (S)-Sulpiride). The activity of single units was recorded for additional 40 minutes. In both IB2 WT and KO mice, the blockade of D1-like and D2-like receptors did not affect the response to DN stimulation as a pause, but the basal firing of the recorded units was indeed modified. In particular, the basal frequency of the recoded units of both WT and KO PrL showed either an increase or a decrease (WT n=4, percentage of increase= 106.4± 13.3, n=6 percentage of decrease= 19.0 ± 11.0; KO n=4, percentage of increase= 105.6± 55.6, n=5 percentage of decrease= -33.9 ± 15.2). The pause depth changes observed correlated well with the corresponding changes in basal frequency (WT n= 4, increase in pause depth=133.4 ± 22.5%, n=6, decrease in pause depth= -33.9 ± 15.2%; KO n=4 increase in pause depth= 87.4 ± 59.1%, n=5 decrease in pause depth= -40.2 ± 6.0%) as shown in figure 6.4. No significant difference was found between the KO and their WT littermates.

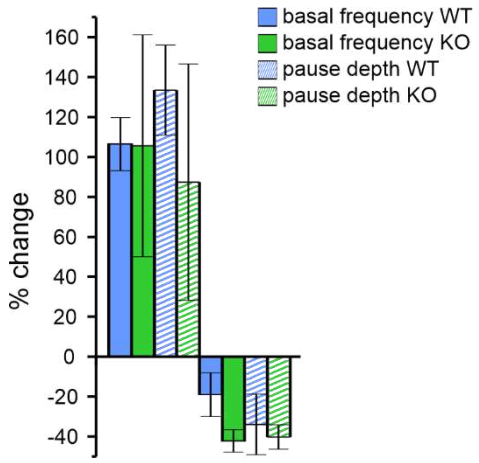

Figure 6.4| Histograms showing the percent change of the basal frequency and pause depth in IB2 WT and KO mice. The plot shows the effects of D1-like and D2-like receptor antagonists blockade on the basal frequency and pause depth in the Prelimbic cortex (PrL) units recorded during stimulation of the dentate nucleus (DN). Comparing the effects of this blockade in the pathological (IB2 KO) versus the control condition (IB2 WT), no significant differences were found.

6.3.5 Effect of $GABA_A$ receptor blockade on IB2 WT and KO PrL

Since the interplay between the GABAergic and the dopaminergic systems is fundamental in maintaining a good E/I balance in the mPFC (Di Domenico and Mapelli 2023, chapter 4), we tested whether this might be altered in the IB2 KO mouse model of autism. To this end, we perfused a $GABA_A$ receptor antagonist (gabazine) after blocking the D1-like and D2-like receptors. The activity of PrL neurons and their responses to DN stimulation were recorded in control, after blocking D1-like and D2-like receptors, and after blocking $GABA_A$ receptors. Gabazine perfusion determined an increase in the basal frequency of all the recorded units in both IB2 KO and WT (WT n=10, percent change of basal frequency after 30 minutes of gabazine superfusion= 157.4±53.4 %; KO n=7, percent change of basal frequency after 30 minutes of gabazine superfusion = 417.0±128.7 %). A similar result was obtained for the pause depth, with an increase of 165.4±68.5% in and four times larger in KO (420.2±118.5 %). The increase of both the basal frequency and the pause depth with gabazine perfusion follows a positive linear correlation with the changes induced after D1-like and D2-like receptors block, as shown in figure 6.5. There is a clear difference in the KO behaviour with respect to the control condition: KO units show a shift upward compared to WT units, also evident from the

percent change of both the basal frequency and the pause depth which is clearly enhanced in the KO mouse model.

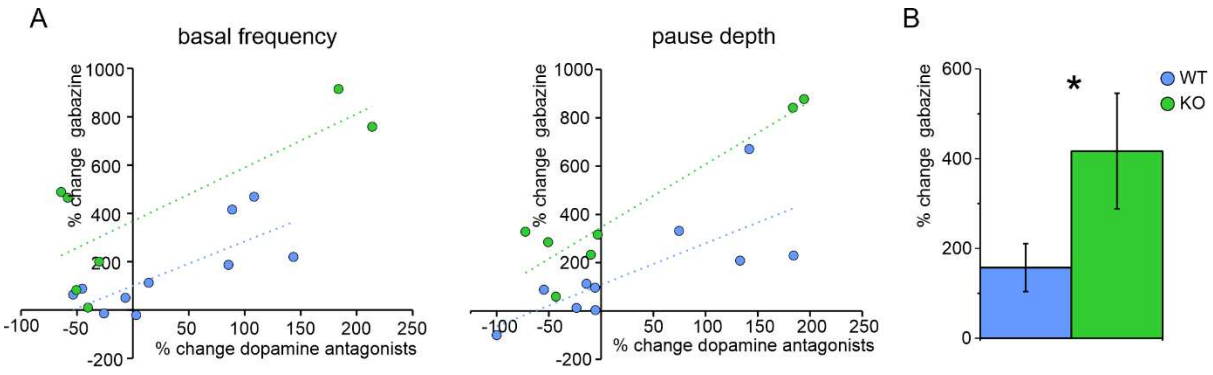

Figure 6.5| Correlation plots of both basal frequency and pause depth. A) The plot on the left shows the positive correlation between changes in PrL neurons basal frequencies after perfusion of dopamine receptor antagonists and gabazine with respect to the control condition, the correlation of the IB2 KO group (green) is shifted upward compared to the WT group (blue) (KO R^2=0.62; WT R^2=0.577). The plot on the right shows the positive correlation between changes in pause depth after perfusion of dopamine receptor antagonists and gabazine with respect to the control condition, the correlation of the IB2 KO group is shifted upward compared to the WT group (KO R^2=0.87; WT R^2=0.56). **B)** The histogram shows the show the % changes in basal frequency after gabazine perfusion, it is clear how the IB2 KO increase is four times larger than the one of their WT littermates.

6.3.6 Effect of inhibition blockade on the regularity of PrL neurons firing

To evaluate whether the blockade of inhibition by perfusing gabazine had an effect on the regularity of firing, we analysed the coefficient of variation (CV2) and inter-spike interval (ISI).

The CV2 showed that both IB2 WT and KO have a similar firing in all the evaluated conditions (control, dopamine receptors blockade, and gabazine). No significant differences were found comparing WT and KO in similar conditions. While blocking the dopaminergic receptors did not have a significant effect of the CV2, gabazine perfusion determined a decrease in CV2 of both IB2 WT and KO (WT: CV2 control= 1.25±0.01, gabazine=0.98±0.01, $p=1.03x10^{-8}$; KO: CV2 control= 1.25±0.03, gabazine=0.90±0.08, p=0.004).

More information was given by the analysis of the ISI. The histograms of ISI distribution in the recorded units showed two different peaks, both influenced by gabazine perfusion (Fig. 6.6). The two peaks might indicate the presence of up and down states in the spontaneous firing

of PrL neurons of both IB2 WT and KO, with high frequency activity nested in the up states (Gretenkord et al. 2017) (Fig. 6.7).

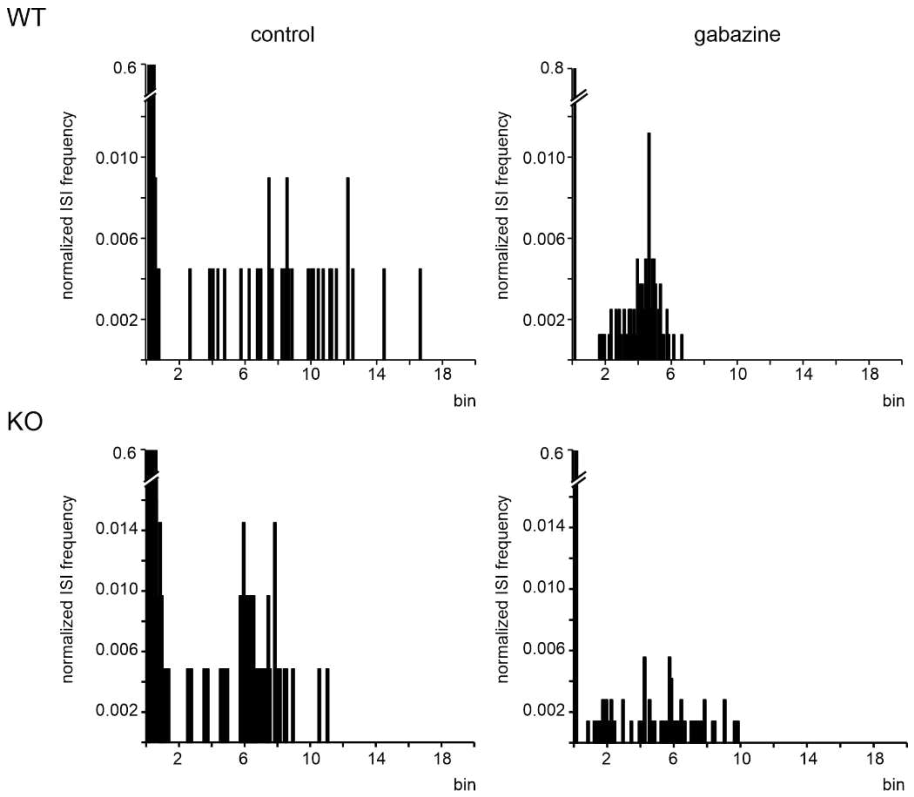

Figure 6.6|ISI distribution histograms. The figure shows examples of ISI distribution histograms for one WT (*top panels*) and one KO (*bottom panels*) unit, in control (*left*) and after gabazine perfusion (*right*). In both IB2 WT and KO histograms, two peaks are present, reflecting the up and down states of spontaneous activity of prelimbic cortex pyramidal neurons. The regularity of firing changed after gabazine perfusion.

The histograms of ISI distribution were fitted to estimate the peaks parameters. The first peak shifted to the left after gabazine perfusion in both WT and KO units (peak centre: WT=73±19 ms, KO=72±10 ms; after gabazine perfusion: WT=46±38, KO=50±0). No significant differences were found between IB2 WT and KO, but the difference was significant when comparing the control condition and the blockade of inhibition inside the same group (control vs. gabazine perfusion WT p=0.001; KO p=0.0002) (Fig. 6.6).

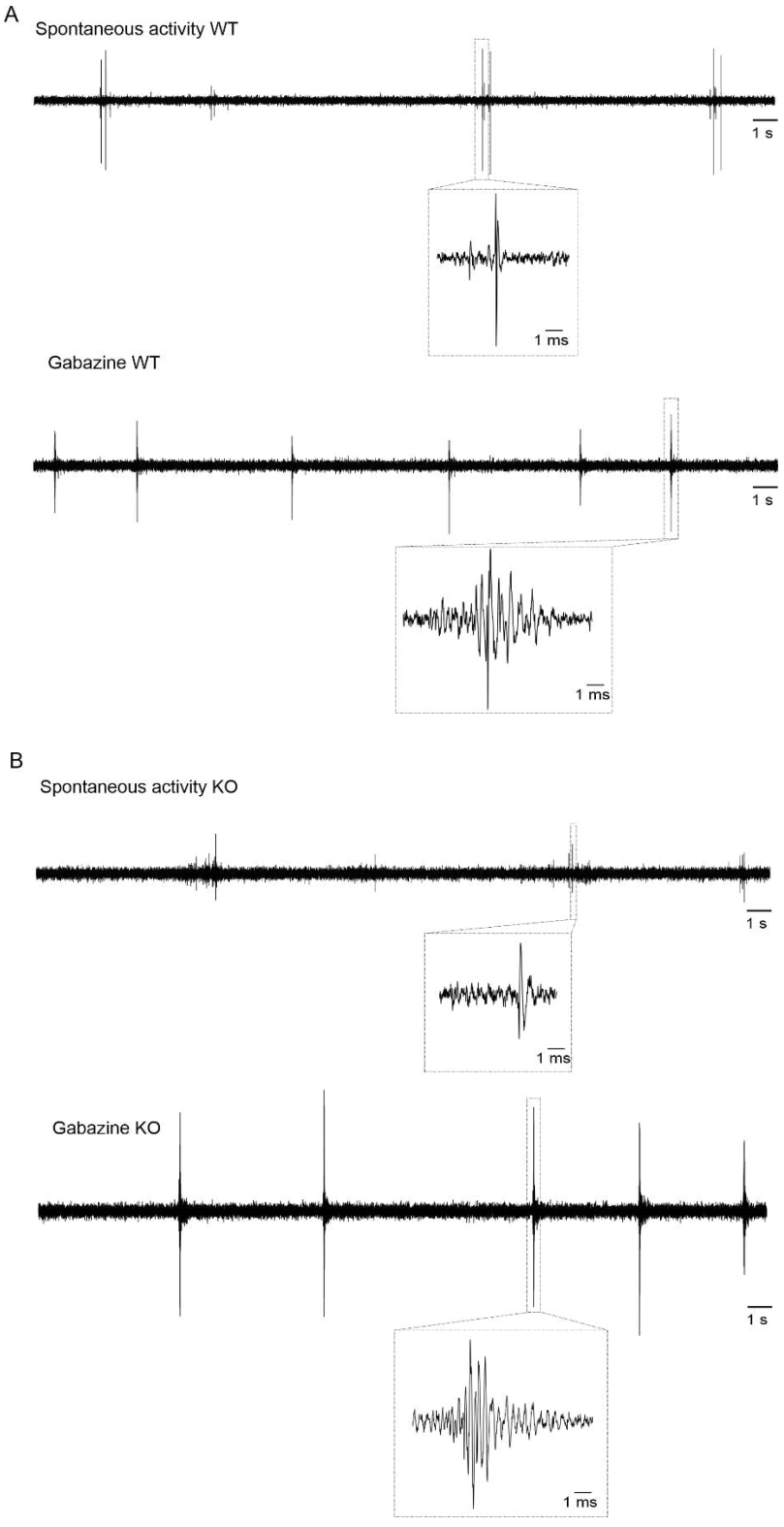

Figure 6.7| Examples of PrL neurons spontaneous activity. The figure shows examples of raw traces of spontaneous activity in control and after gabazine perfusion in IB2 WT **(A)** and KO **(B)**. Panel **A** shows the spontaneous activity before and after gabazine perfusion for the IB2 WT group; an example of spike during spontaneous activity (*up*) and a burst emerging after gabazine perfusion (*down*) are magnified in the boxes. Panel **B** shows the same condition for an IB2 KO unit. In both IB2 WT and KO is evident the presence of up and down states.

On the other hand, the second peak in the ISI distribution histograms showed a significant difference between IB2 WT and KO (centre: WT=6.41±0.45 s, KO=1.47±0.47 s; p=0.0001) showing a shift of the ISI distribution towards the left in the KO group. Moreover, when perfusing gabazine the opposite scenario took place. The peak significantly became sharper in the WT group (width=1.13±0.02 s) while it significantly broadened in the KO group (width=15.92±5.09 s) compared to controls (respectively p=0.0003; p=0.05) (Fig. 6.8).

Finally, we calculated the minimum ISI in control condition and after gabazine perfusion, to be sure that the bursts that occurred during gabazine perfusion were not a sign of epileptogenic activity. The minimum ISI in control and after gabazine perfusion were not significantly different, though a trend in reduction could be identified (minimum ISI: control= 3.5±0.9 ms, gabazine=1.4±0.1 ms, p=0.07).

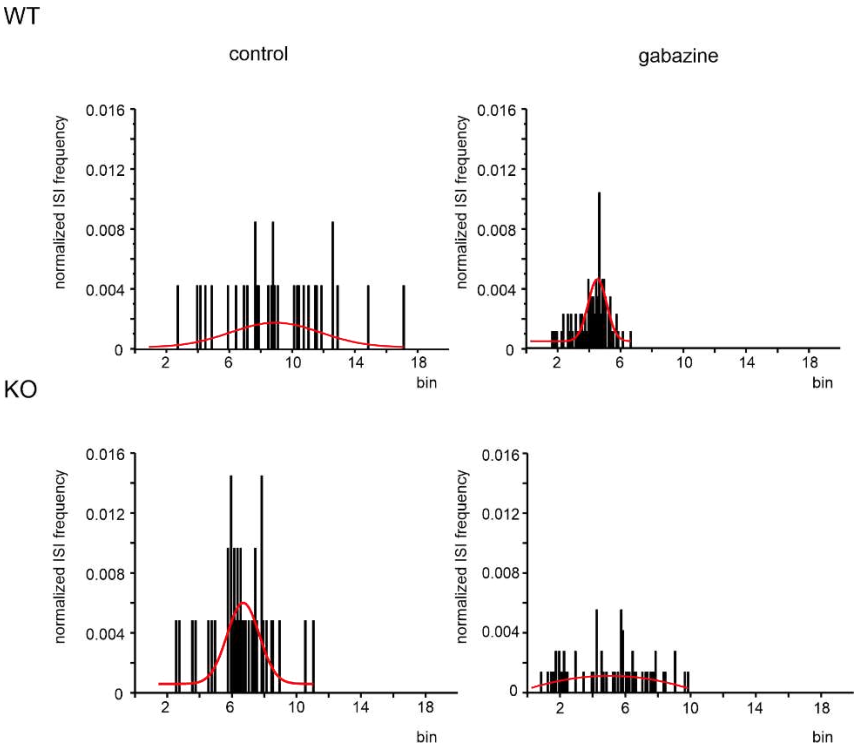

Figure 6.8|distribution histograms of the second peak of the basal frequency in control condition and after perfusion of gabazine. The histograms show the distribution of the ISI in the second peak. The upper panel shows the distribution of the ISI in the WT group in control condition (control, *left*) and after perfusion of gabazine (*right*). The same is shown in the bottom panel for the KO group. Notice the opposite distribution pattern: while in the control condition the WT group has a less regular distribution than the KO one, after gabazine perfusion the distribution sharpens in the WT groups and becomes less regular in the KO one.

6.4 Discussion

The IB2 KO mouse is a very intriguing model of ASD, since the human IB2 orthologous gene is virtually co-deleted with SHANK3 gene in almost all Phelan-McDermid syndrome cases and in some other ASD cases as well. The behavioural phenotype and significant cerebellar alterations have already been investigated (Giza et al. 2010; Soda et al. 2019), further supporting cerebellar role in ASD.

The logical prosecution of the IB2 model characterization was revolving the attention to the prefrontal cortex. Indeed, cerebellum-PFC functional connections are known to be relevant for both physiological and pathological conditions (McKimm et al. 2014; Thomas C. Watson, Jones, and Apps 2009). Particularly, alterations in this connectivity seem to play a crucial role in predisposition of ASD-relevant phenotypes (E. Kelly et al. 2020; Mittleman et al. 2008).

Therefore, we first investigated the E/I balance in the microcolumns of the prelimbic (PrL) subdivision of the prefrontal cortex using voltage sensitive dye imaging (VSDi). The results showed that the E/I balance is increased, meaning that the excitation column is larger in KO mice, with little lateral inhibition. This unbalance was more evident in layer V of the IB2 KO PrL. This led us to further investigate the electrophysiological properties of layer V pyramidal neurons using the patch-clamp technique in both IB2 KO and WT littermates. The results showed a significant difference in the intrinsic excitability of IB2 KO layer V pyramidal neurons with respect to the WT, evident as an upward shift in the frequency/intensity plot. Moreover, the transient inward current density, corresponding to the fast sodium current, was significantly larger in IB2 KO layer V pyramidal neurons than in WT. These preliminary results might demonstrate an enhanced intrinsic excitability in IB2 KO layer V pyramidal cells. This evidence was similar to what reported for cerebellar granule cells, which show increased excitability in KO mice (Soda et al. 2019).

Therefore, we explored the influence of the cerebellum over PFC activity with electrophysiological recordings *in vivo*. Interestingly, IB2 KO pyramidal cells show a lower basal frequency than WT, but the effect of DN stimulation is not significantly different in the two groups. Given the hyper-excitability of KO PrL pyramidal neurons in slices, the decreased basal firing was not expected. Nevertheless, the four times larger increase in basal frequency in KO units after blocking inhibition might provide an explanation. *In vivo*, the increased

excitability of KO neurons might be compensated with an increase in the GABAergic tone. In ASD, the dopaminergic system is known to be involved as well. In our conditions, no difference was found between WT and KO units basal firing and responses to DN stimulation after blocking the dopaminergic transmission. In both cases, the main effects were either an increase or a decrease in the basal firing frequency, probably reflecting the distribution of D1-like and D2-like dopamine receptors in the different neurons recorded. It is known that these two receptors subfamilies mediate opposite effects on neuronal excitability (Di Domenico and Mapelli 2023, chapter 4).

The GABAergic and dopaminergic systems are known to be functionally inter-dependent. Therefore, we investigated the effect of blocking inhibition after blocking the dopaminergic transmission.

Under this condition, the effect evoked in PrL pyramidal neurons (both considering the basal frequency and the response to DN stimulation) is shifted upwards. This result strongly stands for an altered modulation of PFC network activity, which is likely to impact the cognitive phenotype, as reported for several pathologies and ASD (Rinaldi, Perrodin, and Markram 2008; Uzunova, Pallanti, and Hollander 2016). Another interesting aspect was provided by the analysis of the ISI. Indeed, when comparing the ISI distribution of IB2 KO and WT, it is evident that both groups showed up and down states. Moreover, a more regular ISI distribution was found in IB2 KO units with respect to WT. This pattern of distribution seems to be switched by blocking inhibition, with a pattern of ISI distribution dysregulated in the IB2 KO compared to their WT littermates. This evidence suggest that the increased inhibitory tone in IB2 KO mice is crucial for maintaining the regularity of pyramidal neurons activity. The minimum detected ISI shows a trend of reduction after gabazine perfusion, suggesting an increase in the maximum firing rate. Nevertheless, our data do not support the development of epileptogenic-like activity induced by gabazine perfusion. Indeed, the minimum ISI in the control condition is already very low (and not statistically different from the one following gabazine perfusion), reflecting the presence of duplets and triplets at high frequency in the spontaneous firing of PrL pyramidal neurons. After gabazine perfusion, the spontaneous firing of pyramidal neurons rearranges in high frequency bursts, but these bursts are extremely short. Indeed, the epileptogenic activity is described in literature as high frequency bursts (200-500 Hz) that last longer than 30 seconds (Jefferys 2002, 2010; Paschen et al. 2020;

Yekhlef et al. 2015), whilst in our case burst duration with high frequency (200Hz) activity lasted no longer than 30 ms.

Literature has already shown a hyperactive and hyperplastic microcircuit in the prefrontal cortex of a valproic acid mouse model (Rinaldi, Perrodin, and Markram 2008), and the World Intense Syndrome theory has proposed an excessive neuronal activity inside the neocortical minicolumns as a crucial event underlying ASD (Markram and Markram 2010). Taken together, our results, suggest an *in vivo* inhibitory compensation of the E/I unbalance in favour of the excitatory component found *ex vivo*, thus adding new insights on such a complex pathology. Further investigations will be needed to assess the consequences of these alterations on network processing, as synaptic plasticity and further connectivity.

Chapter 7

GENERAL DISCUSSION

We investigated the potential contribution of the cerebellum to neocortical processing, starting from the considerable amount of evidence of the interconnection between the cerebellum and cerebral associative areas of the brain, such as the mPFC. The integral tractographic reconstruction of human cerebellar projections originating from the DCN and passing through the superior cerebellar peduncle showed a prominent cerebello-prefrontal cortex connection (Palesi et al. 2015). The same conclusion was sustained by *in vivo* electrophysiological studies in rodents reporting a bidirectional functional connection between these brain regions (Thomas C. Watson et al. 2014; Thomas C. Watson, Jones, and Apps 2009). Moreover, clinical studies support the hypothesis of a cerebellar role in cognitive function following the observation that cerebellar abnormalities are related to several cognitive dysfunctions. Despite this recent interest in cerebello-prefrontal connections, the cerebellar influence on mPFC functioning is still highly neglected in most investigations (Laubach et al. 2018).

Following these observations, we characterized neuronal responses in the PrL of the mPFC, during electrical stimulation of DN in anesthetized mice. Particularly, a pharmacological approach allowed to explore whether and how PrL neurons activities are influenced by different pathways driven by cerebellar activation. Our results suggest that the cerebellum may exert a crucial role in regulating mPFC activity, by controlling the level of excitation/inhibition in mPFC circuitry and presumably the intrinsic excitability of cortical neurons. Herein, our findings demonstrate the existence of physiological interactions between the cerebellum and the PrL, thus allowing to speculate that the functional interplay between these two regions might have an important role in cognition. Notably, cerebellar activation seems to preferentially lead to mPFC inhibition. Understanding the neuronal correlates underlying cerebello-prefrontal connectivity might explain the involvement of cerebellar abnormalities in various cognitive deficits. Overall, the findings reported in this thesis provide new insights for understanding cerebellar role in driving PrL neurons activity.

The results described in chapter 5provide strong evidence of a cerebellar drive over neuronal activity in PrL, presumably involving both the dopaminergic neuromodulatory system and the

thalamic glutamatergic system activating both pyramidal neurons and inhibitory interneurons of the PrL. Therefore, it is evident that the cerebellum should be considered as an important contributor to general brain processing, including high order cognitive functions, going beyond its role in the motor system. Further investigations on physiological cerebello-prefrontal interactions should include the application of optogenetics in order to specifically address the impact of cerebello-thalamic pathway and cerebello-VTA pathway onto mPFC activity. Indeed, the viral-induced expression of opsins in cerebellar axons projecting to other brain areas would allow their selective photo-stimulation whilst recording from the mPFC *in vivo* in both anesthetized and awake animals, thus ensuring the detection of responses elicited by specific stimulation of afferent projections through different pathways.

Moreover, considering the number of studies reporting abnormal cerebello-prefrontal interaction in several cognitive disorders such as autism and schizophrenia (D'Angelo and Casali 2012; E. Kelly et al. 2020; Schmahmann 2004), the last part of this thesis focused on exploring the cerebellar contribution on mPFC in both normal and pathological condition in animal models. To that end, we used the IB2 KO mouse model of autism, which is associated to the Phelan-McDermid syndrome in which the behavioural deficits are proved to be linked to alterations in cerebellar morphology and synaptic transmission (Giza et al. 2010). A previous study has already described the hyperexcitability in the granular layer of the cerebellar cortex associated with the IB2 KO mouse model (Soda et al. 2019). Considering the functional connection between the cerebellum and the PFC, in chapter 8 we focused on assessing possible disruptions of the PrL in the same mouse model. Our results shed light on impairments in the PFC of IB2 KO mice investigating: i)the PrL microcircuit *ex vivo* with the VSDi approach showing a disrupted E/I balance shifted toward the excitation component predominantly in layer V ; ii) electrophysiological properties of layer V pyramidal neurons with the patch-clamp technique showing an enhanced intrinsic excitability; iii) the influence of the cerebellum on the PrL microcircuit with *in vivo* electrophysiological recordings showing disrupted mechanisms of PFC modulation.

In vivo recordings of mPFC neurons activity during activation of cerebellar afferents either to thalamus or VTA might represent a good approach to give better insights into the pathophysiology of cognitive impairments related to cerebellar dysfunction. Pharmacological

tools might be employed to analyse the impact of cerebellum-mediated release of neurotransmitters and neuromodulators in mPFC in both normal and pathological conditions. Moreover, starting from the observation that cerebellar stimulation can be used to rescue neural mechanisms underlying cognition and alleviate symptoms in epilepsy (Cooper 1976) and schizophrenia (Demirtas-Tatlidede et al. 2010) patients, another interesting approach in studying cerebellar contribution to autism might be represented by cerebellar stimulation in awake, freely behaving animals. Once again, optogenetics could represent the finest tool to specifically stimulate the cerebellar circuit either at the level of the cortex or DCN, in such a way to restore cerebellar physiological activity and test whether cerebellar stimulation in autistic mice models is able to impact their behaviour. In conclusion, the cerebellar contribution to cortical activity has been demonstrated to represent a crucial aspect in processes of sensation, movement, and cognition, thus enlightening the need for further investigation in cerebellar physiology and interaction with other cortical areas in order to better understand brain functioning as a whole.

BIBLIPOGRAPHY

Abrahams, Brett S., and Daniel H. Geschwind. 2010. “Connecting Genes to Brain in the Autism Spectrum Disorders.” *Archives of Neurology* 67(4).

Akakin, Akin et al. 2014. “The Dentate Nucleus and Its Projection System in the Human Cerebellum: The Dentate Nucleus Microsurgical Anatomical Study.” *Neurosurgery* 74(4).

Alitto, Henry J., and W. Martin Usrey. 2003. “Corticothalamic Feedback and Sensory Processing.” *Current Opinion in Neurobiology* 13(4).

Allen, Greg. 2006. “Cerebellar Contributions to Autism Spectrum Disorders.” *Clinical Neuroscience Research* 6(3–4): 195–207.

Amaral, David G. 2011. “The Promise and the Pitfalls of Autism Research: An Introductory Note for New Autism Researchers.” *Brain Research* 1380.

Ambrosi, Glauco et al. 2007. “Non-Traditional Large Neurons in the Granular Layer of the Cerebellar Cortex.” *European Journal of Histochemistry* 51(SUPPL.1).

Anastasiades, Paul G., Christina Boada, and Adam G. Carter. 2019. “Cell-Type-Specific D1 Dopamine Receptor Modulation of Projection Neurons and Interneurons in the Prefrontal Cortex.” *Cerebral Cortex* 29(7): 3224–42.

Anastasiades, Paul G., and Adam G. Carter. 2021. “Circuit Organization of the Rodent Medial Prefrontal Cortex.” *Trends in Neurosciences* 44(7): 550–63. https://doi.org/10.1016/j.tins.2021.03.006.

Andreasen, Nancy C. et al. 1996. “Schizophrenia and Cognitive Dysmetria: A Positron-Emission Tomography Study of Dysfunctional Prefrontal-Thalamic-Cerebellar Circuitry.” *Proceedings of the National Academy of Sciences of the United States of America* 93(18).

Andreasen, Nancy C., and Ronald Pierson. 2008. “The Role of the Cerebellum in Schizophrenia.” *Biological Psychiatry* 64(2).

Antoine, Michelle W., Tomer Langberg, Philipp Schnepel, and Daniel E. Feldman. 2019. “Increased Excitation-Inhibition Ratio Stabilizes Synapse and Circuit Excitability in Four

Autism Mouse Models." *Neuron* 101(4): 648-661.e4. https://doi.org/10.1016/j.neuron.2018.12.026.

Apps, Richard, and Richard Hawkes. 2009. "Cerebellar Cortical Organization: A One-Map Hypothesis." *Nature Reviews Neuroscience* 10(9).

Ariano, Marjorie A. et al. 1997. "Cellular Distribution of the Rat D4 Dopamine Receptor Protein in the CNS Using Anti-Receptor Antisera." *Brain Research* 752(1–2).

Arnsten, Amy F.T., Min J. Wang, and Constantinos D. Paspalas. 2012. "Neuromodulation of Thought: Flexibilities and Vulnerabilities in Prefrontal Cortical Network Synapses." *Neuron* 76(1): 223–39. http://dx.doi.org/10.1016/j.neuron.2012.08.038.

Aron, Adam R., Trevor W. Robbins, and Russell A. Poldrack. 2004. "Inhibition and the Right Inferior Frontal Cortex." *Trends in Cognitive Sciences* 8(4): 170–77.

Ascoli, Giorgio A. et al. 2008. "Petilla Terminology: Nomenclature of Features of GABAergic Interneurons of the Cerebral Cortex." *Nature Reviews Neuroscience* 9(7).

Banerjee, Swati, Maeveen Riordan, and Manzoor A. Bhat. 2014. "Genetic Aspects of Autism Spectrum Disorders: Insights from Animal Models." *Frontiers in Cellular Neuroscience* 8(FEB).

Beaulieu, Jean Martin, and Raul R. Gainetdinov. 2011. "The Physiology, Signaling, and Pharmacology of Dopamine Receptors." *Pharmacological Reviews* 63(1): 182–217.

Benes, Francine M. 1997. "The Role of Stress and Dopamine-GABA Interactions in the Vulnerability for Schizophrenia." *Journal of Psychiatric Research* 31(2): 257–75.

———. 2015. "The GABA System in Schizophrenia: Cells, Molecules and Microcircuitry." *Schizophrenia Research* 167(1–3): 1–3. http://dx.doi.org/10.1016/j.schres.2015.07.017.

Betancur, Catalina. 2011. "Etiological Heterogeneity in Autism Spectrum Disorders: More than 100 Genetic and Genomic Disorders and Still Counting." *Brain Research* 1380.

Bey, Alexander, and Yong Hui Jiang. 2014. 4 Current Protocols in Pharmacology *Current Protocols in Pharmacology: Overview of Mouse Models of Autism Spectrum Disorders*.

Bohne, Pauline, Martin K. Schwarz, Stefan Herlitze, and Melanie D. Mark. 2019. "A New

Projection From the Deep Cerebellar Nuclei to the Hippocampus via the Ventrolateral and Laterodorsal Thalamus in Mice." *Frontiers in Neural Circuits* 13.

Britt, Jonathan P. et al. 2012. "Synaptic and Behavioral Profile of Multiple Glutamatergic Inputs to the Nucleus Accumbens." *Neuron* 76(4).

Brunel, Nicolas, Ecole Normale Sup, and Xiao-jing Wang. 2001. "Effects of Neuromodulation in a Cortical Network Model of Object Working." : 63–85.

Buchta, William C. et al. 2017. "Dopamine Terminals from the Ventral Tegmental Area Gate Intrinsic Inhibition in the Prefrontal Cortex." *Physiological Reports* 5(6).

Buschman, Timothy J, and Earl K Miller. 2007. "Of Attention in the Prefrontal And." *Science* 315(Ci): 1860–62. http://www.ncbi.nlm.nih.gov/pubmed/17395832.

Bushnell, M. Catherine, Marta Čeko, and Lucie A. Low. 2013. "Cognitive and Emotional Control of Pain and Its Disruption in Chronic Pain." *Nature Reviews Neuroscience* 14(7): 502–11.

Carlén, Marie. 2017. "What Constitutes the Prefrontal Cortex?" *Science* 358(6362).

Carper, Ruth A., and Eric Courchesne. 2005. "Localized Enlargement of the Frontal Cortex in Early Autism." *Biological Psychiatry* 57(2).

Carta, Ilaria et al. 2019. "Cerebellar Modulation of the Reward Circuitry and Social Behavior." *Science* 363(6424).

Casanova, Manuel F. 2003. "Modular Concepts of Brain Organization and the Neuropathology of Psychiatric Conditions." *Psychiatry Research* 118(1).

———. 2006. "Neuropathological and Genetic Findings in Autism: The Significance of a Putative Minicolumnopathy." *Neuroscientist* 12(5).

Chiu, Chiayu Q., Nagore Puente, Pedro Grandes, and Pablo E. Castillo. 2010. "Dopaminergic Modulation of Endocannabinoid-Mediated Plasticity at GABAergic Synapses in the Prefrontal Cortex." *Journal of Neuroscience* 30(21): 7236–48.

Chris Muly, E., Klara Szigeti, and Patricia S. Goldman-Rakic. 1998. "D1 Receptor in Interneurons of Macaque Prefrontal Cortex: Distribution and Subcellular Localization."

Journal of Neuroscience 18(24): 10553–65.

Cobb, S. R. et al. 1995. "Synchronization of Neuronal Activity in Hippocampus by Individual GABAergic Interneurons." *Nature* 378(6552): 75–78.

Cooper, Irving S. 1976. "Chronic Cerebellar Stimulation in Epilepsy." *Archives of Neurology* 33(8).

Crabtree, Gregg W., Alan J. Park, Joshua A. Gordon, and Joseph A. Gogos. 2016. "Cytosolic Accumulation of L-Proline Disrupts GABA-Ergic Transmission through GAD Blockade." *Cell Reports* 17(2): 570–82. http://dx.doi.org/10.1016/j.celrep.2016.09.029.

Cruikshank, Scott J. et al. 2012. "Thalamic Control of Layer 1 Circuits in Prefrontal Cortex." *Journal of Neuroscience* 32(49).

D'Angelo, Egidio, and Stefano Casali. 2012. "Seeking a Unified Framework for Cerebellar Function and Dysfunction: From Circuit Operations to Cognition." *Frontiers in Neural Circuits* (DEC).

Dani, Vardhan S. et al. 2005. "Reduced Cortical Activity Due to a Shift in the Balance between Excitation and Inhibition in a Mouse Model of Rett Syndrome." *Proceedings of the National Academy of Sciences of the United States of America* 102(35).

Defelipe, Javier et al. 2013. "New Insights into the Classification and Nomenclature of Cortical GABAergic Interneurons." *Nature Reviews Neuroscience* 14(3).

Delahaye, A. et al. 2009. "Chromosome 22q13.3 Deletion Syndrome with a de Novo Interstitial 22q13.3 Cryptic Deletion Disrupting SHANK3." *European Journal of Medical Genetics* 52(5): 328–32. http://dx.doi.org/10.1016/j.ejmg.2009.05.004.

DeLorey, Timothy M. et al. 2008. "Gabrb3 Gene Deficient Mice Exhibit Impaired Social and Exploratory Behaviors, Deficits in Non-Selective Attention and Hypoplasia of Cerebellar Vermal Lobules: A Potential Model of Autism Spectrum Disorder." *Behavioural Brain Research* 187(2).

Dembrow, Nikolai, and Daniel Johnston. 2014. "Subcircuit-Specific Neuromodulation in the Prefrontal Cortex." *Frontiers in Neural Circuits* 8(JUNE).

Demirtas-Tatlidede, Asli et al. 2010. "Safety and Proof of Principle Study of Cerebellar

Vermal Theta Burst Stimulation in Refractory Schizophrenia." *Schizophrenia Research* 124(1–3).

Di Domenico, Danila, and Lisa Mapelli. 2023. "Dopaminergic Modulation of Prefrontal Cortex Inhibition." *Biomedicines* 11(5).

Douglas, Rodney J., and Kevan A.C. Martin. 2004. "Neuronal Circuits of the Neocortex." *Annual Review of Neuroscience* 27.

Durand, Christelle M. et al. 2007. "Mutations in the Gene Encoding the Synaptic Scaffolding Protein SHANK3 Are Associated with Autism Spectrum Disorders." *Nature Genetics* 39(1).

Durstewitz, Daniel, and Jeremy K. Seamans. 2002. "The Computational Role of Dopamine D1 Receptors in Working Memory." *Neural Networks* 15(4–6): 561–72.

———. 2008. "The Dual-State Theory of Prefrontal Cortex Dopamine Function with Relevance to Catechol-O-Methyltransferase Genotypes and Schizophrenia." *Biological Psychiatry* 64(9): 739–49.

Ellegood, J. et al. 2015. "Clustering Autism: Using Neuroanatomical Differences in 26 Mouse Models to Gain Insight into the Heterogeneity." *Molecular Psychiatry* 20(1).

Elliott, Rebecca. 2003. "Executive Functions and Their Disorders." *British Medical Bulletin* 65: 49–59.

Fatemi, S. Hossein et al. 2012. "Consensus Paper: Pathological Role of the Cerebellum in Autism." *Cerebellum* 11(3).

Ferguson, Brielle R., and Wen Jun Gao. 2018. "Pv Interneurons: Critical Regulators of E/I Balance for Prefrontal Cortex-Dependent Behavior and Psychiatric Disorders." *Frontiers in Neural Circuits* 12.

Ferron, A., A. M. Thierry, C. Le Douarin, and J. Glowinski. 1984. "Inhibitory Influence of the Mesocortical Dopaminergic System on Spontaneous Activity or Excitatory Response Induced from the Thalamic Mediodorsal Nucleus in the Rat Medial Prefrontal Cortex." *Brain Research* 302(2).

Floresco, Stan B. et al. 2006. "Multiple Dopamine Receptor Subtypes in the Medial

Prefrontal Cortex of the Rat Regulate Set-Shifting." *Neuropsychopharmacology* 31(2).

Floresco, Stan B., and Anthony A. Grace. 2003. "Gating of Hippocampal-Evoked Activity in Prefrontal Cortical Neurons by Inputs from the Mediodorsal Thalamus and Ventral Tegmental Area." *Journal of Neuroscience* 23(9).

Floresco, Stan B., and Orsolya Magyar. 2006. "Mesocortical Dopamine Modulation of Executive Functions: Beyond Working Memory." *Psychopharmacology* 188(4).

Froula, Jessica M., Shayne D. Hastings, and Esther Krook-Magnuson. 2023. "The Little Brain and the Seahorse: Cerebellar-Hippocampal Interactions." *Frontiers in Systems Neuroscience* 17(March): 1–27.

Gandolfi, Daniela et al. 2014. "The Spatiotemporal Organization of Cerebellar Network Activity Resolved by Two-Photon Imaging of Multiple Single Neurons." *Frontiers in Behavioral Neuroscience* 8(APR).

Gao, Wen Jun, and Patricia S. Goldman-Rakic. 2003. "Selective Modulation of Excitatory and Inhibitory Microcircuits by Dopamine." *Proceedings of the National Academy of Sciences of the United States of America* 100(5): 2836–41.

Garbutt, J. C., and D. P. Van Kammen. 1983. "The Interaction between GABA and Dopamine: Implications for Schizophrenia." *Schizophrenia Bulletin* 9(3): 336–53.

Garris, P. A., and R. M. Wightman. 1994. "Different Kinetics Govern Dopaminergic Transmission in the Amygdala, Prefrontal Cortex, and Striatum: An in Vivo Voltammetric Study." *Journal of Neuroscience* 14(1): 442–50.

Garris, Paul A., Leonard B. Collins, Sara R. Jones, and R. Mark Wightman. 1993. "Evoked Extracellular Dopamine In Vivo in the Medial Prefrontal Cortex." *Journal of Neurochemistry* 61(2): 637–47.

Gaspar, Patricia, Bertrand Bloch, and Catherine Le Moine. 1995. "D1 and D2 Receptor Gene Expression in the Rat Frontal Cortex: Cellular Localization in Different Classes of Efferent Neurons." *European Journal of Neuroscience* 7(5): 1050–63.

Gill, Jason S., and Roy V. Sillitoe. 2019. "Functional Outcomes of Cerebellar Malformations." *Frontiers in Cellular Neuroscience* 13.

Giza, Joanna et al. 2010. “Behavioral and Cerebellar Transmission Deficits in Mice Lacking the Autism-Linked Gene Islet Brain-2.” *Journal of Neuroscience* 30(44).

Glausier, Jill R., Zafar U. Khan, and E. Chris Muly. 2009. “Dopamine D1 and D5 Receptors Are Localized to Discrete Populations of Interneurons in Primate Prefrontal Cortex.” *Cerebral Cortex* 19(8): 1820–34.

Gogolla, Nadine et al. 2009. “Common Circuit Defect of Excitatory-Inhibitory Balance in Mouse Models of Autism.” *Journal of Neurodevelopmental Disorders* 1(2).

Goldman-Rakic, P. S. 1995. “Cellular Basis of Working Memory.” *Neuron* 14(3): 477–85.

Goldman-Rakic, Patricia S. 1997. “The Cortical Dopamine System: Role in Memory and Cognition.” *Advances in Pharmacology* 42(C): 707–11.

———. 1999. “The Physiological Approach: Functional Architecture of Working Memory and Disordered Cognition in Schizophrenia.” *Biological Psychiatry* 46(5): 650–61.

Gonzalez-Islas, C., and J. J. Hablitz. 2001. “Dopamine Inhibition of Evoked IPSCs in Rat Prefrontal Cortex.” *Journal of Neurophysiology* 86(6): 2911–18.

Gorelova, Natalia, Jeremy K. Seamans, and Charles R. Yang. 2002. “Mechanisms of Dopamine Activation of Fast-Spiking Interneurons That Exert Inhibition in Rat Prefrontal Cortex.” *Journal of Neurophysiology* 88(6): 3150–66.

Grace, Anthony A. 2016. “Dysregulation of the Dopamine System in the Pathophysiology of Schizophrenia and Depression.” *Nature Reviews Neuroscience* 17(8): 524–32.

Graziane, Nicholas M., Eunice Y. Yuen, and Zhen Yan. 2009. “Dopamine D4 Receptors Regulate GABAA Receptor Trafficking via an Actin/Cofilin/Myosin-Dependent Mechanism.” *Journal of Biological Chemistry* 284(13): 8329–36. http://dx.doi.org/10.1074/jbc.M807387200.

Gretenkord, Sabine et al. 2017. “Dorsal vs. Ventral Differences in Fast Up-State-Associated Oscillations in the Medial Prefrontal Cortex of the Urethane-Anesthetized Rat.” *Journal of Neurophysiology* 117(3): 1126–42.

Gulledge, Allan T., and David B. Jaffe. 1998. “Dopamine Decreases the Excitability of Layer V Pyramidal Cells in the Rat Prefrontal Cortex.” *Journal of Neuroscience* 18(21).

Gunaydin, Lisa A. et al. 2014. “Natural Neural Projection Dynamics Underlying Social Behavior.” *Cell* 157(7): 1535–51. http://dx.doi.org/10.1016/j.cell.2014.05.017.

Hampson, David R., and Gene J. Blatt. 2015. “Autism Spectrum Disorders and Neuropathology of the Cerebellum.” *Frontiers in Neuroscience* 9(NOV).

Hara, Koji, and R. Adron Harris. 2002. “The Anesthetic Mechanism of Urethane: The Effects on Neurotransmitter-Gated Ion Channels.” *Anesthesia and Analgesia* 94(2).

Haroun, Heshmat SW. 2016. “Cerebellar Nuclei and Connections in Man.” *Anatomy Physiology & Biochemistry International Journal* 1(1).

Heidbreder, Christian A., and Henk J. Groenewegen. 2003. “The Medial Prefrontal Cortex in the Rat: Evidence for a Dorso-Ventral Distinction Based upon Functional and Anatomical Characteristics.” *Neuroscience and Biobehavioral Reviews* 27(6): 555–79.

Heinricher, Mary M. 2004. “Principles of Extracellular Single-Unit Recording.” *Microelectrode Recording in Movement Disorder Surgery* c: 8–13.

Henze, Romy et al. 2011. “Gray Matter Alterations in First-Admission Adolescents with Schizophrenia.” *Journal of Neuroimaging* 21(3).

Hoover, Walter B., and Robert P. Vertes. 2007. “Anatomical Analysis of Afferent Projections to the Medial Prefrontal Cortex in the Rat.” *Brain Structure and Function* 212(2).

Houck, Brenda D., and Abigail L. Person. 2014. “Cerebellar Loops: A Review of the Nucleocortical Pathway.” *Cerebellum* 13(3).

Huang, Shuo et al. 2020. “Dopamine Inputs from the Ventral Tegmental Area into the Medial Prefrontal Cortex Modulate Neuropathic Pain-Associated Behaviors in Mice.” *Cell Reports* 31(12): 107812. https://doi.org/10.1016/j.celrep.2020.107812.

Huang, Shuo, Stephanie L. Borgland, and Gerald W. Zamponi. 2019. “Dopaminergic Modulation of Pain Signals in the Medial Prefrontal Cortex: Challenges and Perspectives.” *Neuroscience Letters* 702(November 2018): 71–76. https://doi.org/10.1016/j.neulet.2018.11.043.

Huang, Yan You, Eleanor Simpson, Christoph Kellendonk, and Eric R. Kandel. 2004. “Genetic Evidence for the Bidirectional Modulation of Synaptic Plasticity in the Prefrontal Cortex

by D1 Receptors." *Proceedings of the National Academy of Sciences of the United States of America* 101(9): 3236–41.

Humeau, Yann et al. 2005. "Dendritic Spine Heterogeneity Determines Afferent-Specific Hebbian Plasticity in the Amygdala." *Neuron* 45(1).

Hutsler, Jeffrey J., and Manuel F. Casanova. 2016. "Review: Cortical Construction in Autism Spectrum Disorder: Columns, Connectivity and the Subplate." *Neuropathology and Applied Neurobiology* 42(2).

Ito, Masao. 2008. "Control of Mental Activities by Internal Models in the Cerebellum." *Nature Reviews Neuroscience* 9(4).

Ivry, Richard B., and Rebecca M.C. Spencer. 2004. "The Neural Representation of Time." *Current Opinion in Neurobiology* 14(2).

Jefferys, John G.R. 2010. "Advances in Understanding Basic Mechanisms of Epilepsy and Seizures." *Seizure* 19(10): 638–46. http://dx.doi.org/10.1016/j.seizure.2010.10.026.

Jefferys, John G R. 2002. "Basic Mechanisms of Epilepsy." *European Journal of Neurology* 9(S2): 8–9.

Johnson, Matthew B. et al. 2009. "Functional and Evolutionary Insights into Human Brain Development through Global Transcriptome Analysis." *Neuron* 62(4).

Kana, Rajesh K., Lauren E. Libero, and Marie S. Moore. 2011. "Disrupted Cortical Connectivity Theory as an Explanatory Model for Autism Spectrum Disorders." *Physics of Life Reviews* 8(4).

Kehr, W., Margit Lindqvist, and A. Carlsson. 1976. "Distribution of Dopamine in the Rat Cerebral Cortex." *Journal of Neural Transmission* 38(3–4): 173–80.

Kelly, Elyza et al. 2020. "Regulation of Autism-Relevant Behaviors by Cerebellar–Prefrontal Cortical Circuits." *Nature Neuroscience* 23(9).

Kelly, Roberta M., and Peter L. Strick. 2003. "Cerebellar Loops with Motor Cortex and Prefrontal Cortex of a Nonhuman Primate." *Journal of Neuroscience* 23(23).

Kemper, Thomas L., and Margaret Bauman. 1998. "Neuropathology of Infantile Autism."

Journal of Neuropathology and Experimental Neurology 57(7).

Kesner, Raymond P., and John C. Churchwell. 2011. "An Analysis of Rat Prefrontal Cortex in Mediating Executive Function." *Neurobiology of Learning and Memory* 96(3): 417–31. http://dx.doi.org/10.1016/j.nlm.2011.07.002.

Kim, Hyopil, Chae Seok Lim, and Bong Kiun Kaang. 2016. "Neuronal Mechanisms and Circuits Underlying Repetitive Behaviors in Mouse Models of Autism Spectrum Disorder." *Behavioral and Brain Functions* 12(1).

Koekkoek, S. K.E. et al. 2005. "Deletion of FMR1 in Purkinje Cells Enhances Parallel Fiber LTD, Enlarges Spines, and Attenuates Cerebellar Eyelid Conditioning in Fragile X Syndrome." *Neuron* 47(3).

Kolevzon, Alexander et al. 2014. "Phelan-McDermid Syndrome: A Review of the Literature and Practice Parameters for Medical Assessment and Monitoring." *Journal of Neurodevelopmental Disorders* 6(1).

Kosillo, Polina, and Helen S. Bateup. 2021. "Dopaminergic Dysregulation in Syndromic Autism Spectrum Disorders: Insights From Genetic Mouse Models." *Frontiers in Neural Circuits* 15(July).

Koziol, Leonard F. et al. 2014. "Consensus Paper: The Cerebellum's Role in Movement and Cognition." *Cerebellum* 13(1): 151–77.

Kruse, Andreas O., and Juan R. Bustillo. 2022. "Glutamatergic Dysfunction in Schizophrenia." *Translational Psychiatry* 12(1).

Kummer, Kai K., Miodrag Mitrić, Theodora Kalpachidou, and Michaela Kress. 2020. "The Medial Prefrontal Cortex as a Central Hub for Mental Comorbidities Associated with Chronic Pain." *International Journal of Molecular Sciences* 21(10).

Kuroda, Masaru et al. 1993. "Direct Synaptic Connections between Thalamocortical Axon Terminals from the Mediodorsal Thalamic Nucleus (MD) and Corticothalamic Neurons to MD in the Prefrontal Cortex." *Brain Research* 612(1–2).

Kuroda, Masaru, Kunio Murakami, Hiroaki Igarashi, and Akiko Okada. 1996. "The Convergence of Axon Terminals from the Mediodorsal Thalamic Nucleus and Ventral

Tegmental Area on Pyramidal Cells in Layer V of the Rat Prelimbic Cortex." *European Journal of Neuroscience* 8(7).

Kvitsiani, D. et al. 2013. "Distinct Behavioural and Network Correlates of Two Interneuron Types in Prefrontal Cortex." *Nature* 498(7454): 363–66.

Kyriakopoulos, Marinos et al. 2008. "A Diffusion Tensor Imaging Study of White Matter in Early-Onset Schizophrenia." *Biological Psychiatry* 63(5).

Laubach, Mark, Linda M. Amarante, Kyra Swanson, and Samantha R. White. 2018. "What, If Anything, Is Rodent Prefrontal Cortex?" *eNeuro* 5(5).

Law-Tho, D., J. M. Desce, and F. Crepel. 1995. "Dopamine Favours the Emergence of Long-Term Depression versus Long-Term Potentiation in Slices of Rat Prefrontal Cortex." *Neuroscience Letters* 188(2): 125–28.

Lawyer, Glenn et al. 2009. "Grey and White Matter Proportional Relationships in the Cerebellar Vermis Altered in Schizophrenia." *Cerebellum* 8(1).

Lebarton, Eve Sauer, and Jana M. Iverson. 2013. "Fine Motor Skill Predicts Expressive Language in Infant Siblings of Children with Autism." *Developmental Science* 16(6).

Lee, Anthony T., Steven M. Gee, et al. 2014. "Pyramidal Neurons in Prefrontal Cortex Receive Subtype-Specific Forms of Excitation and Inhibition." *Neuron* 81(1).

Lee, Anthony T., Daniel Vogt, John L. Rubenstein, and Vikaas S. Sohal. 2014. "A Class of GABAergic Neurons in the Prefrontal Cortex Sends Long-Range Projections to the Nucleus Accumbens and Elicits Acute Avoidance Behavior." *Journal of Neuroscience* 34(35).

Lee, Samuel P. et al. 2004. "Dopamine D1 and D2 Receptor Co-Activation Generates a Novel Phospholipase C-Mediated Calcium Signal." *Journal of Biological Chemistry* 279(34): 35671–78.

Lee, Yunjin et al. 2018. "Excessive D1 Dopamine Receptor Activation in the Dorsal Striatum Promotes Autistic-Like Behaviors." *Molecular Neurobiology* 55(7): 5658–71.

Leroi, Iracema et al. 2002. "Psychopathology in Patients with Degenerative Cerebellar Diseases: A Comparison to Huntington's Disease." *American Journal of Psychiatry*

159(8).

Lew, Sergio E., and Kuei Y. Tseng. 2014. “Dopamine Modulation of GABAergic Function Enables Network Stability and Input Selectivity for Sustaining Working Memory in a Computational Model of the Prefrontal Cortex.” *Neuropsychopharmacology : official publication of the American College of Neuropsychopharmacology* 39(13): 3067–76. http://dx.doi.org/10.1038/npp.2014.160.

Lewis, Barbara L., and Patricio O’Donnell. 2000. “Ventral Tegmental Area Afferents to the Prefrontal Cortex Maintain Membrane Potential ‘up’ States in Pyramidal Neurons via D1 Dopamine Receptors.” *Cerebral Cortex* 10(12): 1168–75.

Lewis, David A., and Guillermo Gonzalez-Burgos. 2006. “Pathophysiologically Based Treatment Interventions in Schizophrenia.” *Nature Medicine* 12(9): 1016–22.

Li, Yan Chun et al. 2011. “D2 Receptor Overexpression in the Striatum Leads to a Deficit in Inhibitory Transmission and Dopamine Sensitivity in Mouse Prefrontal Cortex.” *Proceedings of the National Academy of Sciences of the United States of America* 108(29): 12107–12.

Lisman, John E., and Anthony A. Grace. 2005. “The Hippocampal-VTA Loop: Controlling the Entry of Information into Long-Term Memory.” *Neuron* 46(5).

Little, Justin P., and Adam G. Carter. 2013. “Synaptic Mechanisms Underlying Strong Reciprocal Connectivity between the Medial Prefrontal Cortex and Basolateral Amygdala.” *Journal of Neuroscience* 33(39).

Liu, Yi et al. 2021. “A Selective Review of the Excitatory-Inhibitory Imbalance in Schizophrenia: Underlying Biology, Genetics, Microcircuits, and Symptoms.” *Frontiers in Cell and Developmental Biology* 9(October): 1–15.

Lorente de No, R. 1947. “A Study of Nerve Physiology.” *Studies from the Rockefeller institute for medical research. Reprints. Rockefeller Institute for Medical Research* 131.

Manning, Melanie A. et al. 2004. “Terminal 22q Deletion Syndrome: A Newly Recognized Cause of Speech and Language Disability in the Autism Spectrum.” *Pediatrics* 114(2 I).

Mapelli, Jonathan, and Egidio D’Angelo. 2007. “The Spatial Organization of Long-Term

Synaptic Plasticity at the Input Stage of Cerebellum." *Journal of Neuroscience* 27(6).

Mapelli, Lisa, Teresa Soda, Egidio D'Angelo, and Francesca Prestori. 2022. "The Cerebellar Involvement in Autism Spectrum Disorders: From the Social Brain to Mouse Models." *International Journal of Molecular Sciences* 23(7).

Markram, Kamila et al. 2008. "Abnormal Fear Conditioning and Amygdala Processing in an Animal Model of Autism." *Neuropsychopharmacology* 33(4).

Markram, Kamila, and Henry Markram. 2010. "The Intense World Theory - A Unifying Theory of the Neurobiology of Autism." *Frontiers in Human Neuroscience* 4.

McKimm, Eric et al. 2014. "Glutamate Dysfunction Associated with Developmental Cerebellar Damage: Relevance to Autism Spectrum Disorders." *Cerebellum* 13(3).

McKlveen, Jessica M. et al. 2019. "'Braking' the Prefrontal Cortex: The Role of Glucocorticoids and Interneurons in Stress Adaptation and Pathology." *Biological Psychiatry* 86(9): 669–81. https://doi.org/10.1016/j.biopsych.2019.04.032.

Middleton, Frank A., and Peter L. Strick. 1994. "Anatomical Evidence for Cerebellar and Basal Ganglia Involvement in Higher Cognitive Function." *Science* 266(5184).

———. 2001. "Cerebellar Projections to the Prefrontal Cortex of the Primate." *Journal of Neuroscience* 21(2).

Miller, E. K., and J. D. Cohen. 2001. "An Integrative Theory of Prefrontal Cortex Function." *Annual Review of Neuroscience* 24.

Minshew, Nancy J., and Diane L. Williams. 2007. "The New Neurobiology of Autism: Cortex, Connectivity, and Neuronal Organization." *Archives of Neurology* 64(7).

Mittleman, Guy, Daniel Goldowitz, Detlef H. Heck, and Charles D. Blaha. 2008. "Cerebellar Modulation of Frontal Cortex Dopamine Efflux in Mice: Relevance to Autism and Schizophrenia." *Synapse* 62(7).

Monteverdi, Anita, Danila Di Domenico, Egidio D Angelo, and Lisa Mapelli. 2023. "Anisotropy and Frequency Dependence of Signal Propagation in the Cerebellar Circuit Revealed by High-Density Multielectrode Array Recordings."

Mosconi, Matthew W. et al. 2015. “The Role of Cerebellar Circuitry Alterations in the Pathophysiology of Autism Spectrum Disorders.” *Frontiers in Neuroscience* 9(SEP).

Mrzljak, L. et al. 1996. “Localization of Dopamine D4 Receptors in GABAergic Neurons of the Primate Brain.” *Nature* 381(6579).

Nakazawa, Kazu, and Kiran Sapkota. 2020. “The Origin of NMDA Receptor Hypofunction in Schizophrenia.” *Pharmacology and Therapeutics* 205: 107426. https://doi.org/10.1016/j.pharmthera.2019.107426.

Negri, Stéphanie et al. 2000. “CDNA Cloning and Mapping of a Novel Islet-Brain/JNK-Interacting Protein.” *Genomics* 64(3).

Nestor, A., Ying Wan Lam, and J. A. Gray. 1996. “Latent Inhibition: A Neural Network Approach.” *Journal of Experimental Psychology: Animal Behavior Processes* 22(3).

Nguyen, Michael et al. 2014. “Decoding the Contribution of Dopaminergic Genes and Pathways to Autism Spectrum Disorder (ASD).” *Neurochemistry International* 66(1): 15–26. http://dx.doi.org/10.1016/j.neuint.2014.01.002.

Nieoullon, A., A. Cheramy, and J. Glowinski. 1978. “Release of Dopamine in Both Caudate Nuclei and Both Substantia Nigrae in Response to Unilateral Stimulation of Cerebellar Nuclei in the Cat.” *Brain Research* 148(1).

O’Donnell, Patricio. 2011. “Adolescent Onset of Cortical Disinhibition in Schizophrenia: Insights from Animal Models.” *Schizophrenia Bulletin* 37(3): 484–92.

O’Donnell, Patricio, and Anthony A. Grace. 1998. “Dysfunctions in Multiple Interrelated Systems as the Neurobiological Bases of Schizophrenic Symptom Clusters.” *Schizophrenia Bulletin* 24(2): 267–83.

Okugawa, Gaku, Kenji Nobuhara, Katsunori Takase, and Toshihiko Kinoshita. 2008. “Cerebellar Posterior Superior Vermis and Cognitive Cluster Scores in Drug-Naive Patients with First-Episode Schizophrenia.” *Neuropsychobiology* 56(4).

Opris, Ioan et al. 2013. “Prefrontal Cortical Microcircuits Bind Perception to Executive Control.” *Scientific Reports* 3.

Otani, Satoru, Jing Bai, and Kevin Blot. 2015. “Dopaminergic Modulation of Synaptic

Plasticity in Rat Prefrontal Neurons." *Neuroscience Bulletin* 31(2).

Ott, Torben, and Andreas Nieder. 2017. "Dopamine D2 Receptors Enhance Population Dynamics in Primate Prefrontal Working Memory Circuits." *Cerebral Cortex* 27(9): 4423–35.

———. 2019. "Dopamine and Cognitive Control in Prefrontal Cortex." *Trends in Cognitive Sciences* 23(3).

Paine, Tracie A., Lauren E. Slipp, and William A. Carlezon. 2011. "Schizophrenia-like Attentional Deficits Following Blockade of Prefrontal Cortex GABA a Receptors." *Neuropsychopharmacology* 36(8).

Palesi, Fulvia et al. 2015. "Contralateral Cerebello-Thalamo-Cortical Pathways with Prominent Involvement of Associative Areas in Humans in Vivo." *Brain Structure and Function* 220(6).

Palmen, Saskia J.M.C., Herman Van Engeland, Patrick R. Hof, and Christoph Schmitz. 2004. "Neuropathological Findings in Autism." *Brain* 127(12).

Palmer, Lucy, Masanori Murayama, and Matthew Larkum. 2012. "Inhibitory Regulation of Dendritic Activity in Vivo." *Frontiers in Neural Circuits* 6(MAY2012): 1–10.

Parfitt, K. D., A. Gratton, and P. C. Bickford-Wimer. 1990. "Electrophysiological Effects of Selective D1 and D2 Dopamine Receptor Agonists in the Medial Prefrontal Cortex of Young and Aged Fischer 344 Rats." *Journal of Pharmacology and Experimental Therapeutics* 254(2).

Parnaudeau, Sébastien, Scott S. Bolkan, and Christoph Kellendonk. 2018. "The Mediodorsal Thalamus: An Essential Partner of the Prefrontal Cortex for Cognition." *Biological Psychiatry* 83(8).

Paschen, E. et al. 2020. "Hippocampal Low-Frequency Stimulation Prevents Seizure Generation in a Mouse Model of Mesial Temporal Lobe Epilepsy." *eLife* 9: 1–57.

Penit-Soria, Jacqueline, Etienne Audinat, and Francis Crepel. 1987. "Excitation of Rat Prefrontal Cortical Neurons by Dopamine: An in Vitro Electrophysiological Study." *Brain Research* 425(2).

Pezzulo, Giovanni. 2012. “An Active Inference View of Cognitive Control.” *Frontiers in Psychology* 3(NOV): 2011–12.

Phelan, Mary C. 2008. “Deletion 22q13.3 Syndrome.” *Orphanet Journal of Rare Diseases* 3(1): 1–6.

Piochon, Claire et al. 2015. “Correction: Corrigendum: Cerebellar Plasticity and Motor Learning Deficits in a Copy-Number Variation Mouse Model of Autism.” *Nature Communications* 6(1).

Pirot, S. et al. 1992. “Inhibitory Effects of Ventral Tegmental Area Stimulation on the Activity of Prefrontal Cortical Neurons: Evidence for the Involvement of Both Dopaminergic and GABAergic Components.” *Neuroscience* 49(4).

Pisano, Thomas John et al. 2021. “Parallel Organization of Cerebellar Pathways to Sensory, Motor, and Associative Forebrain.” *SSRN Electronic Journal*.

Polleux, Franck, and Jean M. Lauder. 2004. “Toward a Developmental Neurobiology of Autism.” *Mental Retardation and Developmental Disabilities Research Reviews* 10(4).

Povysheva, N. V. et al. 2006. “Properties of Excitatory Synaptic Responses in Fast-Spiking Interneurons and Pyramidal Cells from Monkey and Rat Prefrontal Cortex.” *Cerebral Cortex* 16(4).

Puig, M. Victoria, Jonas Rose, Robert Schmidt, and Nadja Freund. 2014. “Dopamine Modulation of Learning and Memory in the Prefrontal Cortex: Insights from Studies in Primates, Rodents, and Birds.” *Frontiers in Neural Circuits* 8(AUG): 1–15.

Qiu, Shenfeng, Kimberly A. Aldinger, and Pat Levitt. 2012. “Modeling of Autism Genetic Variations in Mice: Focusing on Synaptic and Microcircuit Dysfunctions.” *Developmental Neuroscience* 34(2–3).

Rall, Wilfrid. 1962. “Electrophysiology of a Dendritic Neuron Model.” *Biophysical Journal* 2(2).

Rao, Srinivas G., Graham V. Williams, and Patricia S. Goldman-Rakic. 2000. “Destruction and Creation of Spatial Tuning by Disinhibition: GABA(A) Blockade of Prefrontal Cortical Neurons Engaged by Working Memory.” *Journal of Neuroscience* 20(1).

Riga, Danai et al. 2014. “Optogenetic Dissection of Medial Prefrontal Cortex Circuitry.” *Frontiers in Systems Neuroscience* 8(DEC): 1–19.

Rinaldi, Tania, Karina Kulangara, Katia Antoniello, and Henry Markram. 2007. “Elevated NMDA Receptor Levels and Enhanced Postsynaptic Long-Term Potentiation Induced by Prenatal Exposure to Valproic Acid.” *Proceedings of the National Academy of Sciences of the United States of America* 104(33).

Rinaldi, Tania, Catherine Perrodin, and Henry Markram. 2008. “Hyper-Connectivity and Hyper-Plasticity in the Medial Prefrontal Cortex in the Valproic Acid Animal Model of Autism.” *Frontiers in Neural Circuits* 2(OCT): 1–7.

Rogers, Tiffany D. et al. 2011. “Connecting the Dots of the Cerebro-Cerebellar Role in Cognitive Function: Neuronal Pathways for Cerebellar Modulation of Dopamine Release in the Prefrontal Cortex.” *Synapse* 65(11).

Rotaru, Diana C. et al. 2011. “Glutamate Receptor Subtypes Mediating Synaptic Activation of Prefrontal Cortex Neurons: Relevance for Schizophrenia.” *Journal of Neuroscience* 31(1).

Rotaru, Diana C., German Barrionuevo, and Susan R. Sesack. 2005. “Mediodorsal Thalamic Afferents to Layer III of the Rat Prefrontal Cortex: Synaptic Relationships to Subclasses of Interneurons.” *Journal of Comparative Neurology* 490(3).

Rowland, Nathan C., and Dieter Jaeger. 2008. “Responses to Tactile Stimulation in Deep Cerebellar Nucleus Neurons Result from Recurrent Activation in Multiple Pathways.” *Journal of Neurophysiology* 99(2).

Roy John, E. 2002. 39 Brain Research Reviews *The Neurophysics of Consciousness*.

De Rubeis, Silvia, and Joseph D. Buxbaum. 2015. “Genetics and Genomics of Autism Spectrum Disorder: Embracing Complexity.” *Human Molecular Genetics* 24(R1).

Rubenstein, J. L.R., and M. M. Merzenich. 2003. “Model of Autism: Increased Ratio of Excitation/Inhibition in Key Neural Systems.” *Genes, Brain and Behavior* 2(5).

Rubinstein, Marcelo et al. 2001. “Dopamine D4 Receptor-Deficient Mice Display Cortical Hyperexcitability.” *Journal of Neuroscience* 21(11): 3756–63.

Rudy, Bernardo, Gordon Fishell, Soo Hyun Lee, and Jens Hjerling-Leffler. 2011. “Three Groups of Interneurons Account for Nearly 100% of Neocortical GABAergic Neurons.” *Developmental Neurobiology* 71(1).

Saffari, R. et al. 2016. “NPY+-, but Not PV+-GABAergic Neurons Mediated Long-Range Inhibition from Infra-to Prelimbic Cortex.” *Translational Psychiatry* 6(2).

Sahu, Asha et al. 2009. “D 5 Dopamine Receptors Are Required for Dopaminergic Activation of Phospholipase C.” *Molecular Pharmacology* 75(3): 447–53.

Santana, Noemí, Guadalupe Mengod, and Francesc Artigas. 2009. “Quantitative Analysis of the Expression of Dopamine D1 and D2 Receptors in Pyramidal and GABAergic Neurons of the Rat Prefrontal Cortex.” *Cerebral Cortex* 19(4): 849–60.

Sawaguchi, T., M. Matsumura, and K. Kubota. 1989. “Delayed Response Deficits Produced by Local Injection of Bicuculline into the Dorsolateral Prefrontal Cortex in Japanese Macaque Monkeys.” *Experimental Brain Research* 75(3).

Sceniak, Michael P. et al. 2016. “Mechanisms of Functional Hypoconnectivity in the Medial Prefrontal Cortex of Mecp2 Null Mice.” *Cerebral Cortex* 26(5).

Schmahmann, Jeremy D. 1996. “From Movement to Thought: Anatomic Substrates of the Cerebellar Contribution to Cognitive Processing.” *Human Brain Mapping* 4(3).

———. 2004. “Disorders of the Cerebellum: Ataxia, Dysmetria of Thought, and the Cerebellar Cognitive Affective Syndrome.” *Journal of Neuropsychiatry and Clinical Neurosciences* 16(3).

Schmahmann, Jeremy D, and Janet C Sherman. 1998. “The Cerebellar Cognitive Affective Syndrome.” : 561–79.

De Schutter, E., and V. Steuber. 2009. “Patterns and Pauses in Purkinje Cell Simple Spike Trains: Experiments, Modeling and Theory.” *Neuroscience* 162(3).

Seamans, Jeremy K., Daniel Durstewitz, et al. 2001. “Dopamine D1/D5 Receptor Modulation of Excitatory Synaptic Inputs to Layer V Prefrontal Cortex Neurons.” *Proceedings of the National Academy of Sciences of the United States of America* 98(1): 301–6.

Seamans, Jeremy K., Natalia Gorelova, Daniel Durstewitz, and Charles R. Yang. 2001.

"Bidirectional Dopamine Modulation of GABAergic Inhibition in Prefrontal Cortical Pyramidal Neurons." *Journal of Neuroscience* 21(10): 3628–38.

Seamans, Jeremy K., Christopher C. Lapish, and Daniel Durstewitz. 2008a. "Comparing the Prefrontal Cortex of Rats and Primates: Insights from Electrophysiology." *Neurotoxicity Research* 14(2–3).

———. 2008b. "Comparing the Prefrontal Cortex of Rats and Primates: Insights from Electrophysiology." *Neurotoxicity Research* 14(2–3): 249–62.

Seamans, Jeremy K., and Charles R. Yang. 2004. "The Principal Features and Mechanisms of Dopamine Modulation in the Prefrontal Cortex." *Progress in Neurobiology* 74(1): 1–58.

Sesack, S. R., and B. S. Bunney. 1989. "Pharmacological Characterization of the Receptor Mediating Electrophysiological Responses to Dopamine in the Rat Medial Prefrontal Cortex: A Microiontophoretic Study." *Journal of Pharmacology and Experimental Therapeutics* 248(3).

Shadmehr, Reza, and John W. Krakauer. 2008. "A Computational Neuroanatomy for Motor Control." *Experimental Brain Research* 185(3).

Shen, Lie Hang, Mei Hsiu Liao, and Yu Chin Tseng. 2012. "Recent Advances in Imaging of Dopaminergic Neurons for Evaluation of Neuropsychiatric Disorders." *Journal of Biomedicine and Biotechnology* 2012.

Shepherd, Gordon M. 2004. The Synaptic Organization of the Brain *The Synaptic Organization of the Brain*.

Shyian, D. N. 2016. "Morphological Features of the Globose Nucleus of the Cerebellum." *Morphologia* 10(1).

da Silva Alves, Fabiana et al. 2008. "The Revised Dopamine Hypothesis of Schizophrenia: Evidence from Pharmacological MRI Studies with Atypical Antipsychotic Medication." *Psychopharmacology bulletin* 41(1).

Smiley, John F., Allan I. Levey, Brian J. Ciliax, and Patricia S. Goldman-Rakic. 1994. "D1 Dopamine Receptor Immunoreactivity in Human and Monkey Cerebral Cortex: Predominant and Extrasynaptic Localization in Dendritic Spines." *Proceedings of the*

National Academy of Sciences of the United States of America 91(12): 5720–24.

Snider, Ray S., and A. Maiti. 1976. "Cerebellar Contributions to the Papez Circuit." *Journal of Neuroscience Research* 2(2).

Snider, Ray S., A. Maiti, and Stuart R. Snider. 1976. "Cerebellar Pathways to Ventral Midbrain and Nigra." *Experimental Neurology* 53(3).

Soda, Teresa et al. 2019. "Erratum: Hyperexcitability and Hyperplasticity Disrupt Cerebellar Signal Transfer in the Ib2 Ko Mouse Model of Autism (Journal of Neuroscience (2019) (2383-2397) DOI: 10.1523/JNEUROSCI.1985-18.2019)." *Journal of Neuroscience* 39(35): 7029.

Soorya, Latha et al. 2013. "Prospective Investigation of Autism and Genotype-Phenotype Correlations in 22q13 Deletion Syndrome and SHANK3 Deficiency." *Molecular Autism* 4(1).

Stanfield, Andrew C. et al. 2008. "Towards a Neuroanatomy of Autism: A Systematic Review and Meta-Analysis of Structural Magnetic Resonance Imaging Studies." *European Psychiatry* 23(4).

Stoner, Rich et al. 2014. "Patches of Disorganization in the Neocortex of Children with Autism." *New England Journal of Medicine* 370(13).

Stoodley, Catherine J. et al. 2017. "Altered Cerebellar Connectivity in Autism and Cerebellar-Mediated Rescue of Autism-Related Behaviors in Mice." *Nature Neuroscience* 20(12).

Strick, Peter L., Richard P. Dum, and Julie A. Fiez. 2009. "Cerebellum and Nonmotor Function." *Annual Review of Neuroscience* 32.

Suska, Anna et al. 2013. "Selective Presynaptic Enhancement of the Prefrontal Cortex to Nucleus Accumbens Pathway by Cocaine." *Proceedings of the National Academy of Sciences of the United States of America* 110(2).

Swadlow, Harvey A., Alexander G. Gusev, and Tatiana Bezdudnaya. 2002. "Activation of a Cortical Column by a Thalamocortical Impulse." *Journal of Neuroscience* 22(17).

Swenson, Rand S., Ross J. Kosinski, and Anthony J. Castro. 1984. "Topography of Spinal, Dorsal Column Nuclear, and Spinal Trigeminal Projections to the Pontine Gray in Rats."

Journal of Comparative Neurology 222(2).

SWENSON, Rand S. 2006. “Review of Clinical and Functional Neuroscience, Chapter 9.” *Educational Review Manual in Neurology*.

Sydnor, Lindsey M, and Kimberly A Aldinger. 2021. “Structure, Function, and Genetics of the Cerebellum in Autism.” *Journal of Psychiatry and Brain Science*: 1–22.

Terraneo, Alberto et al. 2016. “Transcranial Magnetic Stimulation of Dorsolateral Prefrontal Cortex Reduces Cocaine Use: A Pilot Study.” *European Neuropsychopharmacology* 26(1).

Testa-Silva, Guilherme et al. 2012. “Hyperconnectivity and Slow Synapses during Early Development of Medial Prefrontal Cortex in a Mouse Model for Mental Retardation and Autism.” *Cerebral Cortex* 22(6).

Thomson, Alex M., and A. Peter Bannister. 2003. “Interlaminar Connections in the Neocortex.” In *Cerebral Cortex*,.

Townsend, Jeanne et al. 1999. “Spatial Attention Deficits in Patients with Acquired or Developmental Cerebellar Abnormality.” *Journal of Neuroscience* 19(13).

Trantham-Davidson, Heather, Sven Kröner, and Jeremy K. Seamans. 2008. “Dopamine Modulation of Prefrontal Cortex Interneurons Occurs Independently of DARPP-32.” *Cerebral Cortex* 18(4).

Trantham-Davidson, Heather, Laurence C. Neely, Antonieta Lavin, and Jeremy K. Seamans. 2004. “Mechanisms Underlying Differential D1 versus D2 Dopamine Receptor Regulation of Inhibition in Prefrontal Cortex.” *Journal of Neuroscience* 24(47): 10652–59.

Trevathan, James K. et al. 2021. “Calcium Imaging in Freely Moving Mice during Electrical Stimulation of Deep Brain Structures.” *Journal of Neural Engineering* 18(2).

Tritsch, Nicolas X., and Bernardo L. Sabatini. 2012. “Dopaminergic Modulation of Synaptic Transmission in Cortex and Striatum.” *Neuron* 76(1): 33–50. http://dx.doi.org/10.1016/j.neuron.2012.09.023.

Trobe, Jonathan D. 2008. “Netter’s Atlas of Human Neuroscience.” *Journal of Neuro-*

Ophthalmology 28(2).

Tsai, Peter T. et al. 2012. “Autistic-like Behaviour and Cerebellar Dysfunction in Purkinje Cell Tsc1 Mutant Mice.” *Nature* 488(7413).

Tseng, Kuei Y. et al. 2006. “Excitatory Response of Prefrontal Cortical Fast-Spiking Interneurons to Ventral Tegmental Area Stimulation in Vivo.” *Synapse* 59(7): 412–17.

Tseng, Kuei Y., R. Andrew Chambers, and Barbara K. Lipska. 2009. “The Neonatal Ventral Hippocampal Lesion as a Heuristic Neurodevelopmental Model of Schizophrenia.” *Behavioural Brain Research* 204(2): 295–305.

Tseng, Kuei Y., and Patricio O’Donnell. 2004. “Dopamine-Glutamate Interactions Controlling Prefrontal Cortical Pyramidal Cell Excitability Involve Multiple Signaling Mechanisms.” *Journal of Neuroscience* 24(22): 5131–39.

Tseng, Kuei Yuan, and Patricio O’Donnell. 2007. “Dopamine Modulation of Prefrontal Cortical Interneurons Changes during Adolescence.” *Cerebral Cortex* 17(5): 1235–40.

Uusisaari, Marylka, Kunihiko Obata, and Thomas Knöpfel. 2007. “Morphological and Electrophysiological Properties of GABAergic and Non-GABAergic Cells in the Deep Cerebellar Nuclei.” *Journal of Neurophysiology* 97(1).

Uusisaari, Marylka, and Erik de Schutter. 2011. “The Mysterious Microcircuitry of the Cerebellar Nuclei.” *Journal of Physiology* 589(14).

Uylings, Harry B.M., Henk J. Groenewegen, and Bryan Kolb. 2003. “Do Rats Have a Prefrontal Cortex?” *Behavioural Brain Research* 146(1–2).

Uzunova, Genoveva, Stefano Pallanti, and Eric Hollander. 2016. “Excitatory/Inhibitory Imbalance in Autism Spectrum Disorders: Implications for Interventions and Therapeutics.” *World Journal of Biological Psychiatry* 17(3).

Vargas, Diana L. et al. 2005. “Neuroglial Activation and Neuroinflammation in the Brain of Patients with Autism.” *Annals of Neurology* 57(1).

Vertes, Robert P. 2006. “Interactions among the Medial Prefrontal Cortex, Hippocampus and Midline Thalamus in Emotional and Cognitive Processing in the Rat.” *Neuroscience* 142(1).

Volk, David, and David Lewis. 2005. “GABA Targets for the Treatment of Cognitive Dysfunction in Schizophrenia.” *Current Neuropharmacology* 3(1): 45–62.

Vranesic, Ivo et al. 1994. “Signal Transmission in the Parallel Fiber-Purkinje Cell System Visualized by High-Resolution Imaging.” *Proceedings of the National Academy of Sciences of the United States of America* 91(26).

Wang, Samuel S.H., Alexander D. Kloth, and Aleksandra Badura. 2014. “The Cerebellum, Sensitive Periods, and Autism.” *Neuron* 83(3).

Wang, Xun, Ping Zhong, Zhenglin Gu, and Zhen Yan. 2003. “Regulation of NMDA Receptors by Dopamine D4 Signaling in Prefrontal Cortex.” *Journal of Neuroscience* 23(30): 9852–61.

Wang, Xun, Ping Zhong, and Zhen Yan. 2002. “Dopamine D4 Modulate GABAergic Signaling in Pyramidl Neurons.PDF.” *The Journal of Neuroscience* 22(21): 9185–93.

Watson, Charles, George Paxinos, and Luis Puelles. 2011. The Mouse Nervous System *The Mouse Nervous System*.

Watson, Thomas C., Nadine Becker, Richard Apps, and Matthew W. Jones. 2014. “Back to Front: Cerebellar Connections and Interactions with the Prefrontal Cortex.” *Frontiers in Systems Neuroscience* 8(FEB).

Watson, Thomas C., Matthew W. Jones, and Richard Apps. 2009. “Electrophysiological Mapping of Novel Prefrontal - Cerebellar Pathways.” *Frontiers in Integrative Neuroscience* 3(AUG).

Watson, Thomas Charles et al. 2019. “Anatomical and Physiological Foundations of Cerebello-Hippocampal Interaction.” *eLife* 8.

Wędzony, K. et al. 2000. “Cortical Localization of Dopamine D4 Receptors in the Rat Brain - Immunocytochemical Study.” *Journal of Physiology and Pharmacology* 51(2): 205–21.

West, Anthony R., and Anthony A. Grace. 2002. “Opposite Influences of Endogenous Dopamine D1 and D2 Receptor Activation on Activity States and Electrophysiological Properties of Striatal Neurons: Studies Combining in Vivo Intracellular Recordings and Reverse Microdialysis.” *Journal of Neuroscience* 22(1): 294–304.

Whitney, Elizabeth R. et al. 2008. “Cerebellar Purkinje Cells Are Reduced in a Subpopulation of Autistic Brains: A Stereological Experiment Using Calbindin-D28k.” *Cerebellum* 7(3).

———. 2009. “Density of Cerebellar Basket and Stellate Cells in Autism: Evidence for a Late Developmental Loss of Purkinje Cells.” *Journal of Neuroscience Research* 87(10).

Whittington, Miles A., and Roger D. Traub. 2003. “Interneuron Diversity Series: Inhibitory Interneurons and Network Oscillations in Vitro.” *Trends in Neurosciences* 26(12): 676–82.

Wise, Roy A. 2008. “Dopamine and Reward: The Anhedonia Hypothesis 30 Years On.” *Neurotoxicity Research* 14(2–3): 169–83.

Yan, Rongzhen, Tianyu Wang, and Qiang Zhou. 2019. “Elevated Dopamine Signaling from Ventral Tegmental Area to Prefrontal Cortical Parvalbumin Neurons Drives Conditioned Inhibition.” *Proceedings of the National Academy of Sciences of the United States of America* 116(26): 13077–86.

Yekhlef, Latefa et al. 2015. “Selective Activation of Parvalbumin- or Somatostatin-Expressing Interneurons Triggers Epileptic Seizurelike Activity in Mouse Medial Entorhinal Cortex.” *Journal of Neurophysiology* 113(5): 1616–30.

Yizhar, Ofer et al. 2011. “Neocortical Excitation/Inhibition Balance in Information Processing and Social Dysfunction.” *Nature* 477(7363).

———. 2012. “Optogenetic Insights into Social Behavior Function.” *Biological Psychiatry* 71(12).

De Zeeuw, C. I., and A. S. Berrebi. 1995. “Postsynaptic Targets of Purkinje Cell Terminals in the Cerebellar and Vestibular Nuclei of the Rat.” *European Journal of Neuroscience* 7(11): 2322–33.

Zeidán-Chuliá, Fares et al. 2016. “Up-Regulation of Oligodendrocyte Lineage Markers in the Cerebellum of Autistic Patients: Evidence from Network Analysis of Gene Expression.” *Molecular Neurobiology* 53(6).

Zhang, Wen et al. 2021. “The Role of the GABAergic System in Diseases of the Central Nervous System.” *Neuroscience* 470: 88–99.

https://doi.org/10.1016/j.neuroscience.2021.06.037.

Zhang, Xiao Yang, Jian Jun Wang, and Jing Ning Zhu. 2016. “Cerebellar Fastigial Nucleus: From Anatomic Construction to Physiological Functions.” *Cerebellum and Ataxias* 3(1).

Zhou, Fu Ming, and John J. Hablitz. 1999. “Dopamine Modulation of Membrane and Synaptic Properties of Interneurons in Rat Cerebral Cortex.” *Journal of Neurophysiology* 81(3): 967–76.

APPENDIX- During my PhD program I also participated in a project for the investigation of cerebellar circuitry frequency dependence using a high-density multi-electrode array (HD-MEA). This project led to a paper that is currently under revision.

Anisotropy and frequency-dependence of signal propagation in the cerebellar circuit revealed by high-density multielectrode array recordings.

Anita Monteverdi[1], Danila Di Domenico[2], Egidio D'Angelo [2,1], Lisa Mapelli [2*]

Original article. Biomedicines, 11(5), 1475; doi: 10.3390/biomedicines11051475. May 2023

biomedicines

MDPI

Article

Anisotropy and Frequency Dependence of Signal Propagation in the Cerebellar Circuit Revealed by High-Density Multielectrode Array Recordings

Anita Monteverdi [1], Danila Di Domenico [2], Egidio D'Angelo [1,2] and Lisa Mapelli [2,*]

[1] Brain Connectivity Center, IRCCS Mondino Foundation, 27100 Pavia, Italy
[2] Department of Brain and Behavioral Sciences, University of Pavia, 27100 Pavia, Italy
* Correspondence: lisa.mapelli@unipv.it

Abstract: The cerebellum is one of the most connected structures of the central nervous system and receives inputs over an extended frequency range. Nevertheless, the frequency dependence of cerebellar cortical processing remains elusive. In this work, we characterized cerebellar cortex responsiveness to mossy fibers activation at different frequencies and reconstructed the spread of activity in the sagittal and coronal planes of acute mouse cerebellar slices using a high-throughput high-density multielectrode array (HD-MEA). The enhanced spatiotemporal resolution of HD-MEA revealed the frequency dependence and spatial anisotropy of cerebellar activation. Mossy fiber inputs reached the Purkinje cell layer even at the lowest frequencies, but the efficiency of transmission increased at higher frequencies. These properties, which are likely to descend from the topographic organization of local inhibition, intrinsic electroresponsiveness, and short-term synaptic plasticity, are critical elements that have to be taken into consideration to define the computational properties of the cerebellar cortex and its pathological alterations.

Keywords: cerebellum; multielectrode arrays; granule cells; Purkinje cells; electrophysiology

Citation: Monteverdi, A.; Di Domenico, D.; D'Angelo, E.; Mapelli, L. Anisotropy and Frequency Dependence of Signal Propagation in the Cerebellar Circuit Revealed by High-Density Multielectrode Array Recordings. *Biomedicines* **2023**, *11*, 1475. https://doi.org/10.3390/biomedicines11051475

Academic Editor: Zhenglin Gu

Received: 24 March 2023
Revised: 5 May 2023
Accepted: 12 May 2023
Published: 18 May 2023

1. Introduction

The cerebellar network displays a well-organized modular architecture repeating itself almost identically along the entire cerebellar cortex [1]. Briefly, inputs are provided by climbing fibers (from the inferior olive, directly contacting Purkinje cells) and mossy fibers (from the rest of the brain), which send collaterals to the deep cerebellar nuclei before reaching the cortex. Here, mossy fibers (MFs) contact granular layer neurons (inhibitory Golgi cells and the most abundant neurons in the entire brain, the excitatory granule cells) in anatomical structures called "glomeruli" [2]. The granular layer is therefore considered the input layer of the cerebellar cortex. In a complex network of inhibitory loops [3], the signals are conveyed to Purkinje cells (PCs), which are the output layer of the cortex. Molecular layer interneurons (MLI) are contacted by granule cells (GrCs) and inhibit PCs. The anatomical orientation of most of these neurons influences their function. Golgi cells (GoCs) develop the axonal plexus in the sagittal plane [4,5], While the parallel fibers, i.e., GrC axons providing excitation to MLI and PCs, are organized orthogonally with respect to this plane (i.e., in the coronal plane). PCs develop their wide dendritic arborization in the sagittal plane and can also be activated by GrC ascending axons (before generating the parallel fibers; see Figure 1). MLI axons contact PCs both in the sagittal (mainly basket cells) and coronal (mainly stellate cells) planes [6–8].

This uniform and ordered network processes inputs in an extremely complex way, and a comprehensive characterization of cerebellar functions and network dynamics currently represents an open challenge. The recently recognized role of the cerebellum in higher cognitive and emotional processes, besides the well-studied sensorimotor integration, makes it even more crucial to address the issue [9–14].

Indeed, the cerebellum operates in different frequency ranges, receiving extensive and heterogeneous inputs from the motor and non-motor areas, and the cerebellar cortical activity is known to be considerably frequency dependent. The granular layer appears to be well equipped for developing and maintaining rhythmic low-frequency activity (theta band, 2–10 Hz), presenting coherent oscillations and resonance [15]. In the 20 Hz input domain, an increase in the responsiveness of GrCs and GoCs and a coherent organization of the granular layer emergent activity has been predicted [16]. At higher frequencies (50–100 Hz), MFs stimulation has been described to maximally evoke the response of PCs located over the excited granular layer area [17]. Recently, a nonlinear frequency dependence of the complex mechanisms regulating neurovascular coupling in the cerebellum has been characterized [18]. Short-term dynamics, through depression and facilitation of synaptic transmission, are known to be powerful modulators of signal transmissions in neuronal networks [6,19–21]. At the mossy fiber–granule cell relay, short-term depression is known to enhance the inhibitory control of synaptic gain, allowing multiplicative operations of the inputs by the postsynaptic neurons [22]. At the same time, the PC output depends on the combination of the short-term plasticity (mainly potentiation) at the parallel fiber connection, and that with MLI, both deeply frequency dependent [20,23]. This explains the diversity of PC response to mossy fiber stimulation, ranging from net increases in the basal firing to complete stops of spontaneous firing. Through these mechanisms, short-term plasticity is able to impact the excitatory/inhibitory balance of the granular and PC layers [20] and modulate the information transfer through the whole network [19]. However, to date, the experimental assessment of granular and PC spikes responses to a varying range of mossy fiber inputs in the sagittal and coronal planes was still missing, and a complete understanding of the frequency dependence of cerebellar cortical processing is yet to be achieved.

In this work, we characterized the frequency dependence of cerebellar processing and its short-term dynamics in the cortical input and output layers both in the sagittal and coronal orientations. We have taken advantage of a high-density multielectrode array (HD-MEA) device, a recent cutting-edge technique that allows simultaneous extracellular recordings from 4096 electrodes, sampling the activity from all the cerebellar cortical layers. Network responses to MFs stimulation at different frequencies (6 Hz, 20 Hz, 50 Hz, 100 Hz), mimicking different ranges of brain activity, were analyzed and compared in two different planes of section (sagittal and coronal) in acute mouse cerebellar slices. Our results integrate previous investigations on cerebellar frequency dependence [17] and, thanks to technological advancement, reveal an unforeseen efficiency of the cerebellar cortical network in transmitting low-frequency inputs. Moreover, cerebellar short-term dynamics showed a marked orientation dependence, revealing anisotropic signal transmission compatible with the anatomical organization of local inhibitory circuits.

2. Materials and Methods

Animal maintenance and experimental procedures were performed according to the international guidelines of the European Union Directive 2010/63/EU on the ethical use of animals and were approved by the local ethical committee of the University of Pavia (Italy) and by the Italian Ministry of Health (authorization following art. 1, comma 4 of the D. Lgs. n. 26/2014 approved on 9 December 2017).

2.1. Slice Preparation and Maintenance

Acute parasagittal or coronal cerebellar slices (220 µm thick) were obtained from 18 to 23-day-old C57BL/6 mice of either sex. Animals were anesthetized with halothane (Aldrich, Milwaukee, WI, USA) and killed by decapitation. The cerebellum was gently removed to isolate the vermis, fixed with cyanoacrilic glue on the specimen support of a vibroslicer (VT1200S, Leica Microsystems, Wetzlar, Germany), used to obtain the slices. The whole procedure was performed in cold and oxygenated Krebs solution which contained (in mM): 120 NaCl, 2 KCl, 1.2 MgSO4, 26 NaHCO3, 1.2 KH2PO4, 2 CaCl2, 11 glucose,

pH 7.4 equilibrated with 95% O_2–5% CO_2. Slices were recovered for 1 hour in the same solution before recording. To record cerebellar activity, slices were gently positioned on the HD-MEA chip improving the coupling with the electrodes array using a platinum ring with a nylon mesh. Oxygenated Krebs solution (2–3 mL/min) was continuously perfused in the glass reservoir during the whole recording session and maintained at 32 °C with a Peltier feedback temperature controller (TC-324B; Warner Instrument Corporation, Holliston, MA, USA).

2.2. High-Resolution Electrophysiological Recordings

The investigation of the cerebellar circuit was conducted using a complementary metal-oxide-semiconductor (CMOS) based high-density multielectrode array (HD-MEA; Biocam X, 3Brain AG, Wädenswil, Switzerland). The chip consisted of 4096 electrodes arranged in a 64 × 64 matrix on an area of 2.67 mm × 2.67 mm. Electrode size was 21 µm × 21 µm with a pitch of 42 µm (Biochip Arena, 3Brain AG, Wädenswil, Switzerland). The whole chip is packaged onto a substrate together with a glass reservoir with a diameter of 25 mm and 7 mm of height. Signals were sampled at 18 kHz/electrode, with a high pass filter at 100 Hz. Electrical stimulation was provided using a bipolar tungsten electrode positioned on the MFs bundle (pulses of 50 µA with a duration of 200 µs per pulse). This stimulation setting is demonstrated to selectively activate MFs, without direct GrC excitation [24]. To investigate cerebellar input processing at different frequencies, 30 single pulses were delivered at 0.1 Hz, followed by 30 trains of 5 impulses at 6 Hz, 20 Hz, 50 Hz, and 100 Hz (in mixed combinations) repeated every 10 s.

2.3. Data Analysis

2.3.1. Local Field Potentials

MFs stimulation elicited GrCs response observed in the form of Local Field Potentials (LFPs) propagating through the granular layer. The LFP was characterized by a typical N_1-N_{2a}-N_{2b}-P_2 complex. In this complex, N1 derives from the activation of the presynaptic volley, N_{2a}, and N_{2b} are informative of GrCs synaptic activation, and P2 represents the current returning from the molecular layer [18,25]. Data were displayed online and stored using the BrainWave X Software (3Brain AG, Wädenswil, Switzerland) and data analysis was performed using ad-hoc routines written in MATLAB (Mathworks). To investigate GrCs synaptic activation, only N_{2a} and N_{2b} peaks were considered for the analysis. Peak amplitudes were calculated by subtracting the negative peaks found in the appropriate time window (1.9 ± 1.1 ms and 4.5 ± 1.2 ms from the stimulus artifact, for N_{2a} and N_{2b}, respectively; [25]) to the baseline derived from the averaged signal in 300 ms before the stimulus onset. LFP signals were considered for the analysis only when the peak amplitude exceeded 3 times (for N_{2a}) and 2.5 times (for N_{2b}) the standard deviation calculated over the baseline period, in response to at least 75% of trials. LFP signals stability (see right inset in Figure 2) over the entire duration of the experiment was verified using an unpaired Student's *t*-test. Channels showing a significant increase or decrease of the N_{2a} peak amplitude in response to single pulse stimulation or to the first stimulation in the pulse trains at the end of the recording were discarded (significance at $p < 0.05$). The percent change of the last response in the train, compared to the first one, within each stimulation, pattern was calculated both for N_{2a} and N_{2b}, and then used to generate colormaps to represent the corresponding spatial distribution. The signals showing a statistically significant change (unpaired Student's *t*-test, $p < 0.05$) in N_{2a} and N_{2b} peak amplitudes at the end of the 5 pulses stimulation compared to the first response in the train were considered undergoing short-term plasticity. Data are reported as mean ± SEM (standard error of the mean).

2.3.2. Purkinje Cell Firing

PCs autorhythmic spiking activity was recorded using the BrainWave X software (3Brain AG, Wädenswil, Switzerland). The analysis of PCs firing was performed using

BrainWave 4 software (3Brain AG, Wädenswil, Switzerland) and ad-hoc routines written in MATLAB (Mathworks). PCs were identified based on three main parameters: (i) their location on the slice, between the granular and molecular layers following the lobule layout; (ii) their firing frequency, ranging from 10 to more than 100 Hz; (iii) the spike amplitude exceeding 100 µV. Possible contamination by basket cells cannot be completely ruled out, given that these cells have their cell bodies located in the internal molecular layer and some can be found near PCs. However, basket cells are smaller than PCs and usually have lower spontaneous discharge frequency, so their spikes are unlikely to be detected and confused with those of the PCs. Therefore, although we cannot exclude that some basket cells could have been included in the analysis, their impact on the results should be negligible. Moreover, complex spikes were never observed after MF stimulation but could be elicited by positioning the stimulating electrode underneath the PC layer (see left inset in Figure 2). Spike detection of PC activity was performed in BrainWave 4 using the hard threshold of ±100 µV (refractory period of 1 ms). Spike detection was followed by the waveform extraction in a temporal window of 0.5 ms pre-spike and 3 ms post-spike and the spike sorting using a Principal Component Analysis based on spikes characteristics followed by a clustering k-mean algorithm. Pakhira-Bandyopadhyay-Maulik (PBM) index was used for validating clustering results. Due to the inter-electrode tip distance of 42 µm and the large PC soma (25–40 µm diameter), commonly more than a unit was detected by every single electrode of the HD-MEA. The BrainWave 4 software was used to eliminate common units in nearby channels and retain the signal only in the channel presenting spikes with the largest amplitude. In this way, the same PC was not considered multiple times in different electrodes. The user's supervision of every step of this procedure was performed. Then peri-stimulus time histograms (PSTHs) and raster plots were used for the analysis of PCs' responses to stimulation. PC responses consisted of a transient increase or decrease of the basal discharge. Herein, an increase in PC firing frequency was defined as a peak in the PSTH, while a decrease in firing frequency was defined as a pause in the PSTH. Peaks and pauses detection was performed using one-tailed permutation test [26]. The permutation test was restricted to increased Mean Firing Rate (MFR) for peaks and decreased MFR for pauses. In both cases, it was followed by a false discovery rate correction with alpha at 0.01. PSTHs resolution was set at 5 ms/bin to analyze peaks and 20 ms/bin to analyze pauses. For each PC detected, the basal MFR was calculated on the 500 ms pre-stimulus period and used to generate colormaps. The percent change of the MFR within each stimulation pattern was calculated by comparing the MFR at the end (during the last two pulses) of the trains at different input frequencies to the MFR at the beginning (during the first two pulses) of the trains at different input frequencies. This percent change was used to generate colormaps together with the percent change of N_{2a} peak amplitude obtained from the previous analysis. Data are reported as mean ± SEM.

3. Results

The activity of the granular and PC layers was recorded using a high-density multi-electrode array (HD-MEA), which provides an exceptional spatiotemporal resolution [18]. In both sagittal and coronal slices, MFs were stimulated to activate the cerebellar cortical network. As evident in Figure 1, MFs contact both GrCs and GoCs in the granular layer. GrCs axons originate the parallel fibers, which contact PCs, MLIs, and GoCs. GrCs are then inhibited through feedforward (MF–GoC–GrC) and feedback (GrC–GoC–GrC) loops. In turn, PCs are excited by GrCs and inhibited by MLIs, which provide inhibitory loops in the molecular layer. It is evident that the inhibitory component is predominant both in the granular and molecular layers, to determine cerebellar cortical processing, [2,3]. The architecture of the cerebellar cortex is such that forcing a sagittal or coronal orientation to the circuit activation (by using the slicing procedure) is expected to impact cerebellar processing. In this work, we characterized how cerebellar input and output layers responses are affected, at different activity ranges, by the sagittal or coronal orientation of the circuit.

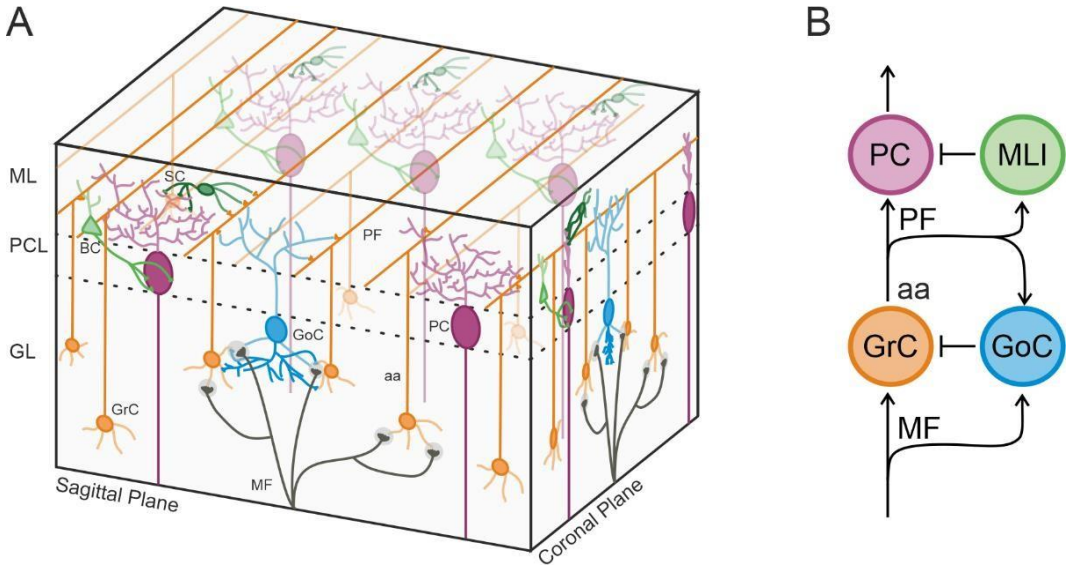

Figure 1. The cerebellar circuit. (**A**) 3D orthographic view of the cerebellar network. As can be seen, mossy fibers (MF) convey an excitatory input in the granular layer (GL), contacting granule cells (GrC) and Golgi cells (GoC). GoC develop their axonal plexus in the sagittal plane and exert a feedforward and a feedback inhibition onto GrC. GrC axon (aa) passes vertically the Purkinje cells layer (PCL) and reaches the molecular layer (ML) originating parallel fibers (PF). These fibers are organized orthogonally in the coronal plane and make excitatory synapses onto Purkinje cells (PC). PC develop their dendritic arborization in the sagittal plane and their activity is under the inhibitory control exerted by stellate cells (SC) and basket cells (BC). Dendrites and axons are of different color grades (lighter and darker, respectively). (**B**) Schematic representation of the cerebellar cortical circuit. Forward and stop arrows indicate excitatory and inhibitory connections, respectively.

3.1. Characterization of Cerebellar Cortical Activity with HD-MEA

HD-MEA recordings are the ideal tool to access the spontaneous activity of PCs and the responses to MFs stimulation on both the granular layer (silent at rest) and the PC layer itself (Figure 2). PCs spontaneous activity was detected by 1859 channels in 9 sagittal slices and 1809 channels in 9 coronal slices, resulting in the characterization of 858 and 1095 single units, respectively (Table 1; see Methods for details on the spike sorting procedure). The basal MFR of the detected units was 58.1 ± 2.8 Hz in sagittal slices (n = 9) and 85.5 ± 8.0 Hz in coronal slices (n = 9; Student's t-test, p = 0.001). PCs showed heterogeneous basal MFR ranging from 10 Hz to more than 100 Hz. A color map representing the spatial organization of PCs with different basal MFR was reconstructed (Figure 3A). Interestingly, in coronal slices PCs with low and high basal MFR tended to alternate in bands, while in sagittal slices no evident pattern could be detected. Though this kind of characterization is beyond the scope of this work, this spatial organization resembles the zebrin-like distribution pattern described for PCs in the coronal plane [27].

Table 1. Recording channels and detected units.

	SAGITTAL	CORONAL	
	n **= 9**	***n*** **= 9**	**tot**
ch granular layer	804	1649	2453
ch Purkinje cells	1859	1809	3668
detected units	858	1095	1953

Single-pulse MFs stimulation evoked GrCs responses, recorded as LFPs propagating through the granular layer of the stimulated lobule, both in sagittal and coronal slices (Figure 2). The LFP showed the typical N1-N_{2a}-N_{2b}-P2 complex in agreement with pre-

vious observations [18,24,25]. Herein, the analysis was focused on N_{2a} and N_{2b} peaks as a measure of postsynaptic GrCs activation (see Methods for details). Over the large sample obtained (804 channels in 9 sagittal slices and 1649 channels in 9 coronal slices; Table 1), the average peak delays and amplitudes for N_{2a} and N_{2b} peaks were as follows. N_{2a}: 1.60 ± 0.02 ms and − 233.3 ± 21.4 µV in parasagittal slices; 1.55 ± 0.04 ms and − 214.0 ± 19.6 µV in coronal slices. N_{2b}: 4.51 ± 0.09 ms and −76.8 ± 3.8 µV in parasagittal slices; 4.25 ± 0.16 ms and −71.8 ± 9 µV in coronal slices. N_{2a} and N_{2b} peaks delays and amplitudes did not present a significant difference in sagittal and coronal slices (unpaired Student's *t*-test, N_{2a} $p = 0.32$ and $p = 0.51$, N_{2b} $p = 0.19$ and $p = 0.26$). The LFP spread through the granular layer was recorded along the stimulated lobule, allowing us to compute the propagation velocity of the signal. In sagittal and coronal slices, signal velocity was respectively 0.66 ± 0.09 m/s and 0.44 ± 0.09 m/s, not presenting significant differences (unpaired Student's *t*-test, $p = 0.12$).

The table shows the number of channels in nine parasagittal and nine coronal slices detecting local field potential (LFP) signals in the granular layer and Purkinje cells firing (ch = channels). The number of units detected in sagittal and coronal slices after spike detection and spike sorting operations is reported. The last column contains the total amount of channels and units analyzed from all cerebellar slices.

To characterize PC responses, raster plots, and PSTHs were reconstructed for each PC detected (Figure 3B,C). Over a total of 1953 units (858 in sagittal slices and 1095 in coronal), two different types of responses were identified: a rapid significant increase of PCs basal firing in the PSTH (within 20 ms after the pulse, here defined as "peak") and a significant decrease of PCs firing in the PSTH (within 40 ms after the pulse, here defined as "pause"). As evident in Figure 3B, PCs' most common response pattern was an increase in their basal discharge after a single pulse stimulation in sagittal slices and a decrease in their basal discharge in coronal slices.

For simplicity, the detailed analysis of cerebellar cortical responses to different frequencies of MFs stimulation is reported separately for the experiments performed in sagittal and coronal slices. The comparison between these two conditions is highlighted in a devoted paragraph at the end of Section 3.

3.2. Short-Term Plasticity on the Sagittal Plane

3.2.1. Granular Layer Responses at Different Input Frequencies

To characterize granular layer responses to different ranges of activity, MFs were stimulated with 5 pulses at 6, 20, 50, and 100 Hz. The amplitude of the LFP N_{2a} and N_{2b} peaks following each pulse was measured and normalized for comparison (Figure 4).

The percent change of the amplitude in response to the last pulse in the train, compared to the first one, was used to determine the direction of the short-term plasticity recorded. The results showed a trend to decrease for N_{2a} peak amplitude, while the N_{2b} peak showed significantly more variability (paired Student's *t*-test, $p = 0.009$) at increasing frequency, increasing or decreasing its amplitude during the stimulation trains (Table 2 and Figure 4). However, while the percentage of channels showing a significant change in N_{2a} peak amplitude was always high in the granular layer (more than 70% of the recorded channels), the percentage of channels detecting a significant change in N_{2b} was more than 40% only at high input frequencies (Table 2).

On average, N_{2a} peak amplitude showed short-term depression, becoming more evident increasing the stimulation frequency. In turn, N_{2b} appeared to weakly tend to increase especially at higher input frequencies, but the heterogeneous profile evident in the channel population needs to be considered (Figure 4).

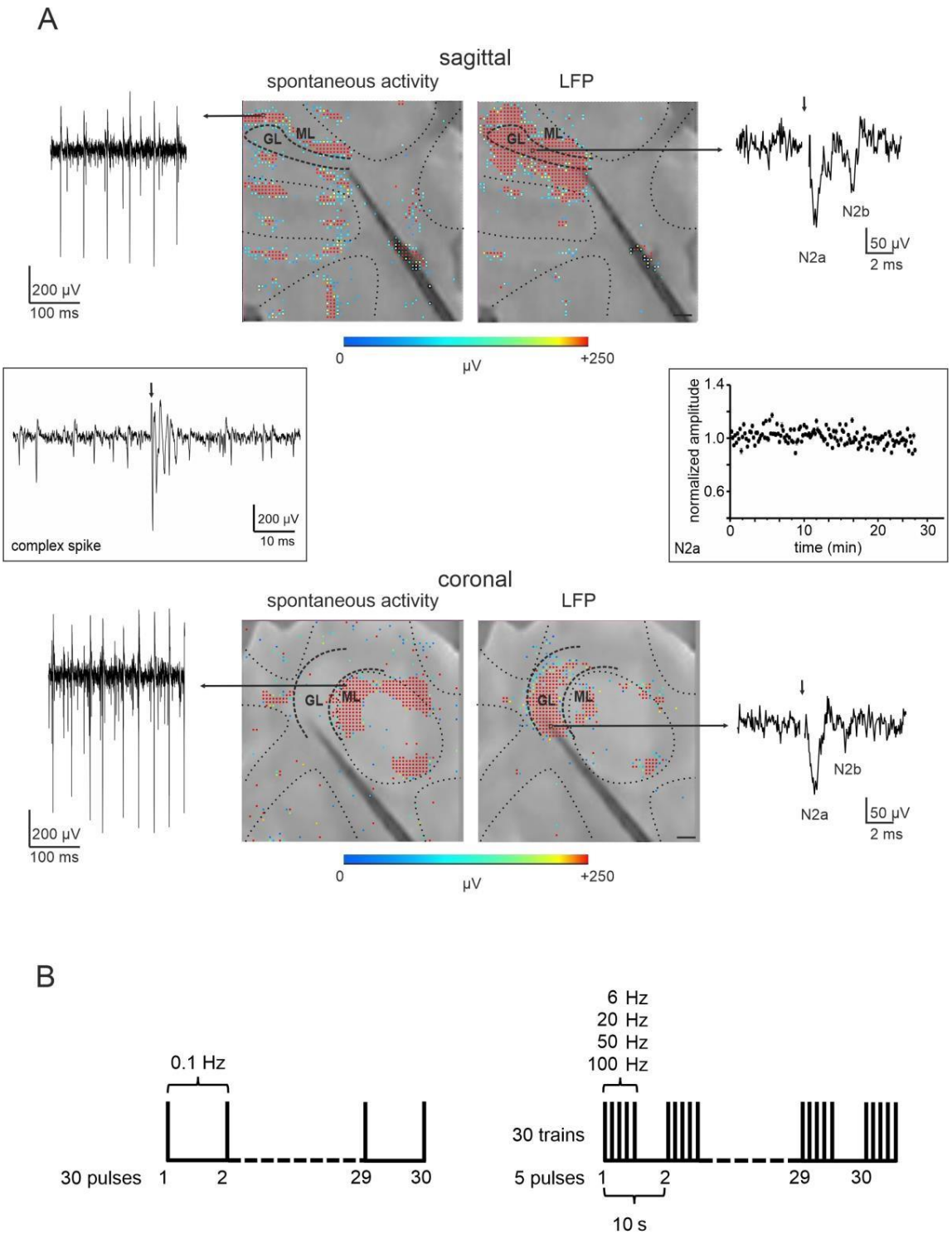

Figure 2. Typical HD-MEA recording. (**A**) For both sagittal (upper panels) and coronal (lower panels) orientations, the images in the center show the cerebellar slice on the chip (scale bar 250 µm), with the stimulating electrode (black line) positioned on the MFs. The colored dots over the slice represent the single HD-MEA channels showing neuronal activity in the selected time-bin (500 ms at left, 3 ms at right). The raw traces represent examples of recordings of PCs' spontaneous activity (left) and local field potential (LFP, right). The N_{2a} and N_{2b} peaks of the LFP are indicated in the electrophysiological trace. The plot in the inset shows the time course of the average N_{2a} peak amplitude in response to single pulse stimulation and to the first stimulation in the trains, for all the channels used for the analysis. (**B**) Schematic representation of the stimulation protocol.

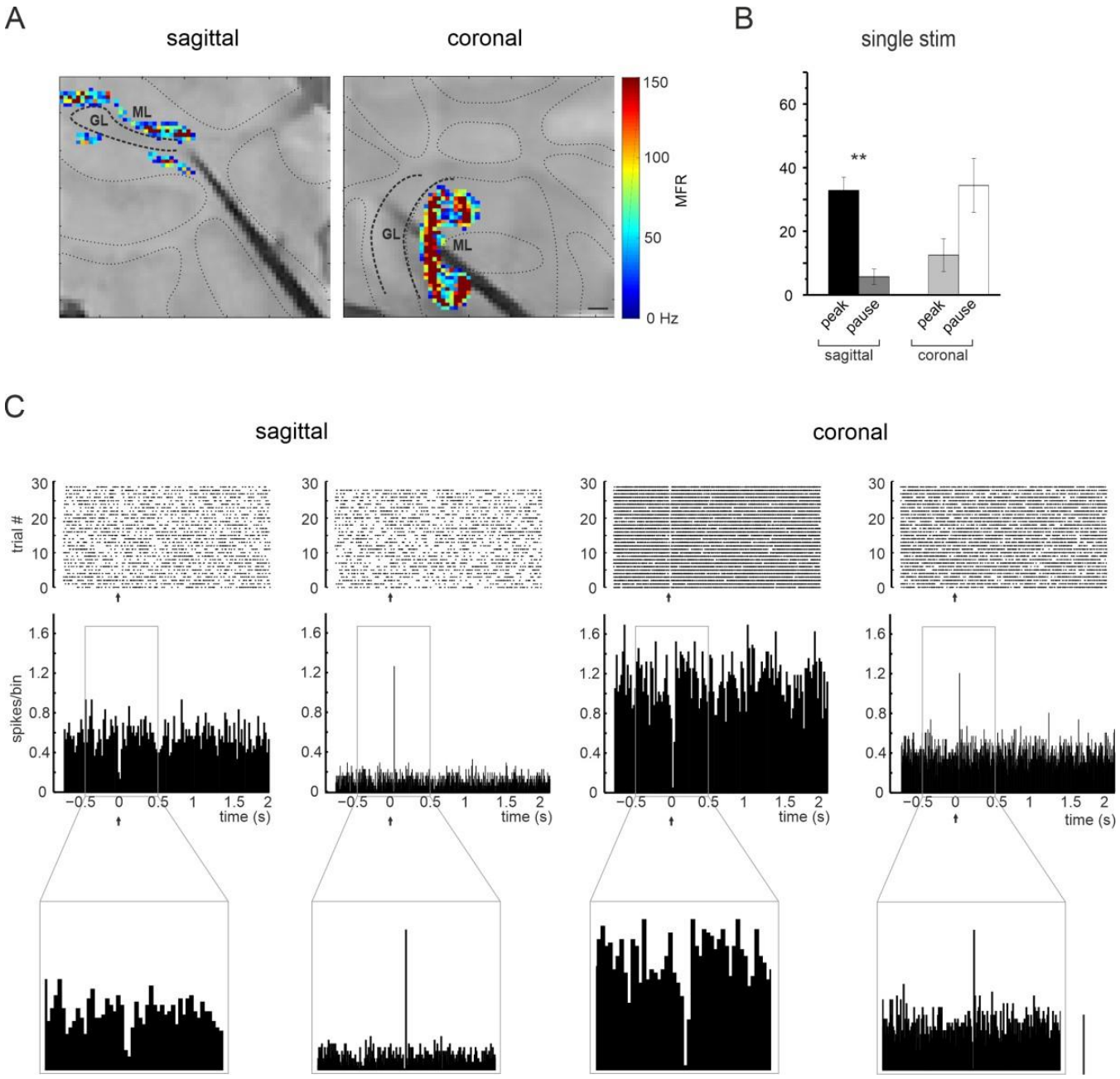

Figure 3. PCs' spontaneous and evoked activity. (**A**) The pictures show the cerebellar slice on the chip, with superimposed the location of the analyzed channels for PCs' spontaneous activity, for a sagittal (left) and coronal (right) experiment. For each channel, the basal mean firing rate (MFR) of a single unit is represented using the color scale on the right. Scale bar 200 μm. (**B**) The histograms show the percentage of PCs showing peaks or pauses in response to single-pulse MF stimulation in sagittal and coronal slices (** $p < 0.01$). (**C**) Examples of raster plots and PSTHs of PCs' activity are reported for both sagittal (left) and coronal (right) slices. The PSTH shows the two main classes of PCs' responses: a significant increase of PCs firing in the PSTH (5 ms-bin, peak) or a significant decrease of PCs firing in the PSTH (20 ms-bin, pause). The PSTH in the time window corresponding to −0.5/0.5 s is magnified below. Scale bar 0.5 sp/bin.

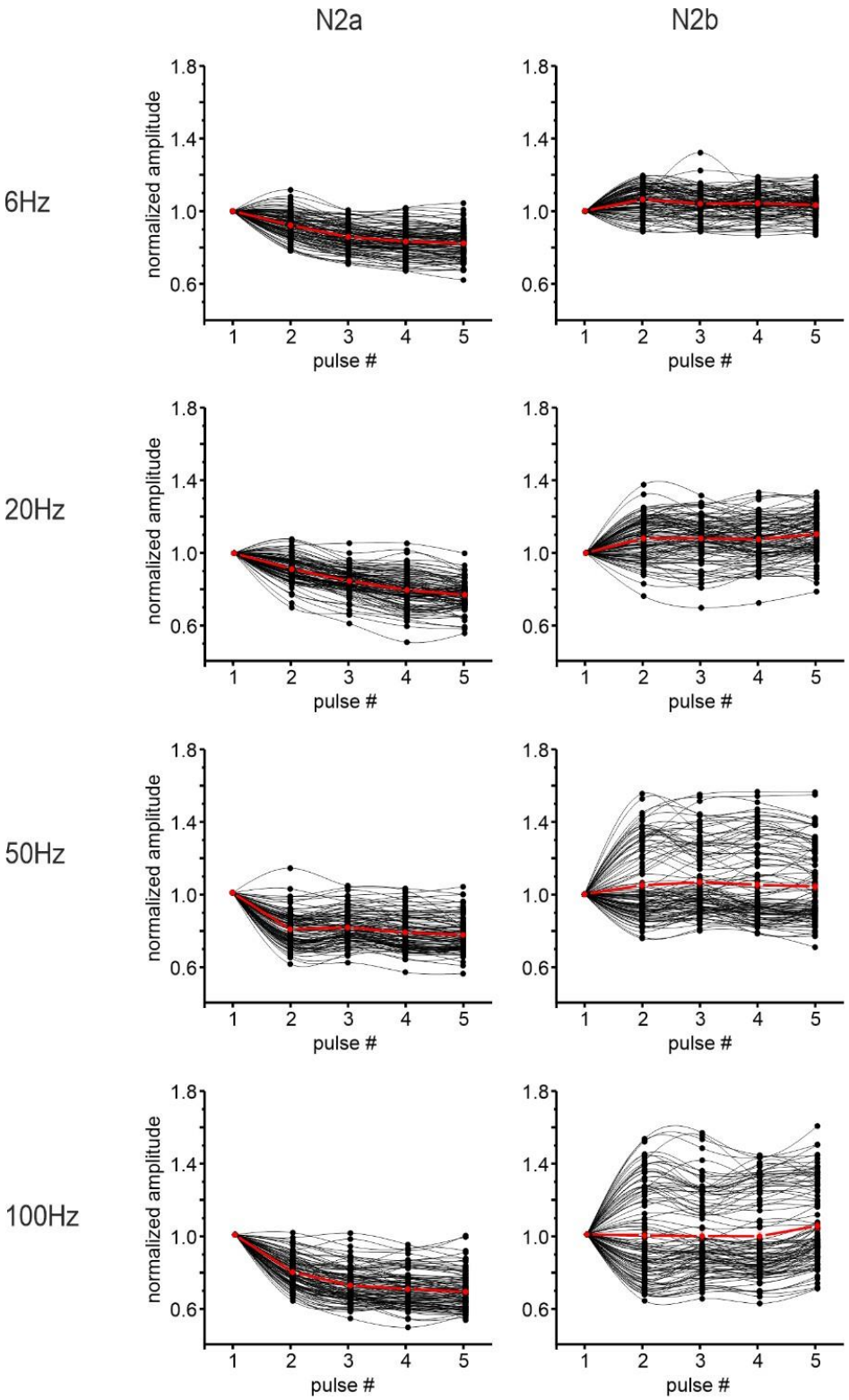

Figure 4. Granular layer responses to stimulation trains in sagittal slices. The plots show the normalized N_{2a} (left column) and N_{2b} (right column) peak amplitudes within the stimulation trains at the different frequencies tested. The responses to each of the five stimulation pulses in the train were normalized to the response to the first pulse. Black dots represent the single channels considered for the analysis. The red dots show the average trend.

Table 2. N_{2a} and N_{2b} peak amplitude changes at different input frequencies (sagittal plane). (A) The table shows the percent change of the peak amplitude in response to the last pulse compared to the first one within each stimulation pattern. (**B**) The table shows the percentage of channels in the granular layer undergoing N_{2a} or N_{2b} short-term plasticity.

A				
	6 Hz	**20 Hz**	**50 Hz**	**100 Hz**
N_{2a}	−13.60 ± 0.99	−15.58 ± 1.45	−19.87 ± 1.41	−27.37 ± 1.92
$N_{2b}\uparrow$	12.33 ± 1.68	13.89 ± 2.01	17.13 ± 2.83	20.09 ± 3.18
$N_{2b}\downarrow$	−10.59 ± 2.42	−13.36 ± 3.08	−17.34 ± 1.85	−13.48 ± 2.10
B				
	6 Hz	**20 Hz**	**50 Hz**	**100 Hz**
%ch N_{2a}	75.82 ± 4.63	72.34 ± 6.48	83.92 ± 3.85	88.82 ± 3.03
%ch $N_{2b}\uparrow$	11.83 ± 3.61	16.94 ± 5.74	25.74 ± 5.88	40.09 ± 9.05
%ch $N_{2b}\downarrow$	16.57 ± 9.41	15.15 ± 8.86	22.81 ± 7.61	13.56 ± 4.49

In both tables, $N_{2b}\uparrow$ stands for N_{2b} amplitude increase during the stimulation trains and $N_{2b}\downarrow$ refers to N_{2b} amplitude decrease during the stimulation trains.

3.2.2. The Spatial Organization of Short-Term Plasticity in the Granular Layer

The spatial resolution of the HD-MEA was exploited to investigate the spatial organization of granular layer responses in the stimulated lobules. The previously calculated percent changes of N_{2a} and N_{2b} peaks following MFs stimulation at the different frequencies tested were used to generate color maps showing the position of each channel (and the relative response) in the cerebellar lobule. Colormaps constructed with N_{2a} peak percent change suggested a spatial organization of short-term plasticity in the granular layer (Figure 5A). Larger short-term depression appeared to be more pronounced in the center of the granular layer, becoming more evident at increasing stimulation frequencies. An average colormap of all the recordings was reconstructed aligning the slices along the MF axis, showing a sort of longitudinal spatial organization of short-term plasticity in the sagittal plane (Figure 5B).

The spatial organization of N_{2b} percent changes in the granular layer appeared to be different than N_{2a}. As evident in Figure 5A, the trend to increase the N_{2b} peak appeared more accentuated in the center of the granular layer, and this phenomenon was more evident increasing the input frequency. The reconstruction of the average color map (Figure 5B) showed that this spatial organization is consistent in the different slices, though less defined in the longitudinal axes at all frequencies compared to the one shown for N_{2a}.

3.2.3. Purkinje Cells Responses at Different Input Frequencies

PCs responses were evaluated at all input frequencies (6 Hz, 20 Hz, 50 Hz, 100 Hz). Unfortunately, the short time interval between pulses at 100 Hz hampered the reconstruction of PC responses within the train at that frequency. The results are reported as a percentage of units presenting MFR increases or decreases in response to the stimulation. As reported in Figure 6A, the PCs' most common response pattern was an increase (PSTH peak) in the basal discharge after each stimulation pulse at all the frequencies examined, while the decrease in the basal discharge (PSTH pause) was less common (see statistics in Figure 6A). This trend was more evident at increasing frequencies.

Finally, the percent change of the MFR during the stimulation train was calculated within each stimulation pattern (6 Hz, 20 Hz, 50 Hz, excluding the 100 Hz case for the above-mentioned limitation). Similar to what was already described for the granular layer, the comparison between the last and the first response in the stimulation train was calculated, here as percent changes in the MFR. A special representation of the units was obtained generating colormaps showing the percent change. These maps were combined with the ones generated for the granular layer to describe the short-term modifications in neuronal activity in both layers of the cerebellar cortex (Figure 6B). Notice that increasing

the input frequency determined a marked decrease in granular N_{2a} amplitude while a marked increase in PCs MFR.

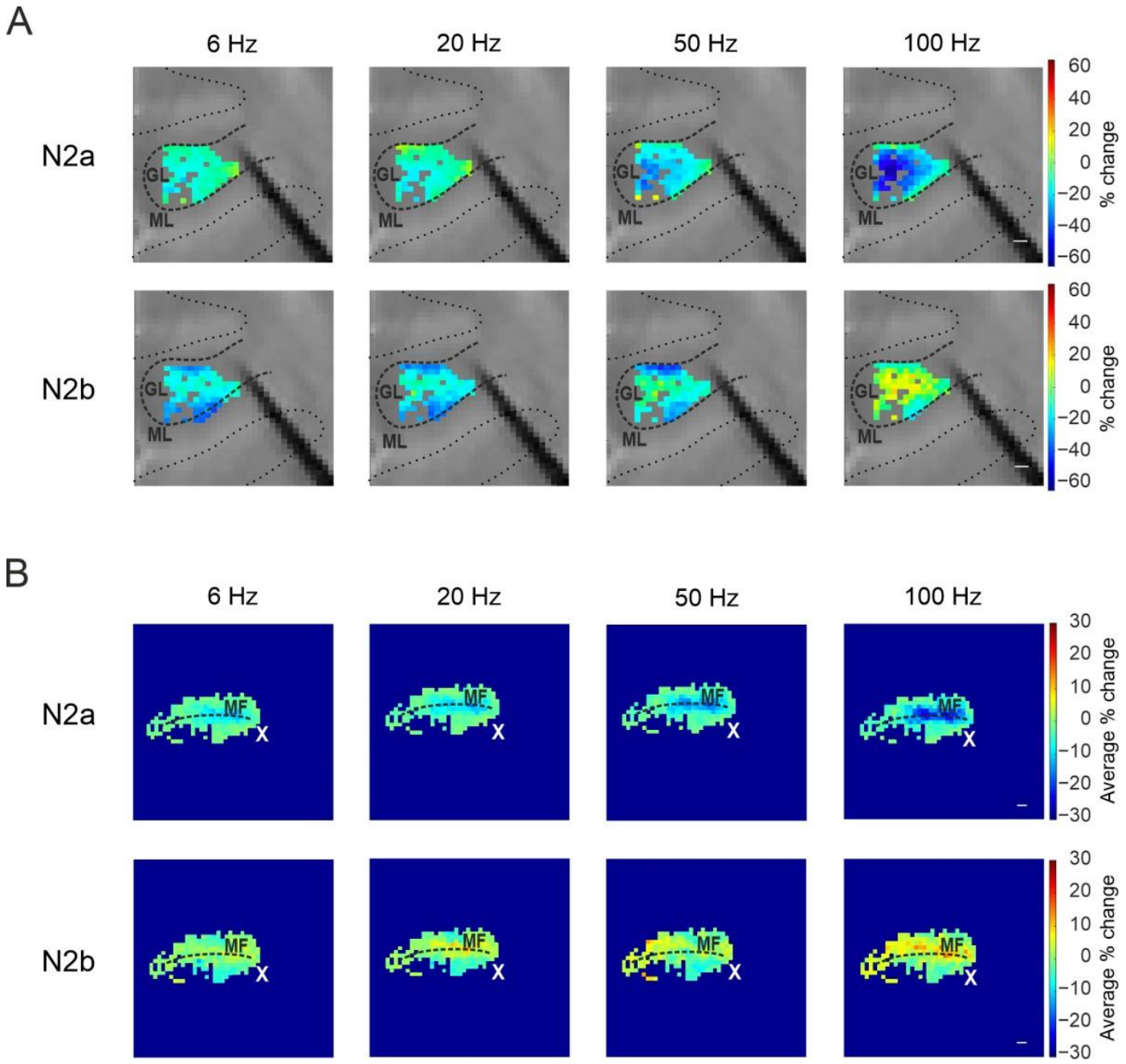

Figure 5. The spatial organization of short-term plasticity in the sagittal plane. (**A**) Color maps were reconstructed for each stimulation pattern with the percent change of N_{2a} (top panels) and N_{2b} (bottom panels) peak amplitude after the last stimulation pulse compared to the first one, from a single experiment. Scale bar 100 μm. (**B**) Average colormaps obtained aligning the recorded slices along the MFs axis, showing the average percent change of N_{2a} (top panels) and N_{2b} (bottom panels) peak amplitude. The white cross indicates the stimulus location.

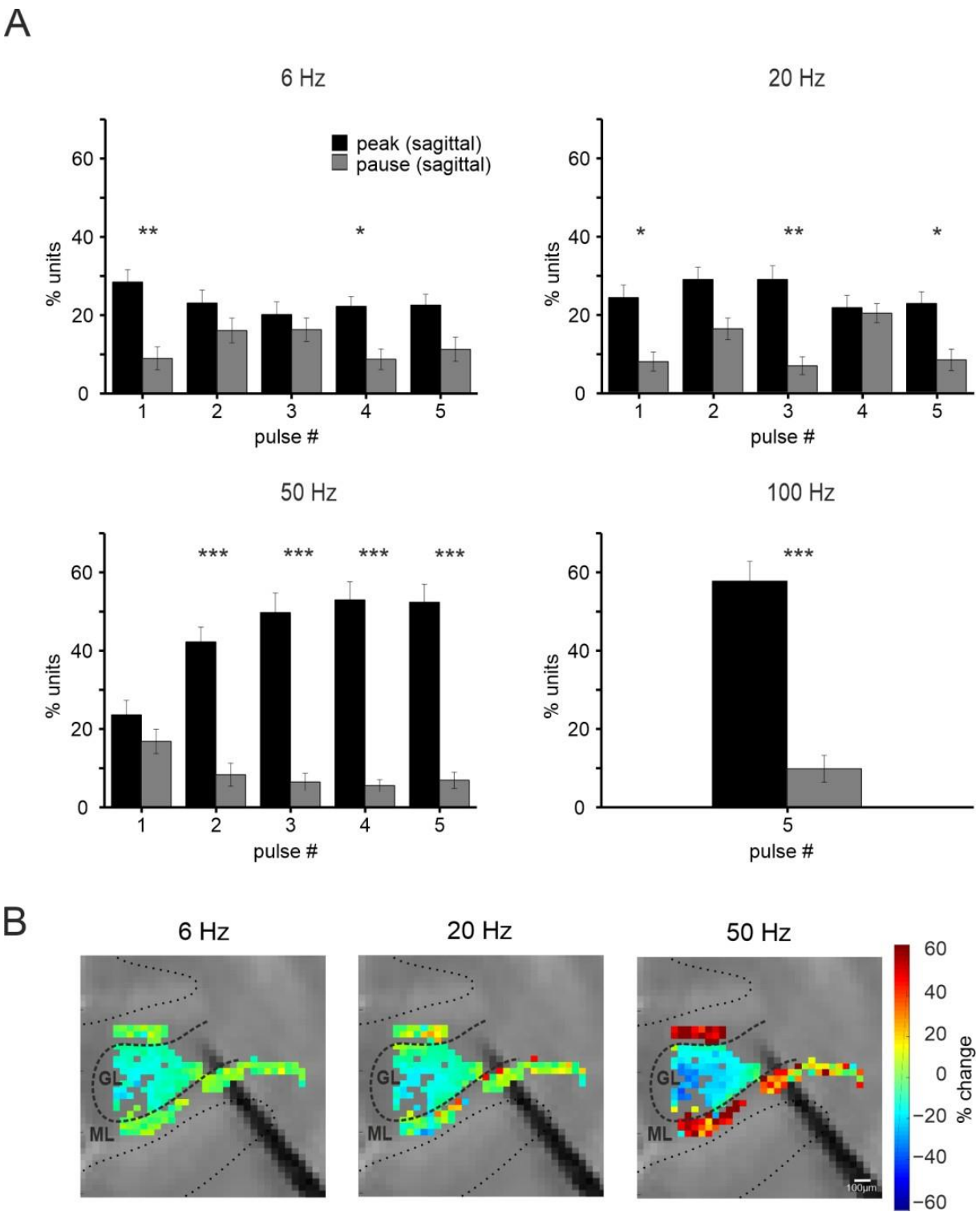

Figure 6. PCs responses to MF stimulation in the sagittal plane. (**A**) The histograms show the average percentage of units responding to MF stimulation at different frequencies with peaks (black) or pauses (grey) in the PSTHs. Asterisks indicate statistical significance (* $p < 0.05$, ** $p < 0.01$, *** $p < 0.001$). (B) Colormaps showing the percent change of PCs MFR at the last stimulation pulse compared to the first one, at 6, 20, and 50 Hz, in a single experiment (scale bar 100 μm). In the same image, the channels in the granular layer showing a response to MF stimulation are reported, for the same experiment, showing the percent change of the N_{2a} peak (as in Figure 5A) using the same color code at right.

3.3. Short-Term Plasticity on the Coronal Plane

3.3.1. Granular Layer Responses at Different Input Frequencies

The same analysis performed on sagittal slices was repeated on 9 coronal slices. The percent change of N_{2a} and N_{2b} peaks was calculated at different input frequencies together with the percentage of channels showing short-term plasticity of N_{2a} and N_{2b} peak amplitudes in the granular layer. Again, the decrease of N_{2a} peak amplitude prevailed within the stimulation trains, becoming more evident increasing the stimulation frequency (Figure 7).

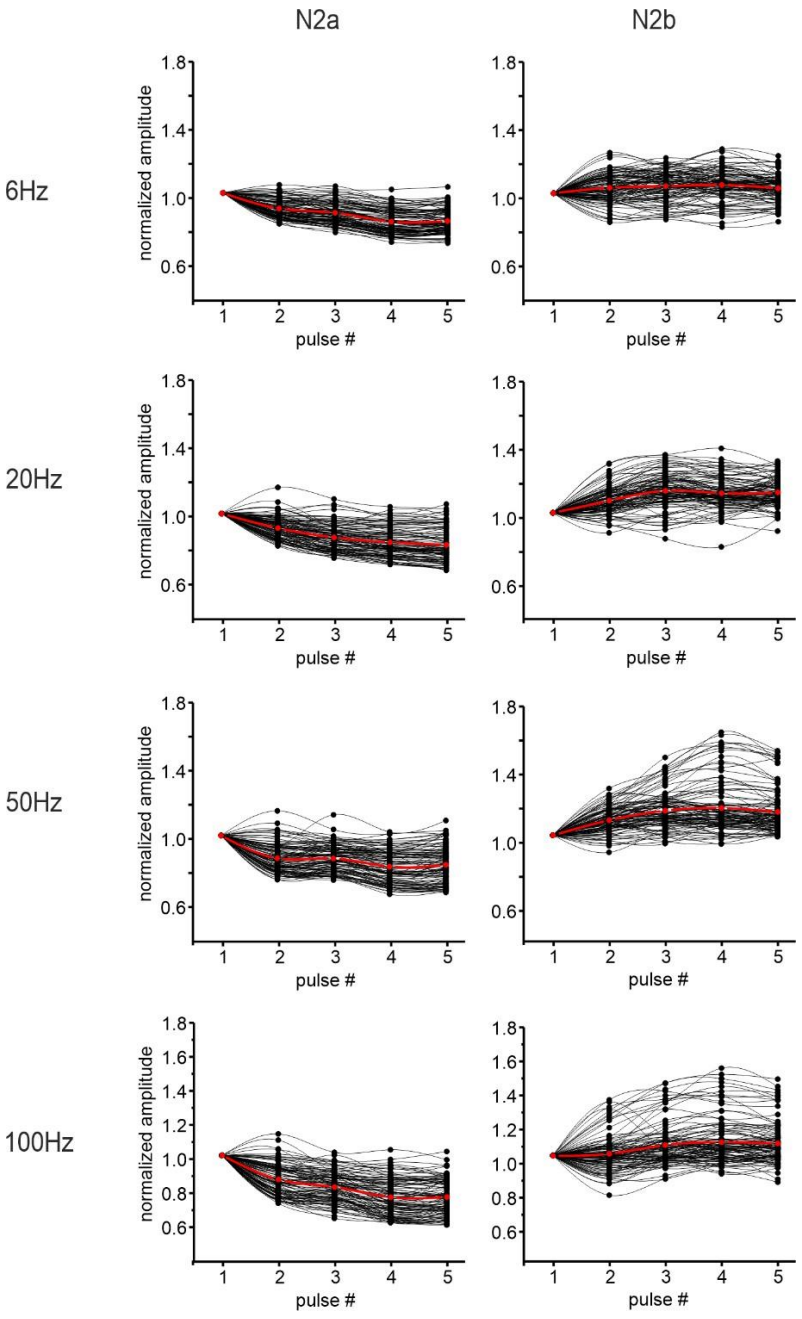

Figure 7. Granular layer responses to stimulation trains in coronal slices. The plots show the normalized N_{2a} (left column) and N_{2b} (right column) peak amplitudes within the stimulation trains at the different frequencies tested. The responses to each of the five stimulation pulses in the train were normalized to the response to the first pulse. Black dots represent the single channels considered for the analysis. The red dots show the average trend.

N_{2b} showed both an increase and a decrease in its amplitude (Table 3), but its variability during the train was not significantly increased (paired Student's *t*-test $p = 0.35$) at increasing frequency. Moreover, among the channels showing a response to the stimulation, the percentage of channels showing short-term plasticity in the N_{2a} peak amplitude was above 50% at every condition, while it reached 40% only at higher input frequencies (50 Hz and 100 Hz) for the N_{2b} peak (Table 3). The percentage of channels showing a significant increase in the N_{2b} peak amplitude was larger than the percentage of channels presenting a decrease (Table 3).

Table 3. N_{2a} and N_{2b} peak amplitude changes at different input frequencies (coronal plane). (**A**) The table shows the percent change of the last response peak compared to the first one within each stimulation pattern. (**B**) The table shows the percentage of channels in the granular layer recording a significant N_{2a} or N_{2b} peak amplitude change.

A				
	6 Hz	**20 Hz**	**50 Hz**	**100 Hz**
N_{2a}	−13.44 ± 0.84	−14.92 ± 1.26	−17.56 ± 0.89	−23.93 ± 1.46
N_{2b} +	14.80 ± 1.44	14.26 ± 1.65	18.23 ± 1.69	17.62 ± 1.41
N_{2b} −	−10.63 ± 1.71	−11.55 ± 2.19	−6.53 ± 2.12	−10.28 ± 2.30
B				
	6 Hz	**20 Hz**	**50 Hz**	**100 Hz**
%ch N_{2a}	53.96 ± 7.18	55.47 ± 6.85	61.59 ± 6.73	78.94 ± 5.37
%ch N_{2b} ↑	18.01 ± 6.02	19.77 ± 4.94	41.60 ± 4.43	39.41 ± 6.78
%ch N_{2b} ↓	4.75 ± 1.60	2.23 ± 0.79	0.74 ± 0.29	2.60 ± 1.12

In both these tables N_{2b}↑stands for N_{2b} amplitude increase during the stimulation trains while N_{2b} ↓refers to N_{2b} amplitude decrease during the stimulation trains.

N_{2a} and N_{2b} peak amplitude changes for each stimulus in the trains are reported in Figure 7, showing an average predominant short-term depression for N_{2a} peak amplitude and an average weak increase for N_{2b} peak amplitude. Again, the heterogeneous profile evident in the channel population when considering N_{2b} peak amplitude needs to be considered.

3.3.2. The Spatial Organization of Short-Term Plasticity in the Granular Layer

The percent change of N_{2a} and N_{2b} peaks in each recorded channel was used to construct colormaps representing the spatial organization of the responses in the granular layer. Again, short-term depression of the N_{2a} peak was more pronounced in the center of the responding region. This was more evident at increasing frequencies, suggesting a frequency dependence (Figure 8A). The average colormap was reconstructed aligning all the recordings along the MF axis, confirming the organization observed in each single experiment (Figure 8B).

The N_{2b} peak amplitude changes during the stimulation showed a less defined spatial organization, compared to N_{2a} (Figure 8A). Nevertheless, the increase in the N_{2b} peak was more concentrated in the center of the responding region nearest to the stimulation site. This was more evident in the average colormaps. Again, this effect was enhanced at increasing stimulation frequencies (Figure 8B).

3.3.3. Purkinje Cells Responses at Different Input Frequencies

Raster plots and PSTHs reconstructed for each stimulation frequency showed a combination of peaks and pauses over a total of 1095 units. During stimulation at different frequencies, PC responses showed pauses prevailing at the beginning and peaks prevailing at the end of the five-pulse train (Figure 9A).

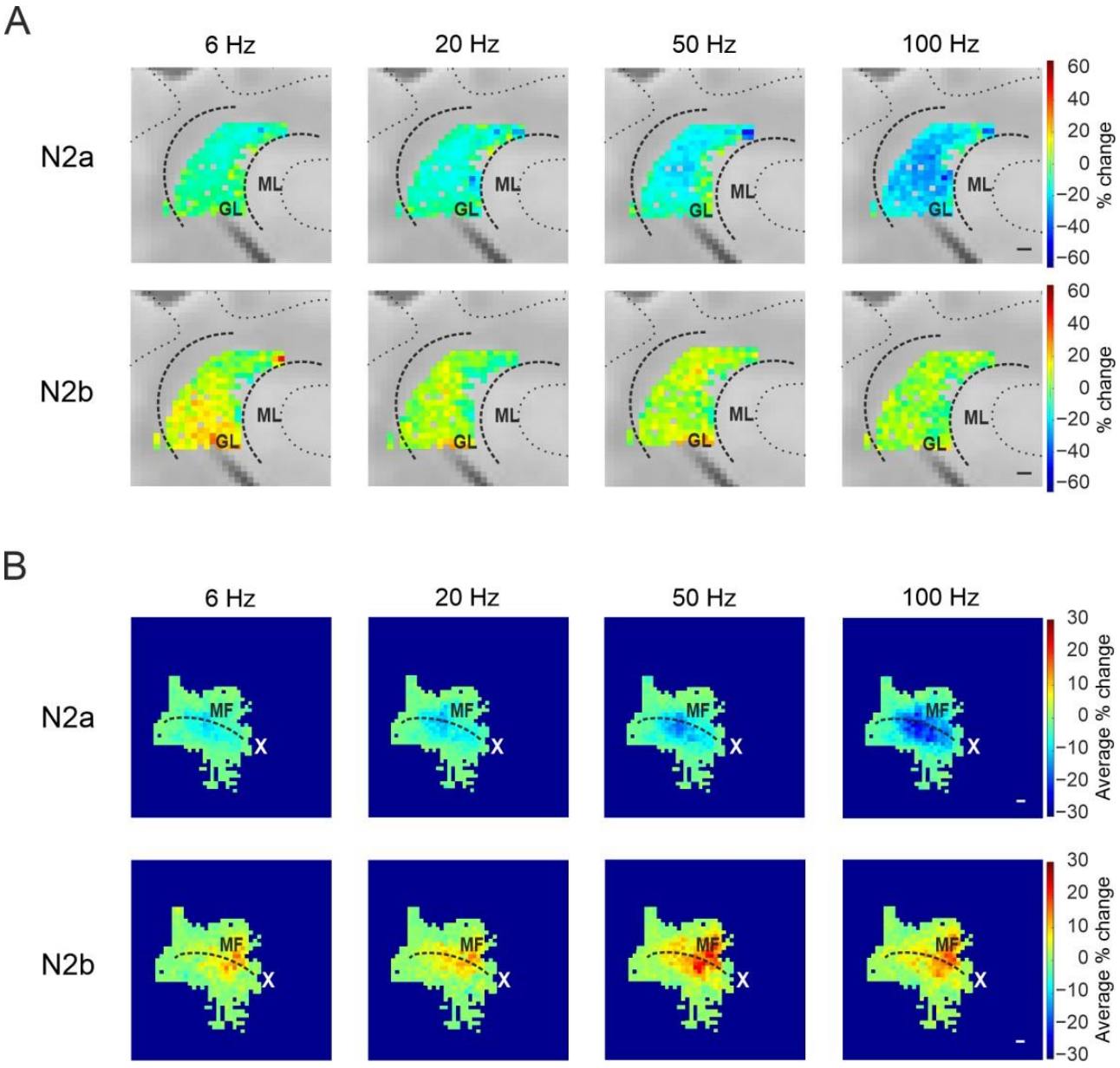

Figure 8. The spatial organization of short-term plasticity in the coronal plane. (**A**) Color maps were reconstructed for each stimulation pattern with the percent change of N_{2a} (top panels) and N_{2b} (bottom panels) peak amplitude after the last stimulation pulse compared to the first one, from a single experiment. Scale bar 100 μm. (**B**) Average colormaps obtained aligning the recorded slices along the MFs axis, showing the average percent change of N_{2a} (top panels) and N_{2b} (bottom panels) peak amplitude. The white cross indicates the stimulus location.

Finally, the percent change of the MFR was calculated within each stimulation pattern (6 Hz, 20 Hz, 50 Hz), excluding the 100 Hz for the limitations specified above. Colormaps were generated using this percent change and combined with the ones describing granular layer short-term plasticity, for each experiment (Figure 9B), representing the spatio-temporal reconstruction of cerebellar cortical responses at different input frequencies in the coronal plane. Notice that increasing the input frequency determined a marked decrease in granular N_{2a} amplitude while a marked increase in PCs MFR.

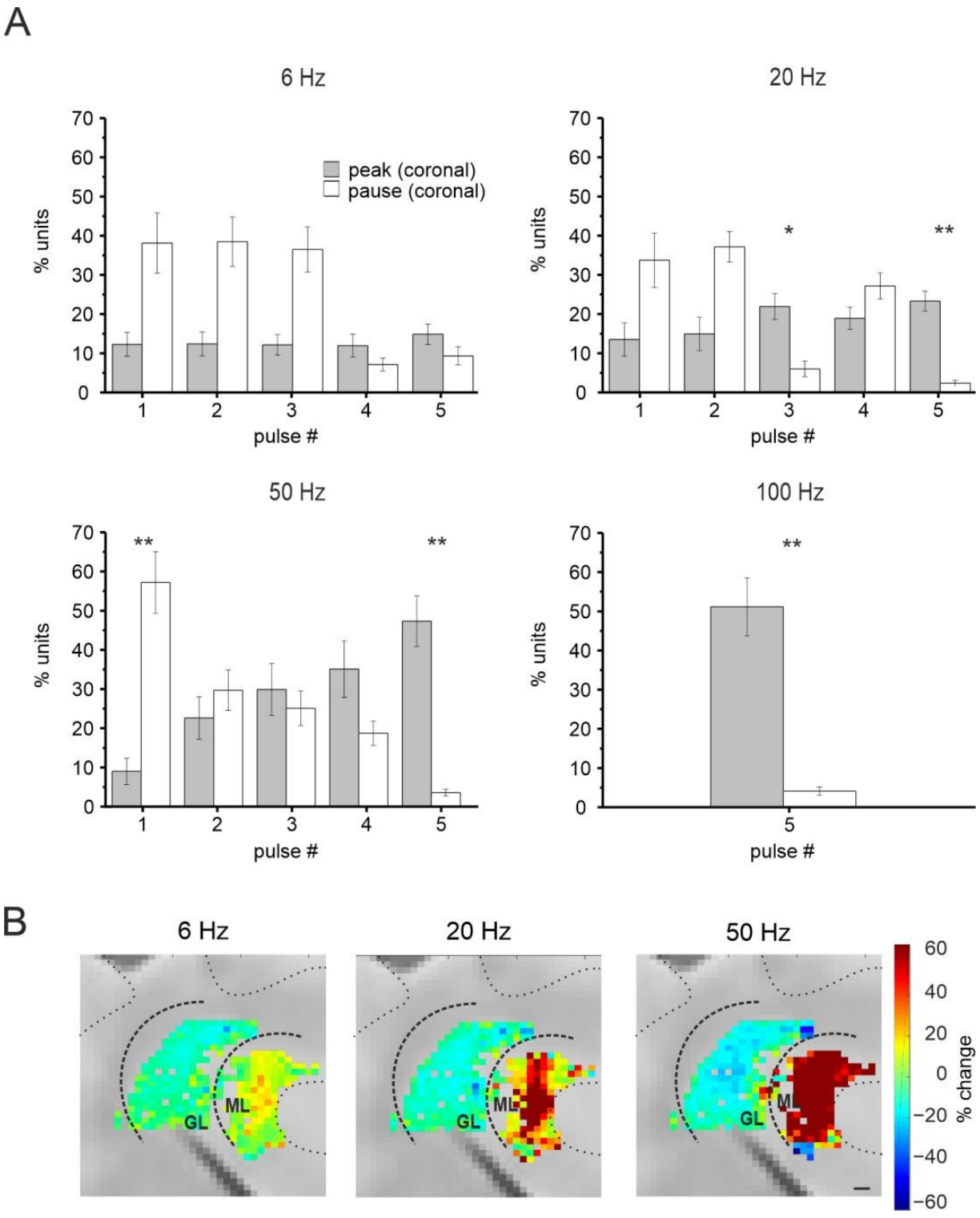

Figure 9. PCs responses to MF stimulation in the coronal plane. (**A**) The histograms show the average percentage of units responding to MFs stimulation at different frequencies with peaks (black) or pauses (grey) in the PSTHs. Asterisks indicate statistical significance (* $p < 0.05$, ** $p < 0.01$). (**B**) Colormaps showing the percent change of PCs' mean firing rate (MFR) at the last stimulation pulse compared to the first one, at 6, 20, and 50 Hz, in a single experiment. In the same image, the channels in the granular layer showing a response to MFs stimulation are reported, for the same experiment, showing the percent change of the N_{2a} peak (as in Figure 5A) using the same color code at right. Scale bar 100 µm.

3.4. Comparison of Cerebellar Network Responses in the Sagittal and Coronal Planes

MFs stimulation evoked an LFP response propagating through the granular layer. The activated granular layer area appeared to be more extended in coronal slices than in sagittal ones. After a single pulse stimulation, N_{2a} and N_{2b} peaks characterizing GrCs responses did not show a statistically significant difference in the two planes of the section. However, at increasing input frequencies, N_{2b} peak amplitude changes during the train appeared to differ in the two conditions, concerning short-term depression. Indeed, while N_{2a} showed short-term depression in both sagittal and coronal slices with similar amplitude, the N_{2b} peak could show an increase or a decrease in its amplitude. The main differences comparing the responses in the sagittal and coronal planes can be detected at higher frequencies (50 Hz and 100 Hz) for the amount of short-term depression shown (at 50 Hz, much smaller in the coronal plane; $p = 0.001$) and the percentage of channels showing depression (at 50 Hz and 100 Hz, much smaller in the coronal plane; $p = 0.01$, $p = 0.03$). This is in agreement with the fact that, at these frequencies, N_{2b} showed short-term potentiation in the coronal plane more than in the sagittal one ($p = 0.04$) (Figure 10A).

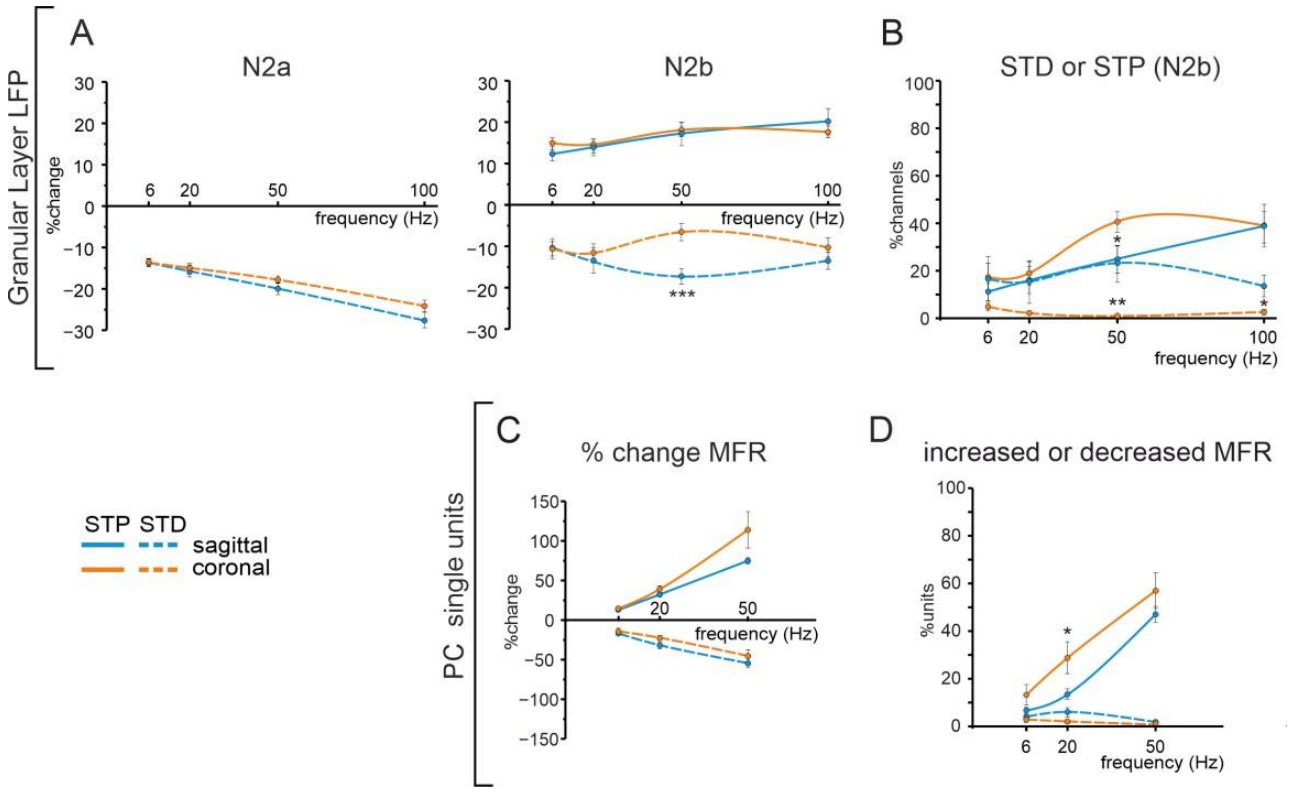

Figure 10. Comparison of the granular layer and PC responses in the sagittal and coronal planes. (**A**) The plots show the average percent change of the granular layer N2a (left) and N2b (right) peak amplitude in the sagittal (blue) and coronal orange planes. (**B**) The plot shows the percentage of units showing a significant change of N2b peak amplitude (as short-term potentiation, STP, full line; and short-term depression, STD, dashed line) in sagittal (blue) and coronal orange slices. (**C**) The plot shows the average percent change of PC mean firing rate (MFR) in sagittal (blue) and coronal orange slices. (**D**) The plot shows the percentage of units showing a significant increase (full line) and decrease (dashed line) of PCs MFR after the last stimulation pulse at different frequencies in the sagittal (blue) and coronal orange planes. Asterisks indicate statistical significance between granular layer and PC responses (either as STP or STD) in sagittal and coronal orientations (* $p < 0.05$, ** $p < 0.01$, *** $p < 0.001$).

Concerning PCs activity, their average basal MFR was significantly higher in coronal than in sagittal slices. As discussed below, this might depend on the different composition

in zebrin positive and negative cells in the coronal and sagittal slices, and on different orientations of MLI axons. Following MFs stimulation, PCs showed marked differences in their response patterns already after a single pulse. While peak responses significantly prevailed in the sagittal plane, pause responses were much more common in the coronal. This difference was conserved in the responses within the trains. In both sagittal and coronal slices, peaks prevailed over pauses at the end of the 5 pulses at any frequency, though more evidently at 50 Hz and 100 Hz. Nevertheless, PCs in the coronal plane maintained a higher degree of pause responses within the train compared to the sagittal plane, where pauses were less represented at any frequency (cfr. Figures 6 and 9). Concerning PC response amplitude, the MFR percent change within each stimulation pattern was not different in sagittal and coronal slices (Figure 10B).

4. Discussion

In this work, last-generation HD-MEA allowed us to characterize cerebellar microcircuit processing with state-of-the-art resolution. HD-MEA provided LFPs recording in the granular layer and PC single-unit spikes over the surface extension of a cerebellar slice, which allowed us to reconstruct the spatiotemporal distribution of activity in response to input patterns at different frequencies. The main observation is that cerebellar network processing is markedly anisotropic and frequency dependent.

Mossy fiber signal transmission through the cerebellar microcircuit was observed over an extended frequency range (0.1–100 Hz) and increased with frequency. Interestingly, we observed a previously underestimated efficiency of the network in processing low-frequency inputs. Moreover, while previous investigations suggested that only the sagittal orientation had an impact on dynamic processing, with a relative frequency independence in the coronal plane [17], here we show that both planes are characterized by an evident frequency dependence. Yet another aspect is that of short-term processing dynamics, which differed between the sagittal and coronal orientations, with an impact on the network output more evident at lower frequencies. All these differences presumably reflect the topographic organization of local inhibition, intrinsic electroresponsiveness, and short-term synaptic plasticity. After a few considerations on HD-MEA recordings, the results are briefly summarized to facilitate the reader in following the logical development of the Discussion leading to the schematic reconstruction of signal transmission summarized in Conclusions.

4.1. Considerations on HD-MEA Recordings

The HD-MEA allowed us to record the granular layer responses from an average of 136 channels per slice (2453 in 18 slices; see Table 1). Considering that 10–15 GrCs are expected to contribute to the LFP recorded in a single channel in these conditions (see [18]), the response detected in a single slice might be provided by approximately 1700 GrCs. However, we cannot exclude that a single GrC contributed to the signal recorded in two nearby channels, though the probability that the contribution was significant is low given the small cell size and the locality of the electrical field generated around it [28]. The average GrC diameter is around 5 µm [29], while the pitch between the electrodes is 42µm. Moreover, the electrode is recessed by about 1.5 µm in the chip insulating layer, restricting the sensitivity to the above neurons. Concerning PCs, the average number of detected units was 108 per slice (1953 in 18 slices; see Table 1). In this case, a single PC may indeed contribute to several nearby channels. For this reason, an automated procedure was used to avoid considering the same PC unit more than once (see Methods for details). Indeed, the average number of channels detecting PC activity was 204 per slice (3668 in 18 slices). This high throughput allowed us to test a large set of input patterns with high spatiotemporal resolution.

A comparison of responses in sagittal and coronal cerebellar slices was also performed. The anatomy of the cerebellar cortical circuit is geometrically orientated: in the granular layer, GoC inhibition over GrCs is exerted more efficiently in the sagittal plane (given the

specific orientation of the GoC axonal bundle); in the molecular layer, excitatory parallel fibers travel in the coronal plane, intersecting PCs and MLI dendrites that are oriented parasagittally. As previously reported [17], thanks to this anatomical organization of the circuit, the use of sagittal and coronal slices is an effective tool to discriminate signal transmission through the two main orientation planes of the cerebellar cortex. Thus, the HD-MEA allowed us a straightforward investigation of the anisotropic activation of GrCs and PCs.

This technique allowed us to resolve spatiotemporal network dynamics with enhanced resolution compared to low-density MEA [25] or voltage-sensitive dye imaging [17]. Low-density MEAs had less than half the HD-MEA pitch and a lower signal-to-noise ratio. Voltage-sensitive dyes allowed a good spatial resolution (<10 μm), but this was diffraction-limited and the quantum yield of the dyes was rather low decreasing the signal-to-noise ratio. Moreover, voltage-sensitive dyes were incapable of resolving single spikes and required a signal average. It should also be noted that HD-MEA signals mainly depend on neuronal firing, both in the granular and Purkinje cell layer, while voltage-sensitive dye imaging informs both about subthreshold and suprathreshold membrane potential changes.

Taken together, these features need to be considered when comparing the present data to previous ones obtained using different techniques.

4.2. Characterization of Spontaneous and Evoked Activity in Granular and PC Layers

GrCs are silent at rest and constitute the majority of cells in the granular layer with a ratio of about 400:1 with respect to GoCs in rodents [18,29,30], while PCs are autorhythmic with a mean firing rate (MFR) ranging from 20 to more than 100 Hz [31]. Interestingly, our data show that PCs' basal MFR in the coronal is significantly higher than in the sagittal plane. Several factors might be involved. First, parallel fibers are intact in the coronal plane, increasing the glutamatergic tone on PCs. Secondly, basket cell axons target PCs in the sagittal plane, so that the inhibitory tone on PC spontaneous firing should be lower in coronal slices, where basket cell axons are severed. Another factor that might have contributed to different PC firing rates in coronal and sagittal slices is zebrin protein expression. Zebrin-positive PCs are reported to have a lower spontaneous firing rate than zebrin-negative PCs [32] (from 36 Hz to 76 Hz in Ref. [33]) The zebrin pattern develops in parasagittal stripes and we do not know whether positive or negative PCs were equally represented in sagittal and coronal slices.

MF stimulation determined responses both in the granular and PC layer. The granular layer response was characterized by an LFP showing a series of peaks [24]. Interestingly, the number of channels showing GrCs responses was larger in the coronal plane. This might depend on the anisotropy of MF rosettes distribution in the granular layer, being three times closer one to the other in the coronal plane compared to the sagittal [34]. An increase in rosettes density might recruit more GrCs and, therefore, result in LFP detection in a larger number of channels. In granular layer LFPs, N_{2a} reflects the synchrony of GrCs firing driven by AMPA receptor-mediated responses, while N_{2b} reflects the NMDA receptor-mediated component of GrC synaptic responses and is modulated by Golgi cell GABAergic inhibition [25,28]. No difference between sagittal and coronal planes was found in the delay and amplitude of N_{2a} and N_{2b}. Conversely, PC responses revealed a significant difference. In the sagittal plane, most PCs showed a transient increase in their firing rate (evident as a peak in the PSTH). (Figure 3B). In the coronal plane, most PCs showed a pause after the stimulation (Figure 3B). The anatomy of the circuit provides hints for the interpretation of these data. In the sagittal plane, PCs are mostly activated by GrCs ascending axons, while the inhibition provided by MLIs is weak (Gr~~C~~→PCs). The functional equivalence of ascending axons and parallel fiber inputs has been demonstrated [35]. MLIs connections are more preserved in the coronal plane, as for parallel fibers. Therefore, GrCs activation by MFs is likely to activate MLIs through parallel fibers and lead to the consequent inhibition of PCs (parallel fiber → MLI ⊣ PC pathway).

4.3. Frequency-Dependent Responses in the Granular and PC Layers

The granular and PC layer responses to stimulation trains at different frequencies reveal a complex scenario.

The granular layer shows N_{2a} short-term depression that increases with frequency, reflecting the short-term depression of the AMPA receptor-mediated component of MF-GrCs responses [36–41]. The spatial organization of N_{2a} short-term depression could be due to the different number of MFs impinging on GrCs at different locations (more abundant along the medial region of the lobule). An increased number of active MFs contacts would amplify GrC AMPARs desensitization. Conversely, the N_{2b} component of the LFP can show either a decrease or an increase. This duality of response changes during the trains probably reflects the different excitatory/inhibitory balance that finally regulates the extent of NMDA receptor activation [2,18,37,42]. N_{2b} variability was significantly increased at an increasing frequency only in the sagittal plane, while N_{2b} depression at 50 Hz was smaller in the coronal orientation. This may reflect the anatomical organization of the GoC axonal plexus, which lies in the sagittal plane [3–5], exerting more effective control over GrCs firing in the sagittal than the coronal plane.

PCs responses differ in the two orientations at lower frequencies, showing mainly an MFR increase in sagittal and MFR decrease in the coronal plane. PCs responses at higher frequencies is a net MFR increase in both orientations. The PC response pattern in the coronal plane is richer than in the sagittal, being characterized by pauses at the beginning of the stimulation trains and peaks at the end. The frequency dependence of MLIs inhibition [6] and the short-term dynamics shaping signal transmission and MLIs activity [20] are likely to contribute to this shift. Indeed, different types of short-term plasticity have been observed at parallel fibers synapses depending on the target neuron, with short-term facilitation at parallel fibers–stellate cells relay and short-term depression at parallel fibers–basket cells relay [43,44]. Parallel fibers–MLIs synapses can be characterized by heterogeneous profiles of short-term potentiation, determining differences in the firing frequencies and delays of MLIs responses at different input frequencies [45]. Since complex spikes were not detected in response to MF stimulation, climbing fibers' contribution to MLIs, and PC activity [46] in our experiments can be excluded. In aggregate, PCs patterns of response in the coronal plane are most likely compound in their origin, and they probably involve a stronger drive from the granular layer in the coronal plane, determining the shift from pause to peak responses observed during prolonged high-frequency stimulation, and determining the loss of the anisotropy typical of low-frequency transmission.

5. Summary and Conclusions

A complex set of spatiotemporal filters regulates signal transmission in the cerebellar cortex, revealing a marked frequency dependence and anisotropy.

In the granular layer, the N_{2a} wave of the LFP always shows increasing depression with frequency, while N_{2b} shows either potentiation or depression depending on the granular layer microdomain. Therefore, N_{2b} can discriminate the bandpass at the input stage. When N_{2b} depresses, the filter sharpens, becomes less permissive at higher frequencies, and decreases the time window for GrC firing (this case is more common on the sagittal plane). When N_{2b} potentiates, the filter dampens, decreases its impact at higher frequencies, and allows longer GrC discharge (this case is more common on the coronal plane). Since N_{2b} depends on GABAergic control over NMDA receptor unblocking, this differential behavior reveals an important role for GoC inhibition in determining granular layer microdomains with diverse filtering properties. PCs add to the richness of signal transmission properties in the network. At low frequencies, PCs show either an increase or decrease in firing, with a clear orientation preference (sagittal or coronal, respectively). Nonetheless, at high frequencies, all PCs show a sharp increase in firing.

In aggregate, on the sagittal plane, the GrC time window for emitting spikes is sharp and PCs increase firing already at low frequencies. On the coronal plane, the GrC time window for emitting spikes is broad and PCs decrease firing at low frequencies (Figure 11).

It is possible that the increased time window of GrC firing on the coronal plane determines the response properties of PCs in synergy with frequency-dependent MLI control. Testing this hypothesis will require computational modeling [47] opening new perspectives for the calculation of network complexity, entropy, and mutual information transfer.

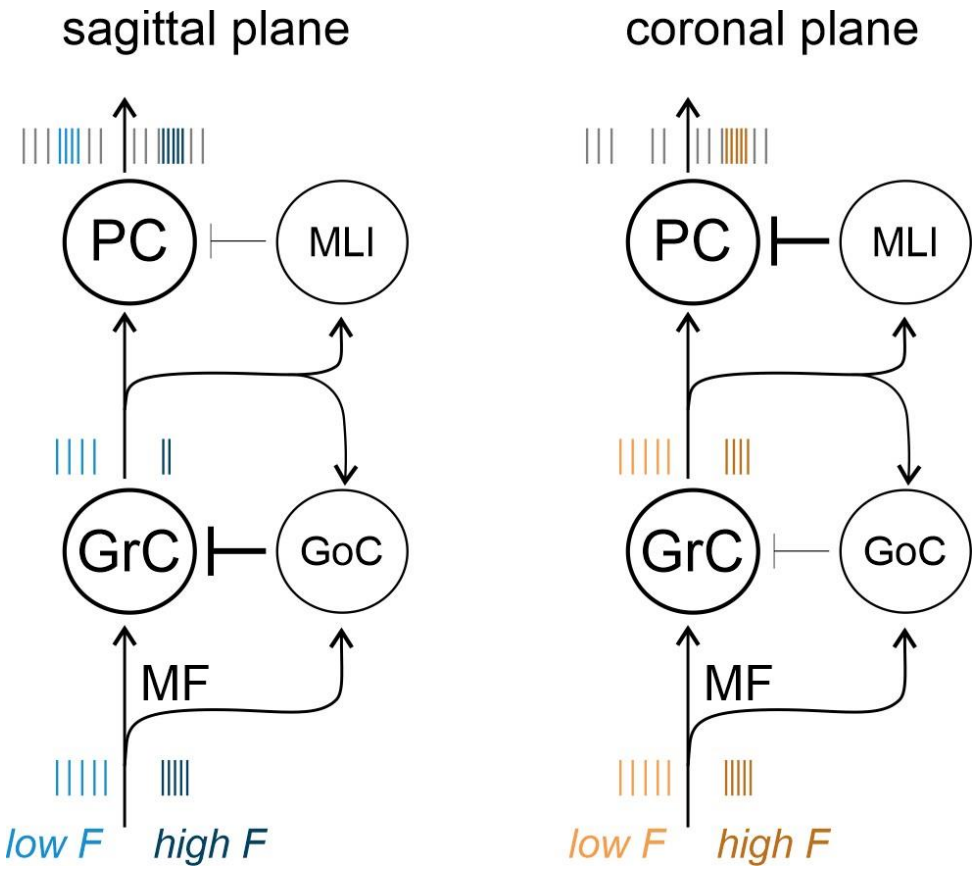

Figure 11. Schematic representation of low and high-frequency signal transmission on the sagittal and coronal planes. Left: on the sagittal plane, granule cells (GrC) receive robust inhibition from Golgi cells (GoC) and Purkinje cells (PC) receive weak inhibition from molecular layer interneurons (MLI). The granular layer filtering of MF input sharpens at high frequency. Right: on the coronal plane, GoC inhibition of GrC activity is less prominent and MLI control of PC activity is more robust. The time window for GrC firing broadens and PC show a decrease in firing at low frequency and an increase in firing at high frequency.

Author Contributions: Conceptualization, E.D. and L.M.; formal analysis, A.M. and D.D.D.; funding acquisition, E.D.; investigation, A.M. and D.D.D.; methodology, A.M. and L.M.; supervision, L.M.; writing—original draft, A.M. and L.M.; writing—review and editing, E.D. and L.M. All authors have read and agreed to the published version of the manuscript.

Funding: This research was funded by the European Union's Horizon 2020 Framework Program for Research and Innovation under the Specific Grant Agreement No. 945539 (Human Brain Project SGA3) to ED. Work supported by #NEXTGENERATIONEU (NGEU) and funded by the Ministry of University and Research (MUR), National Recovery and Resilience Plan (NRRP), project MNESYS (PE0000006)—A Multiscale integrated approach to the study of the nervous system in health and disease (DN. 1553 11.10.2022) to ED.

Institutional Review Board Statement: The animal study protocol was approved by the Institutional Ethics Committee of the University of Pavia (Italy) and by the Italian Ministry of Health with authorization following art.1, comma 4 of the D.Lgs.n. 26/2014 approved on 9 December 2017.

Informed Consent Statement: Not applicable.

Data Availability Statement: All the materials related to the paper are available from the corresponding author upon reasonable request.

Acknowledgments: We thank the animal facility "Centro di servizio per la gestione unificata delle attività di stabulazione e di radiobiologia" of the University of Pavia, Pavia, Italy to host the animals; the OPBA of the University of Pavia for support in animal protocol drawing up. We thank Thierry Nieus and Alessandro Maccione for their contribution in setting data analysis.

Conflicts of Interest: The authors declare no conflict of interest. The funders had no role in the design of the study; in the collection, analyses, or interpretation of data; in the writing of the manuscript; or in the decision to publish the results.

References

1. D'Angelo, E. Chapter 6—Physiology of the cerebellum. In *The Cerebellum: From Embryology to Diagnostic Investigations*; Manto, M., Thierry AGM Huisman, Eds.; Elsevier: Amsterdam, The Netherlands, 2018; Volume 154, pp. 85–108. ISBN 0072-9752.
2. Mapelli, L.; Solinas, S.; D'Angelo, E. Integration and regulation of glomerular inhibition in the cerebellar granular layer circuit. *Front. Cell. Neurosci.* **2014**, *8*, 55. [CrossRef] [PubMed]
3. Prestori, F.; Mapelli, L.; D'Angelo, E. Diverse neuron properties and complex network dynamics in the cerebellar cortical inhibitory circuit. *Front. Mol. Neurosci.* **2019**, *12*, 267. [CrossRef]
4. D'Angelo, E. The critical role of golgi cells in regulating spatio-temporal integration and plasticity at the cerebellum input stage. *Front. Neurosci.* **2009**, *2*, 35–46. [CrossRef]
5. Tabuchi, S.; Gilmer, J.I.; Purba, K.; Person, A.L. Pathway-specific drive of cerebellar golgi cells reveals integrative rules of cortical inhibition. *J. Neurosci.* **2019**, *39*, 1169–1181. [CrossRef] [PubMed]
6. Rizza, M.F.; Locatelli, F.; Masoli, S.; Sánchez-Ponce, D.; Muñoz, A.; Prestori, F.; D'Angelo, E. Stellate cell computational modeling predicts signal filtering in the molecular layer circuit of cerebellum. *Sci. Rep.* **2021**, *11*, 3873. [CrossRef] [PubMed]
7. Rieubland, S.; Roth, A.; Häusser, M. Structured connectivity in cerebellar inhibitory networks. *Neuron* **2014**, *81*, 913–929. [CrossRef]
8. Ango, F.; Wu, C.; Van Der Want, J.J.; Wu, P.; Schachner, M.; Huang, Z.J. Bergmann glia and the recognition molecule CHL1 organize GABAergic axons and direct innervation of purkinje cell dendrites. *PLoS Biol.* **2008**, *6*, 739–756. [CrossRef]
9. D'Angelo, E.; Casali, S. Seeking a unified framework for cerebellar function and dysfunction: From circuit operations to cognition. *Front. Neural Circuits* **2012**, *6*, 116. [CrossRef] [PubMed]
10. D'Angelo, E. The cerebellum gets social. *Science* **2019**, *363*, 229. [CrossRef]
11. Palesi, F.; Tournier, J.D.; Calamante, F.; Muhlert, N.; Castellazzi, G.; Chard, D.; D'Angelo, E.; Wheeler-Kingshott, C.A.M. Contralateral cerebello-thalamo-cortical pathways with prominent involvement of associative areas in humans in vivo. *Brain Struct. Funct.* **2015**, *220*, 3369–3384. [CrossRef]
12. Casiraghi, L.; Alahmadi, A.A.S.; Monteverdi, A.; Palesi, F.; Castellazzi, G.; Savini, G.; Friston, K.; Wheeler-Kingshott, C.A.M.G.; D'Angelo, E. I see your effort: Force-related BOLD effects in an extended action execution-observation network involving the cerebellum. *Cereb. Cortex* **2019**, *29*, 1351–1368. [CrossRef]
13. Mapelli, L.; Soda, T.; D'Angelo, E.; Prestori, F. The cerebellar involvement in autism spectrum disorders: From the social brain to mouse models. *Int. J. Mol. Sci.* **2022**, *23*, 3894. [CrossRef] [PubMed]
14. Schmahmann, J.D.; Guell, X.; Stoodley, C.J.; Halko, M.A. The theory and neuroscience of cerebellar cognition. *Annu. Rev. Neurosci.* **2019**, *42*, 337–364. [CrossRef] [PubMed]
15. D'Angelo, E.; Koekkoek, S.K.E.; Lombardo, P.; Solinas, S.; Ros, E.; Garrido, J.; Schonewille, M.; De Zeeuw, C.I. Timing in the cerebellum: Oscillations and resonance in the granular layer. *Neuroscience* **2009**, *162*, 805–815. [CrossRef]
16. Solinas, S.; Nieus, T.; D'Angelo, E. A realistic large-scale model of the cerebellum granular layer predicts circuit spatio-temporal filtering properties. *Front. Cell. Neurosci.* **2010**, *4*, 12. [CrossRef]
17. Mapelli, J.; Gandolfi, D.; D'Angelo, E. High-pass filtering and dynamic gain regulation enhance vertical bursts transmission along the mossy fiber pathway of cerebellum. *Front. Cell. Neurosci.* **2010**, *4*, 14. [CrossRef] [PubMed]
18. Gagliano, G.; Monteverdi, A.; Casali, S.; Laforenza, U.; Wheeler-Kingshott, C.A.M.G.; D'angelo, E.; Mapelli, L. Non-linear frequency dependence of neurovascular coupling in the cerebellar cortex implies vasodilation–Vasoconstriction competition. *Cells* **2022**, *11*, 1047. [CrossRef]
19. Salmasi, M.; Loebel, A.; Glasauer, S.; Stemmler, M. Short-term synaptic depression can increase the rate of information transfer at a release site. *PLoS Comput. Biol.* **2019**, *15*, e1006666. [CrossRef]
20. Grangeray-Vilmint, A.; Valera, A.M.; Kumar, A.; Isope, P. Short-term plasticity combines with excitation–Inhibition balance to expand cerebellar purkinje cell dynamic range. *J. Neurosci.* **2018**, *38*, 5153–5167. [CrossRef]
21. Tognolina, M.; Monteverdi, A.; D'Angelo, E. Discovering microcircuit secrets with multi-spot imaging and electrophysiological recordings: The example of cerebellar network dynamics. *Front. Cell. Neurosci.* **2022**, *16*, 805670. [CrossRef]
22. Rothman, J.S.; Cathala, L.; Steuber, V.; Silver, R.A. Synaptic depression enables neuronal gain control. *Nature* **2009**, *457*, 1015–1018. [CrossRef] [PubMed]

23. Tang, Y.; An, L.; Yuan, Y.; Pei, Q.; Wang, Q.; Liu, J.K. Modulation of the dynamics of cerebellar purkinje cells through the interaction of excitatory and inhibitory feedforward pathways. *PLoS Comput. Biol.* **2021**, *17*, e1008670. [CrossRef] [PubMed]
24. Maffei, A.; Prestori, F.; Rossi, P.; Taglietti, V.; D'Angelo, E. Presynaptic current changes at the mossy fiber-granule cell synapse of cerebellum during LTP. *J. Neurophysiol.* **2002**, *88*, 627–638. [CrossRef]
25. Mapelli, J.; D'Angelo, E. The spatial organization of long-term synaptic plasticity at the input stage of cerebellum. *J. Neurosci.* **2007**, *27*, 1285–1296. [CrossRef]
26. Nieus, T.; D'Andrea, V.; Amin, H.; Di Marco, S.; Safaai, H.; Maccione, A.; Berdondini, L.; Panzeri, S. State-dependent representation of stimulus-evoked activity in high-density recordings of neural cultures. *Sci. Rep.* **2018**, *8*, 5578. [CrossRef] [PubMed]
27. Hawkes, R. Purkinje cell stripes and long-term depression at the parallel fiber-purkinje cell synapse. *Front. Syst. Neurosci.* **2014**, *8*, 41. [CrossRef]
28. Diwakar, S.; Lombardo, P.; Solinas, S.; Naldi, G.; D'Angelo, E. Local field potential modeling predicts dense activation in cerebellar granule cells clusters under LTP and LTD control. *PLoS ONE* **2011**, *6*, e21928. [CrossRef] [PubMed]
29. D'Angelo, E.; Solinas, S.; Mapelli, J.; Gandolfi, D.; Mapelli, L.; Prestori, F. The cerebellar golgi cell and spatiotemporal organization of granular layer activity. *Front. Neural Circuits* **2013**, *7*, 93. [CrossRef]
30. Korbo, L.; Andersen, B.B.; Ladefoged, O.; Møller, A. Total numbers of various cell types in rat cerebellar cortex estimated using an unbiased stereological method. *Brain Res.* **1993**, *609*, 262–268. [CrossRef]
31. Masoli, S.; D'Angelo, E. Synaptic activation of a detailed purkinje cell model predicts voltage-dependent control of burst-pause responses in active dendrites. *Front. Cell. Neurosci.* **2017**, *11*, 278. [CrossRef]
32. Cerminara, N.L.; Lang, E.J.; Sillitoe, R.V.; Apps, R. Redefining the cerebellar cortex as an assembly of non-uniform purkinje cell microcircuits. *Nat. Rev. Neurosci.* **2015**, *16*, 79–93. [CrossRef] [PubMed]
33. Zhou, H.; Lin, Z.; Voges, K.; Ju, C.; Gao, Z.; Bosman, L.W.J.; Ruigrok, T.J.; Hoebeek, F.E.; De Zeeuw, C.I.; Schonewille, M. Cerebellar modules operate at different frequencies. *Elife* **2014**, *2014*, e02536. [CrossRef] [PubMed]
34. Sultan, F. Distribution of mossy fibre rosettes in the cerebellum of cat and mice: Evidence for a parasagittal organization at the single fibre level. *Eur. J. Neurosci.* **2001**, *13*, 2123–2130. [CrossRef]
35. Walter, J.T.; Dizon, M.J.; Khodakhah, K. The functional equivalence of ascending and parallel fiber inputs in cerebellar computation. *J. Neurosci.* **2009**, *29*, 8462–8473. [CrossRef] [PubMed]
36. Sola, E.; Prestori, F.; Rossi, P.; Taglietti, V.; D'Angelo, E. Increased neurotransmitter release during long-term potentiation at mossy fibre-granule cell synapses in rat cerebellum. *J. Physiol.* **2004**, *557*, 843–861. [CrossRef]
37. Nieus, T.R.; Mapelli, L.; D'Angelo, E. Regulation of output spike patterns by phasic inhibition in cerebellar granule cells. *Front. Cell. Neurosci.* **2014**, *8*, 246. [CrossRef]
38. D'Errico, A.; Prestori, F.; D'Angelo, E. Differential induction of bidirectional long-term changes in neurotransmitter release by frequency-coded patterns at the cerebellar input. *J. Physiol.* **2009**, *587*, 5843–5857. [CrossRef]
39. Gao, Z.; Van Beugen, B.J.; De Zeeuw, C.I. Distributed synergistic plasticity and cerebellar learning. *Nat. Rev. Neurosci.* **2012**, *13*, 619–635. [CrossRef] [PubMed]
40. Wall, M.J. Short-term synaptic plasticity during development of rat mossy fibre to granule cell synapses. *Eur. J. Neurosci.* **2005**, *21*, 2149–2158. [CrossRef]
41. DiGregorio, D.A.; Rothman, J.S.; Nielsen, T.A.; Silver, R.A. Desensitization properties of AMPA receptors at the cerebellar mossy fiber-granule cell synapse. *J. Neurosci.* **2007**, *27*, 8344–8357. [CrossRef]
42. Mapelli, L.; Rossi, P.; Nieus, T.; D'Angelo, E. Tonic activation of GABAB receptors reduces release probability at inhibitory connections in the cerebellar glomerulus. *J. Neurophysiol.* **2009**, *101*, 3089–3099. [CrossRef] [PubMed]
43. Carter, A.G.; Regehr, W.G. Prolonged synaptic currents and glutamate spillover at the parallel fiber to stellate cell synapse. *J. Neurosci.* **2000**, *20*, 4423–4434. [CrossRef] [PubMed]
44. Bao, J.; Reim, K.; Sakaba, T. Target-dependent feedforward inhibition mediated by short-term synaptic plasticity in the cerebellum. *J. Neurosci.* **2010**, *30*, 8171–8179. [CrossRef] [PubMed]
45. Dorgans, K.; Demai, V.; Bailly, Y.; Poulain, B.; Isope, P.; Doussau, F. Short-term plasticity at cerebellar granule cell to molecular layer interneuron synapses expands information processing. *Elife* **2019**, *8*, e41586. [CrossRef] [PubMed]
46. Szapiro, G.; Barbour, B. Multiple climbing fibers signal to molecular layer interneurons exclusively via glutamate spillover. *Nat. Neurosci.* **2007**, *10*, 735–742. [CrossRef] [PubMed]
47. De Schepper, R.; Geminiani, A.; Masoli, S.; Rizza, M.F.; Antonietti, A.; Casellato, C.; D'Angelo, E. Model simulations unveil the structure-function-dynamics relationship of the cerebellar cortical microcircuit. *Commun. Biol.* **2022**, *5*, 1240. [CrossRef]